

CHAPTER 1

FOUNDATIONS AND LINEAGE OF MODERN MAGNETORHEOLOGICAL MATERIALS

1.1 History and Motivation

In 1947 Willins M. Winslow received a patent for the practical application of the “Johnsen Rahbeck Effect”. This was an application of the observation of an attractive force between electrodes separated by certain poor insulators. Winslow found through his experimentation that some liquids become solids when subjected to an electric field. This was known early on as the Winslow effect and is now more commonly referred to as the electrorheological effect. [US Patent 1947].

Electrorheological (ER) and Magnetorheological (MR) materials are composed of dispersed particles in a fluid carrier or polymer matrix that exhibit fast and reversible changes in their rheological characteristics when these fluids are subjected to external electric or magnetic fields. This is a consequence of their electrical and/or magnetic material properties. The particles in these systems experience forces and torques when subjected to electric and/or magnetic fields as a consequence of their material properties. Furthermore, when they are electrically charged or magnetized, closely spaced particles often exhibit strong mutual interactions. The interactions in materials of this type cause

rheological behavior that responds directly to an applied field. Materials that fall into this class are referred to as “smart” or active. These ‘smart’ composites which we refer to as magnetorheological (MR) elastomers have been explored for use in a number of designs from automotive, aerospace and civil engineering applications as shock absorbers, automotive suspension bushings, valves, brakes, clutches, safety restraint systems, semi-active control systems and building vibration isolation.

MR fluid applications have been known for several decades, particularly their use in vacuum-compatible bearings and rotational feedthroughs; MR fluids have been commercialized under the trademark “Ferrofluidics”. Studies of nanocomposite MR fluids have been conducted by Poddar[25], Kristof[18], and Ivanov[14]. These investigations have attempted to understand the dynamic magnetic behavior of colloidal systems. Wiedmann [37] has written on the observed pseudo-crystalline ordering in ferrofluids induced by magnetic fields. However, the extension of MR concepts to solid-state and polymeric materials is relatively recent. There is much work yet to be done in order to understand the basic mechanisms of MR behavior in solid state systems and enable engineering applications of such materials. It is the goal of this dissertation to provide some insights on the dynamic behavior of MR elastomeric materials at the nanoscale level. This is the first such study of its kind.

The revival of interest in magnetorheological (MR) fluids has inspired the development of (MR) elastomers, their solid-state analogues. While MR fluids comprise micron-size, or smaller, soft magnetic (magnetizable) inclusions dispersed in liquids, MR elastomers

contain such particles embedded in an elastomeric or rubber-like matrix. Elastomers that have been used in the formulation of these materials include silicone rubber and natural rubber. The application of a magnetic field to an uncured (pre-crosslinked) MR elastomer can lead to the formation of particle chains or more complex structures with high levels of mechanical anisotropy. Once the matrix has cured or crosslinked, these structures are locked into place although it should be pointed out that some limited particle motion can still take place as if in a very viscous medium. This viscoelastic composite can possess shear and tensile moduli that can be controlled by the application of an external magnetic field. The resulting modulus increase is rapid, continuous, and reversible. For a relatively high-modulus elastomer matrix such as natural rubber (cis-polyisoprene), the fractional modulus increase with field can exceed 50%, while it can be even larger for low-modulus host materials.

Investigation of the physical composition and rheological behavior of ER and MR devices has traditionally been done with such techniques as tensile and shear strength testing, viscosity measurements and dynamic light scattering. A great deal of mechanical testing of both ER and MR fluids and solids has been done in the last two decades. The emphasis of this body of work has been on understanding the magnetostrictive behavior of this class of materials. Experiments have run the range from the composite being an active element in a magnetic system [1][7][2][39] to the examination of single chain strength using optical trapping [5].

Dynamic light scattering has been used to measure the dynamic structure factor of density fluctuations in colloidal suspensions. By monitoring changes in the scattered intensity-intensity autocorrelation function, the dynamics of the inclusions can be studied. It can be shown that the relaxation times of the scattered intensity are determined by the mechanical properties of the material such as diffusion constants and dynamic viscosity. Several authors have used dynamic light scattering [23][35] in this manner.

X-ray photon correlation spectroscopy (XPCS) was recently employed to measure the diffusive behavior of gold colloids and binary fluids[22]. When coherent x-ray fronts are scattered at the particle-host interface they produce a speckle pattern. The time dependence of this intensity pattern can be correlated to explore the characteristic times of the mechanical relaxation of the associated scattering targets. We have extended this technique to MR elastomer composite samples using x-ray synchrotron facilities at the Advanced Photon Source, Argonne National Laboratory.

APS is a third generation x-ray synchrotron source which accelerates relativistic electrons through arrays of permanent magnets known as undulators, thus producing extremely intense quasi-monochromatic x-ray radiation. Excellent transverse and longitudinal coherence of the beam enables interfering wave fronts at the scattering interface to produce an x-ray speckle interference pattern. By studying the temporal fluctuations in the intensities of an x-ray speckle pattern of an (MR) elastomer, we can examine its internal dynamics. X-Ray speckle interferometry correlates the change in the produced speckle field to the relative internal motion of the scattering centers (particles). An (MR)

elastomer sample was placed with the longitudinal cure axis on beam center. X-rays were then scattered from the MR elastomer while an external magnetic field was applied with a Heavyside (step) function. The scattered field was then time correlated over a range of scattering angles. The rate of decay in scattered intensity, $g^{(2)}(t)$, at a given scattering vector, is given by

$$g^{(2)}(t) = \frac{\langle I(t + \Delta t)I(t) \rangle}{\langle I(t) \rangle^2} \quad (1.1)$$

and is due to the change in the internal order due to mechanical relaxation processes.

These mechanical processes are extracted from the scattered electric field vector, $g^{(1)}(t)$, via dynamic light scattering principles and are related to the scattered field intensity by the Siegert relation

$$g^{(2)}(t) = 1 + A |g^{(1)}(t)|^2 \quad (1.2)$$

where A is an experimental optical constant referred to as the speckle constant.

Characteristic material relaxation times and the corresponding relative length changes (particle mean square displacements) can be extracted from the speckle data. The stresses and mechanical constants can then be estimated using the change in stress for a polymer network and the modified viscoelastic elements employed in fractional calculus. We can then use basic continuum mechanics to model the displacements of a rigid spherical

indenter into an elastic half-space. This will allow us to classify the magnetic forces at various length scales associated with the response to a cyclically applied magnetic field for varying degrees of inclusion anisotropy. Understanding these interaction forces are the basis for better design of a magnetorheological material.

1.2 Dissertation Organization

In the chapters that follow I hope to present both an outline for the understanding of the basic mechanics behind a MRE and a novel method to investigate this material using XPCS. The topics to be presented are as follows:

- Fundamental concepts and models specifically needed in MRE mechanics
- Theoretical background of small angle scattering, XPCS, speckle and basic concepts of dynamic light scattering
- Basic continuum and polymer mechanics
- Theory of viscoelasticity and fractional calculus variants
- My XPCS MRE experiments at Argonne National Lab
- Methods, results and conclusions

CHAPTER 2

THEORETICAL BASIS FOR THE WORK

2.1 THEORY OF MRE MECHANICS

2.1.1 MRE Design

(MR) elastomeric materials consist of micron size magnetically permeable particles suspended in a polymeric elastomer. The dispersed phase is usually a soft magnetic material such as iron particles of 0.1-10 μm size and 30 to 50 percent volume fraction. Upon application of a magnetic field, the rheological properties of these materials are rapidly and reversibly altered. The mechanism responsible for this bulk effect is the induced magnetic interaction force between the particles within the matrix. A vulcanized polymer matrix is necessary and the relative MR effect can be increased by using a softer matrix material such as silicone rubber. One of the most important properties of the matrix material besides the rheological properties is that the magnetic permeability should be as low as possible. If the matrix is magnetic, the polarization of the particles will be less effective and the MR effect reduced. The final rigidity of the structure is thus a function of the particle volume fraction and distribution, the matrix material and the applied magnetic field.

Most models of (MR) material behavior are based on the magnetic dipole interactions between adjacent particles. These interparticle interactions are then averaged over the entire sample to yield a model of the bulk magnetostrictive behavior. Magnetizable materials exhibit strongly nonlinear behaviors such as paramagnetism and ferromagnetism. Though magnetization characterization is very complex, it is adequate, for the purposes of describing the forces on magnetizable particles, to group nonlinear magnetic materials into two classifications, namely, “soft” and “hard” materials. Representative magnetization curves of M versus H are shown in Fig. 1 for these two types of materials.

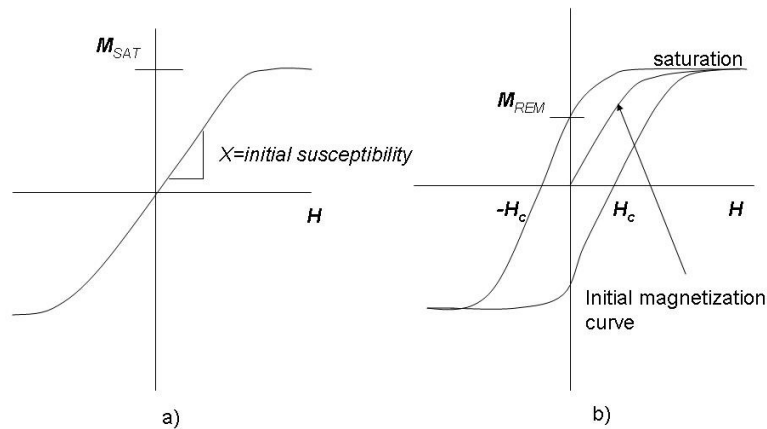


Fig. 1 Representative magnetization curves for ferromagnetic materials
 (a) Magnetically soft material showing saturation.
 (b) Magnetically hard material showing hysteresis loop.

The principal manifestation of this nonlinearity in soft materials is the phenomenon of saturation. Saturation, an attribute of orientational polarization, occurs when all the magnetic domains in a material become aligned, limiting the magnitude of the magnetization vector to a finite value M_{sat} . The influence of saturation upon the effective moment of a particle should be evident. Magnetically hard materials exhibit saturation, but just as importantly, they require significant energy to realign their domain walls once the material is first magnetized. This phenomenon is called hysteresis. The shape of a hysteresis curve is dependent upon the hardness of the material, plus the magnitude and rate of change of the applied magnetic field. Thus, when a uniform magnetic field is superimposed upon the magnetic spherical inclusion and its magnitude is increased from zero to some final value, the material magnetization will follow this curve.

The inclusions interact via a dipolar interaction energy given by

$$E_{12} = \frac{\mu_R \mu_o (MV)^2}{4\pi|r|^3} [(1 - 3\cos^2 \theta)] \quad (2.1)$$

and the associated force in the MRE is given by

$$F_{12} \propto -\frac{dE_{12}}{dr}. \quad (2.2)$$

Where θ is the angle that the vector joining the particle centers forms with the field direction, and r is the distance between particle centers. M is the particle magnetization and V is the particle volume. Therefore it is noted that employing an inclusion material with high permeability and saturation magnetization will provide high interaction energy and subsequently a high MR effect.

We will examine the simple dipole model of particle interaction to aid in characterizing the force distribution within the particle network. This is the basis for the composite magnetostriction.

2.1.2 Dipole-Dipole Interaction

The approach will be to compute the interaction energy, $E(x + \Delta x)$, of a chain of particles with a virtual break Δx at a joint j then calculate the shear force at the j th joint in a chain from

$$F_j = - \left. \frac{dE(x + \Delta x)}{d(\Delta x)} \right|_{\Delta x=0} . \quad (2.3)$$

Harpavat [11] has published an analysis for calculating the magnetic forces at various joints of a chain of spherical beads in a magnetic field. The following fundamental concepts for the magnetic properties of bulk matter can be found in numerous texts [6][10][14].

The net magnetic field at any point in space is the vector sum of the contributions from the original source field plus a contribution from the magnetization of any material in this field.

$$B = B_o + \mu_o M \quad (2.4)$$

Where M is the magnetization or the magnetic moment per unit volume and $\mu_o M$ the contribution of the magnetized object to the field. The effects of free currents are isolated by defining the magnetic intensity, H , as

$$H \equiv \frac{B}{\mu_o} - M \quad (2.5)$$

The dimensions of H are those of M , not of B . By replacing B with $B_o + \mu_o M$ we find

$$B_o = \mu_o H \quad (2.6)$$

We can now write

$$B = \mu_o H + \mu_o M \quad (2.7)$$

and now define the magnetic susceptibility, χ_m , as a coefficient of proportionality between the magnetization and the magnetic intensity

$$M \equiv \chi_m H \quad (2.8)$$

With this definition we can express the relation between the magnetic field in a material and the magnetic intensity

$$B = B_o + \mu_0 M = \mu_0 H + \mu_0 \chi_m H \quad (2.9)$$

$$= \mu_0 (1 + \chi_m) H \quad (2.10)$$

We define the coefficient of H as the permeability, μ , of the material

$$\mu \equiv \mu_0 (1 + \chi_m) \quad (2.11)$$

and the relative permeability as

$$\mu_R = \frac{\mu}{\mu_0} = (1 + \chi_m) \quad (2.12)$$

We will follow the derivation of the dipole-dipole interaction as outlined by Rosenweig [29]. The magnetic field, H , from a point dipole p a distance r away from that source is

$$H = \frac{p}{4\pi\mu_0} \frac{\vec{r}}{|\vec{r}|^3} \quad (2.13)$$

$$H = \frac{p}{4\pi\mu_0} \frac{\hat{r}}{r^2} \quad (2.14)$$

In (SI) an induction field B in tesla is defined in vacuum as

$$B = \mu_0 H \quad (2.15)$$

therefore the induction field B surrounding an (SI) pole is

$$B = \mu_0 H \quad (2.16)$$

$$B = \mu_0 \frac{p}{4\pi\mu_0} \frac{\hat{r}}{r^2} \quad (2.17)$$

$$= \frac{p}{4\pi} \frac{\hat{r}}{r^2} \quad (2.18)$$

The intensity of the magnetization is defined as

$$M \equiv \frac{p}{A\mu_0} = \frac{\rho_s}{\mu_0} \quad (2.19)$$

The external field of a dipole point source is

$$H = \frac{\rho_s a_d}{4\pi\mu_0} \left(-\frac{\vec{r}_1}{r_1^3} + \frac{\vec{r}_2}{r_2^3} \right) \quad (2.20)$$

Where $r_1 = \frac{1}{2}d_1 + r$ and $r_2 = \frac{1}{2}d_2 + r$. Though this relation holds for any separation d ,

what is desired is a good approximation to the field when the separation d is small

compared to r . When $d \ll r$, to a good approximation r_1 and r_2 are given by

$$r_1 \approx r + \frac{d}{2} \cos \theta, \quad r_2 \approx r - \frac{d}{2} \cos \theta \quad (2.21)$$

By the binomial theorem,

$$r_i^{-3} \approx \left(r \pm \frac{d}{2} \cos \theta \right)^{-3} = r^{-3} \left(1 \pm \frac{d}{2r} \cos \theta \right)^{-3} \quad (2.22)$$

$$\approx r^{-3} \left(1 \mp \frac{3d}{2r} \cos \theta \right) \quad (2.23)$$

$$H(r) \approx \frac{\rho_s a_d}{4\pi\mu_0 r^3} \left[\left(-\frac{1}{2}d - r \right) \left(1 - \frac{3d}{2r} \cos \theta \right) + \left(-\frac{1}{2}d + r \right) \left(1 + \frac{3d}{2r} \cos \theta \right) \right] \quad (2.24)$$

Canceling common terms gives

$$H(r) \approx \frac{\rho_s a_d d}{4\pi\mu_0 r^3} \left[-\hat{d} + \hat{r} 3 \cos \theta \right] \quad (2.25)$$

Where \hat{d} is the unit vector \vec{d}/d . However, $\hat{d} \cdot \hat{r} = \cos \theta$, $\rho_s = \mu_o M$, and $V = a_d d$, so the result may be written as

$$H(r) \approx \frac{MV}{4\pi r^3} \left[-\hat{d} + 3(\hat{d} \cdot \hat{r})\hat{r} \right] \quad (2.26)$$

The intrinsic particle polarization is the dipole moment magnitude per unit particle volume, i.e.,

$$|m| = MV_i \quad (2.27)$$

Where M is the induced particle polarization in (SI) units of Tesla.

Note that $\mu_o M$ represents the vector moment per unit volume because the definition of dipole moment m is

$$m \equiv \rho_s a_d d = \mu_o M a_d d = \mu_o MV \quad (2.28)$$

The interaction energy of two dipoles is found from the force per unit volume acting on an elementary volume of dipolar matter in an external magnetic field H . The total force using $\mu_o (M \cdot \nabla)H$ and the definition of m is

$$F = (m \cdot \nabla)H \quad (2.29)$$

With the help of a vector identity, $(m \cdot \nabla)H_0$ can be rewritten as

$$(m \cdot \nabla)H = \nabla(m \cdot H) - (H \cdot \nabla)m - m \times (\nabla \times H) - H \times (\nabla \times m) \quad (2.30)$$

For constant m this simplifies to

$$(m \cdot \nabla)H = \nabla(m \cdot H) - m \times (\nabla \times H) \quad (2.31)$$

When there is no flow of electric current, $\nabla \times H$ is identically zero and thus for a dipole of fixed moment m the force F can be derived from the energy of interaction E_h by

$$F = -\nabla E_h \quad (2.32)$$

Where

$$E_h = -(m \cdot H) \quad (2.33)$$

It is now possible to consider the interaction energy of two point dipoles. If for example dipole (1) is regarded as the source of the magnetic field felt by (2) then

$$H_1(r) = \frac{M_1 V_1}{4\pi r^3} \left[-\hat{d}_1 + 3(\hat{d}_1 \cdot \hat{r})\hat{r} \right] \quad (2.34)$$

Now using this and the relation

$$m_2 = \mu_0 M_2 V_2 = \mu_0 M_2 V_2 \hat{d}_2 \quad (2.35)$$

The interaction energy of the two dipoles m_1 and m_2 of equal magnitude is

$$E_{12} = -(m_2 \cdot H_1) \quad (2.36)$$

$$E_{12} = \frac{\mu_0 (M_1 V_1)(M_2 V_2)}{4\pi r^3} [\hat{d}_1 \cdot \hat{d}_2 - 3(\hat{d}_1 \cdot \hat{r})(\hat{d}_2 \cdot \hat{r})] \quad (2.37)$$

$$E_{12} = \frac{\mu_R \mu_o (MV)^2}{4\pi |r|^3} [(1 - 3\cos^2 \theta)] \quad (2.38)$$

Using the basic trigonometric identities

$$\cos \theta = \frac{A}{H} = \frac{r_0}{r} \quad (2.39)$$

$$\therefore \cos^2 \theta = \frac{r_0^2}{r^2} \quad (2.40)$$

$$\text{Where } r = \sqrt{r_0^2 + x^2} \quad (2.41)$$

This can be rewritten as

$$E_{12} = \frac{\mu_R \mu_o (MV)^2 \left[\left(1 - 3 \frac{r_o^2}{r_o^2 + x^2} \right) \right]}{4\pi (r_o^2 + x^2)^{3/2}} \quad (2.42)$$

and μ_R is the reduced material permeability.

2.1.3 MRE Chain Mechanics Model

Jolly [15] has modeled the shear stress of the chains caused by the interparticle force.

This method is referenced by Zhou [39] in his MR elastomer studies. By defining the

shear strain of the particle chain as $\varepsilon = x/r_o$ (and $r_o \cong L_o = 2\pi/q$)

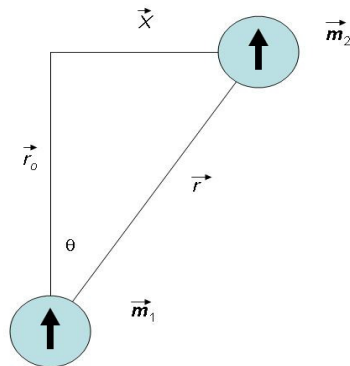


Fig. 2 Shear model for the magnetic interaction between two dipoles

Jolly has written the interaction energy as

$$E_{12} = \frac{\mu_o \mu_r (MV)^2 (\epsilon^2 - 2)}{4\pi |\epsilon^2 + 1|^{5/2}} \quad (2.43)$$

Assuming the composite solid consisting of many spherical particles embedded within a matrix, the total number of particles n , each having volume V_i , can be expressed as

$$n = \phi \frac{V_c}{V_i} = \phi \frac{6V_c}{\pi d^3} \quad (2.44)$$

where ϕ is the volume fraction of the particles in the composite, d is the particle diameter, and V_c is the total volume of the composite. Assuming that the magnetic interaction happens foremost between adjacent particles in a chain, the total energy density (energy per unit volume) can be calculated as

$$U = \frac{n}{V_c} E_{12} = \frac{3\phi \mu_r \mu_o (MV)^2 (\epsilon^2 - 2)}{2\pi^2 d^3 r_o^3 (1 + \epsilon^2)^{5/2}} \quad (2.45)$$

The stress induced by the application of a magnetic field can be computed by taking the derivative of the inter-particle energy density with respect to strain:

$$\sigma(\epsilon) = \frac{\partial U}{\partial \epsilon} = \frac{9\phi \mu_r \mu_o (MV)^2 \epsilon (4 - \epsilon^2)}{2\pi^2 d^3 r_o^3 (1 + \epsilon^2)^{7/2}} \quad (2.46)$$

$$\sigma(\varepsilon) = \left[\frac{9\phi\mu_R\mu_o(MV)^2}{2\pi^2 d^3 r_o^3} \right] \frac{\varepsilon(4 - \varepsilon^2)}{(1 + \varepsilon^2)^{7/2}} \quad (2.47)$$

Therefore

$$\sigma(\varepsilon) = \left[\frac{\phi\mu_R\mu_o M^2}{8h^3} \right] \frac{\varepsilon(4 - \varepsilon^2)}{(1 + \varepsilon^2)^{7/2}} \quad (2.48)$$

Defining $h = L_0/d$ where d is the particle diameter and L_0 the interparticle separation,

we can now write the expression for the stress as

$$\sigma(\varepsilon) = \left[\frac{\phi\mu_R\mu_o M^2}{8h^3} \right] \frac{\varepsilon(4 - \varepsilon^2)}{(1 + \varepsilon^2)^{7/2}} \quad (2.49)$$

A small strain approximation of this stress can be given by

$$\sigma(\varepsilon) \cong \left[\frac{\phi\mu_R\mu_o M^2}{2h^3} \right] \varepsilon \text{ for } (\varepsilon < 0.1) \quad (2.50)$$

For which a 3.6% error results when the strain equals 0.1. The modulus G of the particle network is simply the stress divided by the strain

$$G \cong \left[\frac{\phi \mu_r \mu_o M^2}{2h^3} \right] \quad (2.51)$$

The yield stress of a particle chain occurs at the strain for which the stress is a maximum.

This can be found by taking the first derivative of the stress in the chain to zero

$$\frac{\partial \sigma}{\partial \varepsilon} = \frac{\mu_o \mu_r (4\varepsilon^4 - 27\varepsilon^2 + 4) \phi M^2}{8h^3 (1 + \varepsilon^2)^{9/2}} = 0 \quad (2.52)$$

From which yield strain and corresponding yield stress can be found

$$\varepsilon_y = \frac{\sqrt{27 - \sqrt{665}}}{2^{2/3}} = 0.389 \quad (2.53)$$

$$\sigma_y = \frac{\mu_r \mu_o 0.1143 \phi M^2}{h^3} \quad (2.54)$$

A small strain approximation of the stress has been given as

$$\sigma \cong \frac{\mu_r \mu_o \phi \varepsilon M^2}{2h^3} \quad \text{for } \varepsilon < 0.1 \quad (2.55)$$

We can gain a first approximation to the local deformation mechanics by modeling the dynamics at the inclusion-matrix interface as a rigid sphere into an elastic half-space.

This is the classic Hertz elastic problem.

2.1.4 Hertz Indenter

The stresses and deflections arising from the contact of two elastic solids is referred to as the Hertz contact problem. The most well known scenario is that of contact between a rigid sphere and a flat surface. Landau and Lifshitz[19] have set forth a set of fundamental equations for solid bodies in contact. This is the basic principle of atomic force microscopy (AFM). In AFM a force is applied to a system such to bring a spherical microparticle in contact with an elastic substrate. When the particle is in contact with the elastic substrate, the relative displacement between the microparticle and the elastic substrate due to elastic deformation is measured. This principle is outlined by many works, including the Yang [38] study of the load-displacement relation. Recently, Rudnitsky[30] applied this tool by using dynamic indentation to determine the time-dependent viscoelastic properties of a polymeric material. Therefore, using this as motivation, we will now outline the Hertz problem and later use this force-displacement argument to classify the MRE length scale dependent forces.

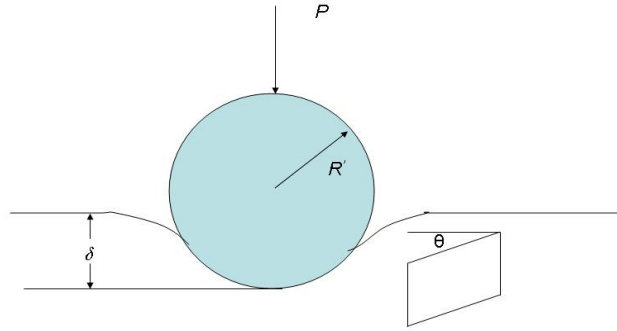


Fig. 3 Simple representation of a rigid spherical indenter with an illustration of the local shear deformation.

Hertz found that the radius of the circle of contact a , is related to the indenter load, P , the indenter radius R , and the elastic properties of the materials by

$$a^3 = \frac{4 kPR}{3 E} \quad (2.59)$$

where k is an elastic mismatch factor given by:

$$k = \frac{9}{16} \left[(1-\nu^2) + \frac{E}{E'} (1-\nu'^2) \right] \quad (2.60)$$

where E and ν are the Young's Modulus and Poisson's ratio of the specimen (unprimed) and indenter (primed). Hertz also found that the maximum tensile stress in the specimen occurs at the edge of the contact circle at the surface and is given by (see Fig.4).

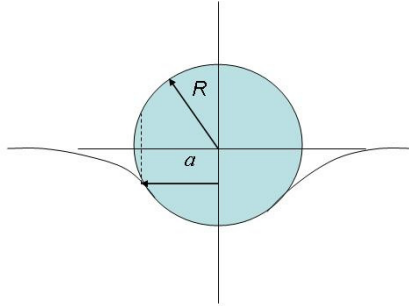


Fig. 4: Representation of the Hertz problem illustrating the difference between the indenter radius R and the contact radius a .

$$\sigma_{\max} = (1 - 2\nu) \frac{P}{2\pi a^2} \quad (2.61)$$

This stress, acting in a radial direction on the surface outside the indenter, decreases as the inverse of the square of the distance away from the center of contact. The maximum tensile stress outside the indenter can be expressed in terms of the indenter radius R

$$\sigma_{\max} = \left(\frac{(1 - 2\nu)P}{2\pi} \right) \left(\frac{3E}{4k} \right)^{2/3} P^{1/3} R^{-2/3} \quad (2.62)$$

The mean contact pressure, p_m , is given by the indenter load divided by the contact area, and it is a useful normalizing parameter which has the additional virtue of having actual physical significance.

$$p_m = \frac{P}{\pi a^2} \quad (2.63)$$

it can be shown that the contact area is proportional to $P^{2/3}$ and therefore p_m is proportional to $P^{1/3}$. This yields

$$p_m = \left(\frac{3E}{4\pi k} \right) \frac{a}{R} \quad (2.64)$$

The mean contact pressure may be referred to as the “indentation stress” and the quantity a/R the “indentation strain”.

If the contacting bodies are in frictionless contact, i.e. only normal pressure is transmitted between the indenter and the specimen, the pressure distribution is given by

$$\frac{\sigma_z}{p_m} = -\frac{3}{2} \left(1 - \frac{R^2}{a^2} \right)^{1/2} \quad (2.65)$$

Consider now the contact of a sphere of radius R' with elastic modulus E' and Poisson's ratio ν' in contact with a flat surface of a specimen. With no load applied, and with the indenter on the point making contact with the specimen, the distance from a point on the periphery of the indenter and the specimen surface is given by

$$\ell = \frac{r^2}{2R} \quad (2.66)$$

where R is the relative curvature of the indenter and the specimen given by

$$\frac{1}{R} = \frac{1}{R'} + \frac{1}{R_s} \quad (2.67)$$

If the load is applied to a flat surface ($R_s = \infty$) such that the point at which the load is applied moves a vertical distance δ . This distance is called the "load-point displacement", it is measured with respect to a distant point in the specimen and may be considered the distance of mutual approach between the indenter and the surface.

In general, both the indenter and the specimen undergo deformation. These deformations are shown by u_z' and u_z at some arbitrary point inside the contact circle for both the indenter and the specimen. The load-point displacement is given by $\delta = u_z' + u_z + \ell$.

If the indenter is perfectly rigid then $u'_z = 0$ and for both rigid and non-rigid indenters, $\ell = 0$ at $r = 0$ and thus the load-point displacement is given by $\delta = u'_z + u_z$. Hertz showed that a distribution of pressure of the form given for that of a sphere results in displacements of the specimen surface, for $r \leq a$

$$u_z = \frac{1-\nu^2}{E} \frac{3}{2} p_m \frac{\pi}{4a} (2a^2 - r^2) \quad r \leq a \quad (2.68)$$

And outside the contact circle $r > a$

$$u_z = \frac{1-\nu^2}{E} \frac{3}{2} p_m \frac{1}{2a} \left[(2a^2 - r^2) \sin^{-1} \frac{a}{r} + r^2 \frac{a}{r} \left(1 - \frac{a^2}{r^2} \right)^{1/2} \right] \quad (2.69)$$

After deformation, the contact surface lies in between the two original surfaces and is also part of a sphere whose radius depends on the relative radii of curvature of the two opposing surfaces and the elastic properties of the two contacting materials. For the special case of contact between a spherical indenter and a flat surface where the two materials have the same elastic properties, the radius of curvature of the contact surface is twice that of the radius of curvature of the indenter. The Hertz pressure distribution acts equally on both the surface of the specimen and the indenter, and the deflections of points on the surface of each are given by both

$$u_z = \frac{1-\nu^2}{E} \frac{3}{2} p_m \frac{\pi}{4a} (2a^2 - r^2) \quad r \leq a \quad (2.70)$$

and

$$u_z = \frac{1-\nu^2}{E} \frac{3}{2} p_m \frac{1}{2a} \left[(2a^2 - r^2) \sin^{-1} \frac{a}{r} + r^2 \frac{a}{r} \left(1 - \frac{a^2}{r^2} \right)^{1/2} \right] \quad (2.71)$$

The Hertz analysis approximates the curved surface of a sphere as a flat surface since the radius of curvature is assumed to be large in comparison to the area of contact. Thus for the general case of a non-rigid indenter and specimen yields

$$u'_z + u_z = \left(\frac{1-\nu'}{E'} + \frac{1-\nu}{E} \right) \frac{\pi}{4a} \frac{3}{2} p_m (2a^2 - r^2) \quad (2.72)$$

$$= \delta - \frac{r^2}{2R_x} \quad (2.73)$$

where R_x is the relative radius of curvature. By setting $r = a$ we can arrive at the Hertz equation and show that at $r = 0$ the distance of mutual approach δ between two distant points within the indenter and the specimen are given by

$$\delta^3 = \left(\frac{4k}{3E} \right)^2 \frac{P^2}{R_x} \quad (2.74)$$

When the indenter is perfectly rigid

$$k = \frac{9}{16}(1-\nu^2) \quad (2.75)$$

Therefore we can write the distance of mutual approach as

$$\delta^3 = \left(\frac{3(1-\nu^2)}{4E} \right)^2 \frac{P^2}{R_x} \quad (2.76)$$

or in terms of the shear modulus

$$\delta^3 = \left(\frac{3(1-\nu)}{8G} \right)^2 \frac{P^2}{R_x} \quad (2.77)$$

Therefore the force responsible for this displacement is written as

$$P = \frac{8G\sqrt{R_x}}{3(1-\nu)} \delta^{3/2} . \quad (2.78)$$

2.2 THEORETICAL BACKGROUND OF SMALL ANGLE SCATTERING, XPCS AND SPECKLE

2.2.1 Small Angle Scattering

Scattering techniques are used to investigate the structure, the organization and the dynamics of matter (e.g. polymers, colloids, micellar systems, aggregates, etc.), with

radiation such as neutrons, electrons, x-rays or light. In general, the specific properties of these sources and their interactions with matter allow for exploring a typical spatial scale from 1 to 20,000 nanometers and a typical dynamic range of seconds to picoseconds. A well collimated beam of radiation with wavelength λ and energy E is incident on a sample of thickness d . Most of the incident radiation is transmitted through the sample without any interaction and some small portion may be absorbed. Only a certain fraction of the incident beam is interacting with the sample and scattered at an angle $\theta > 0$. In general, there is also a non-zero momentum transfer between the sample and the incident beam. A scattering experiment is thus performed, by using some type of convenient detection device, measuring the scattered intensity I as a function of scattering angle θ at a distance L away from the sample and elevated above the incident beam axis by a scattering vector q (see Fig.5).

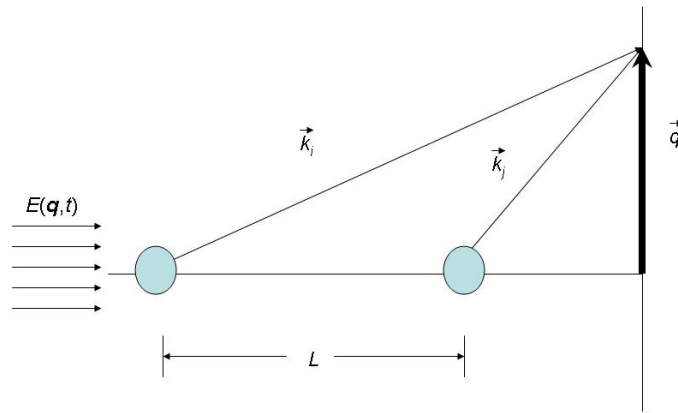


Fig. 5: A representation of the addition of two scattered waves coinciding at a given scattering vector q .

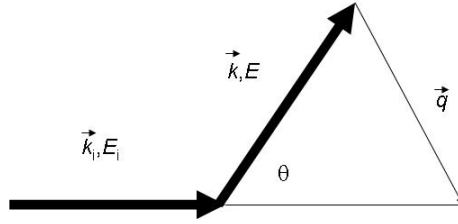


Fig. 6: Definition of the scattering vector q

$$|\vec{q}| = \frac{4\pi \sin(\theta/2)}{\lambda} = |\vec{k}_s - \vec{k}_i| \quad (2.78)$$

Where k_s and k_i are the incident and scattered wave. Substituting this into Bragg's Law of Diffraction

$$\lambda = 2d \sin(\theta/2) \quad (2.79)$$

yields an expression for a characteristic separation distance between scattering sites

$$q = \frac{2\pi}{L} \quad (2.80)$$

The intensity at each spot of the diffraction pattern is the result of interference of the light from many different points in the disordered materials. The essentially random path lengths of the light from these points to the given spot in the measured diffraction pattern leads to the light being the sum of rays with a random set of phases. However, since the light is coherent, the phase of the light, even though it is randomly distributed from point to point, has a definite value at each point. Where the phases add destructively results in a dark spot and where they add constructively, a bright spot appears.

2.2.2 XPCS

If two particles were to fluctuate in position, their interference pattern would also fluctuate. Intensity fluctuation spectroscopy is the technique of measuring these intensity fluctuations and relating them to the kinetics of the materials undergoing diffraction. This technique has been extended to x-rays [16]. X-rays have several advantages over light in that most media are transparent to x-rays, the problems of multiple scattering are not as pronounced or non-existent, and the shorter wavelengths probe smaller distances.

Recent experiments have demonstrated the potential of x-ray intensity-fluctuation spectroscopy (XIFS), which is also known as x-ray photon-correlation spectroscopy (XPCS), to become a powerful probe of sample dynamics at low frequencies ($<10^4$ Hz) and small-length-scales ($\leq 1\mu m$). For example, (XIFS) measurements have been made of the equilibrium dynamics of a binary alloy near critical point [36], of the Brownian motion of gold, palladium, and antimony oxide colloids diffusing in glycerol, and of the

equilibrium dynamics of block-copolymer micelles in a homopolymer matrix[22]. All of these measurements were performed in a regime of wave-vector and frequency space which is inaccessible to various other light, neutron, or x-ray scattering techniques.

2.2.3 Speckle

When coherent light is scattered from a disordered system it gives rise to a random diffraction or “speckle” pattern. Speckle patterns are well known from laser light scattering and are related to the exact special arrangement of the disorder. A speckle pattern can be interpreted as an instantaneous, diffraction limited structure factor

$$S_c(\vec{q}, t) = |A(\vec{q}, t)|^2 = \left| \int_C \rho(r) \exp(-i\vec{q} \cdot \vec{r}) \right|^2 \quad (2.81)$$

where $\rho(r)$ is the electron density and the integral is taken over the coherently illuminated volume $C = \xi_t^2 \cdot \xi_l$ of the sample. When the illuminated volume becomes comparable to the coherence lengths of the source the structure factor $S(\vec{q}, t)$ becomes sensitive to the individual realizations of the ensemble and thus sensitive to the exact atomic arrangement in the illuminated volume. If this spatial arrangement changes with time the corresponding speckle pattern also changes. The observation of intensity fluctuations of a single or equivalent speckle(s) is then a direct measure of the underlying dynamics. By using coherent x-rays, a Photon Correlation Spectroscopy (XPCS) measurement can

probe low frequency dynamics (10^6 Hz to 10^{-3} Hz) in opaque materials with atomic resolution (10^{-3} Å < $g < 1$ Å).

We can define the longitudinal coherence length as

$$\xi_l = \lambda^2 / (2\Delta\lambda) = c / (2\Delta\nu) \quad (2.82)$$

Note that this naturally leads to a definition for coherence time)

$$\tau_c = \xi_l / c = 1 / (2\Delta\nu). \quad (2.83)$$

There are also two transverse coherence lengths which determine approximately how far one must travel parallel to the wave fronts before the wave gets out of phase.

This corresponds to a time interval within which the phase of the wave in the propagation direction (longitudinal) remains within a range of $\pm \pi/2$. Most often, the primary source of this divergence is determined by the finite size of the source σ_s a distance R away.

This gives an equation for the transverse coherence length

$$\xi_t = \lambda R / (2\sigma_s) \quad (2.84)$$

A beam which is sufficiently monochromatic and has a transverse size comparable to its transverse coherence lengths is said to be coherent. When the dimensions of the beam are much larger than the coherence lengths the beam is said to be incoherent. Coherent

effects of the interaction of light with matter happen inside the light's coherence volume. Each coherent region will lead to a speckle pattern, and an image or diffraction pattern is then made up of the average over the sum of all these speckle patterns.

To be more quantitative we need to describe the electric field correlations. The mutual coherence function is described as:

$$\Gamma(\vec{r}_1, \vec{r}_2, \vec{t}_1, \vec{t}_2) = \langle E^*(\vec{r}_1, \vec{t}_1) E(\vec{r}_2, \vec{t}_2) \rangle \quad (2.85)$$

Where $E(\vec{r}, \vec{t})$ is the electric field. Here the averages can be considered either over the different coherence regions or over the distribution of random amplitudes and phases of the electromagnetic (EM) wave. Just as in statistical mechanics, by dealing with the correlation functions directly, the averaging necessary to handle the intrinsic randomness of the wave no longer needs to be explicitly taken care of. Usually the incident EM wave can be considered as having constant intensity and it makes sense to consider the randomness as stationary as this means that the correlation function depends only on the time difference $\tau = t_2 - t_1$. A normalized form of the correlation function, called the degree of coherence, is also useful and it is defined as:

$$\gamma(\vec{r}_1, \vec{r}_2, \tau) = \frac{\Gamma(\vec{r}_1, \vec{r}_2, \tau)}{\Gamma(\vec{r}_1, \vec{r}_1, 0)^{1/2} \Gamma(\vec{r}_2, \vec{r}_2, 0)^{1/2}} \quad (2.86)$$

Regions with $|\gamma| = 1$ can be considered perfectly coherent and those with $|\gamma| = 0$ are incoherent. As is seen from the definition $\Gamma(\vec{r}_1, \vec{r}_2, t_1, t_2)$ is just the intensity of the light at point (\vec{r}, t) .

One can write a similar set of definitions as functions of frequency instead of time. Convention has developed to give the frequency dependent terms different names. Thus the cross-spectral density is the Fourier transform of the mutual coherence function (assumed stationary)

$$W(\vec{r}_1, \vec{r}_2, \nu) = \int_{-\infty}^{\infty} \Gamma(\vec{r}_1, \vec{r}_2, \tau) \exp(i2\pi\nu\tau) d\tau \quad (2.87)$$

and the frequency spectrum of the light $H(\vec{r}, \nu)$ is seen to be $W(\vec{r}_1, \vec{r}_2, \tau)$. The corresponding spectral degree of coherence is:

$$\mu(\vec{r}_1, \vec{r}_2, \nu) = \frac{W(\vec{r}_1, \vec{r}_2, \nu)}{W(\vec{r}_1, \vec{r}_1, \nu)^{1/2} W(\vec{r}_2, \vec{r}_2, \nu)^{1/2}} \quad (2.88)$$

Finally, one can see the relationship of $W(\vec{r}_1, \vec{r}_2, \nu)$ to correlations in the frequency dependent electric fields:

$$\langle E^*(\vec{r}_1, \nu_1) E(\vec{r}_2, \nu_2) \rangle = W(\vec{r}_1, \vec{r}_2, \nu) \delta(\nu_1 - \nu_2) \quad (2.89)$$

Often it is a good approximation to assume that the spatially dependent and frequency (and hence time) dependent parts factor. This is labeled as cross-spectral purity and

implies that the frequency spectrum of the wave is independent of the position in the beam.

In optics, problems in diffraction and interference are often treated by the Huygens principle. This states that wave propagation problems can be treated by imaging the wavefronts as composed of point sources, each of which generates spherical waves. Propagating these spherical waves in a Huygens construction can explain most diffraction effects.

A convenient starting point for the calculations involving coherence is the Huygens-Fresnel principle. The integral form for the solution for to the wave equation states that each point in the wavefront can be considered as a point source of spherical waves which, when added coherently, give the resulting propagation of the wave. Using this principle and the above definitions, one can see how the mutual coherence function or the cross-spectral density can be propagated from one surface S of the wavefront to another. An example of such an equation has been given as [42]:

$$W(\vec{r}_1, \vec{r}_2, \nu) = \iint_S \iint_S W(\vec{r}_1', \vec{r}_2', \nu) \frac{\exp(ik(R_2 - R_1))}{R_1 R_2} \Lambda_1^*(k) \Lambda_2(k) d^2 \vec{r}_1' d^2 \vec{r}_2' \quad (2.90)$$

where R_i are the distances between points \vec{r}_i and \vec{r}_i' and the $\Lambda_i(k)$ are the inclination factors which arise in the Huygens-Fresnel principle. For highly directional beams they are simply $ik/2\pi$.

To help make the above definitions and expressions more concrete it is worthwhile to calculate the cross-spectral density for two arbitrary points distant from an incoherent source. One can argue that the cross-spectral density at an incoherent source with intensity distribution $I(\vec{r}_1)$ and frequency spectrum $H(\nu)$ should have the form:

$$W(\vec{r}_1, \vec{r}_2, \nu) = I(r)H(\nu)\kappa_o\delta(\vec{r}_2 - \vec{r}_1). \quad (2.91)$$

The constant κ_o has dimensions of a length squared in order to compensate for the implied dimensions of the two dimensional delta function defined on the surface S and is equal to λ^2/π .

This function has the properties that any two distinct points in the source are uncorrelated and give the correct relation between the intensity and the cross-spectral density when $\vec{r}_1 = \vec{r}_2$. This gives:

$$W(\vec{r}_1, \vec{r}_2, \nu) = \kappa_o H(\nu) \left(\frac{k}{2\pi} \right)^2 \int_S I(\vec{r}') \frac{\exp(ik(R_2 - R_1))}{R_1 R_2} d^2 \vec{r}' \quad (2.92)$$

$$= H(\nu) \frac{\exp(ik(r_2 - r_1))}{\pi r_1 r_2} \int_S I(\vec{r}') \exp(ik(\hat{s}_2 - \hat{s}_1) \cdot \vec{r}') d^2 \vec{r}' \quad (2.93)$$

where the last line is obtained by defining the unit vectors $\hat{s}_i = \vec{r}_i/r_i$ and using the far field limit so $R_i \approx r_i - \hat{s}_i \cdot \vec{r}'$.

For synchrotron radiation, the intensity distribution is often described as the product of a Gaussian distribution in the vertical position y and one in the horizontal position x ,

$$I(x, y) = \frac{I_o}{2\pi\sigma_h\sigma_v} e^{-\left(\frac{x^2}{2\sigma_h^2} + \frac{y^2}{2\sigma_v^2}\right)} \quad (2.94)$$

With this definition $I_o H(\nu)$ is just the integrated number of photons per second at frequency ν in the source. One can then perform all the integrals to arrive at the cross-spectral density for a plane at a distance z from the source (using $\vec{r}_i = (x_i, y_i, z)$)

$$W(x_1, y_1, x_2, y_2, \nu) = \frac{I_o H(\nu)}{\pi} \frac{e^{i\psi} e^{-\left(\frac{(x_2-x_1)^2}{2\xi_h^2} + \frac{(y_2-y_1)^2}{2\xi_v^2}\right)}}{z^2} \quad (2.95)$$

where the transverse coherence lengths are defined as

$$\xi_i = \frac{z}{k\sigma_i} = \frac{\lambda z}{2\pi\sigma_i} \quad (2.96)$$

and the phase factor is $\psi = \frac{k}{2z} [(x_2^2 + y_2^2) - (x_1^2 + y_1^2)]$. The equation for

$W(x_1, y_1, x_2, y_2, \nu)$ is the primary result of this section and will be used to calculate partial coherence effects on diffraction. It shows explicitly that the transverse coherence dimensions are functions of the source dimensions, the distance and wavelength. It is informative to write this as

$$\left(\frac{\sigma_i}{z}\right)\xi_i = \lambda/2\pi \quad (2.97)$$

which relates the angular size of the source σ_i/z to the coherence length ξ_i and is similar to the angle-position uncertainty relation. Angle and position are the appropriate phase space variables for propagating waves and the phase space density of a coherent wave is $\lambda/2\pi$.

Typically, the frequency spectrum is quasi-monochromatic so that the frequency spectrum is peaked near a central frequency, $\nu_o = \omega_o/2\pi$, with a width, $\delta\nu$. This frequency spread determines the longitudinal coherence length which will be proportional to $c/\delta\nu$ where c is the speed of light. We will use the Lorentzian frequency distribution

$$H(\nu) = \frac{1}{1 + \left(\frac{\nu - \nu_o}{\delta\nu} \right)^2} \quad (2.98)$$

This leads to an exponential time correlation

$$\tilde{H}(\tau) = e^{-\left(\frac{|\tau|}{\tau_{cor}}\right)} e^{i2\pi\nu_o t} \quad (2.99)$$

Where the correlation time is defined as $\tau_{cor} = 1/2\pi\delta\nu$ and the full width at half maximum (FWHM) of the power spectrum is $2\delta\nu$. It follows for a Lorentzian spectrum that the longitudinal coherence length can be defined as $\xi_l = c\tau_{cor} = (k\Delta\lambda/2\lambda)^{-1}$, i.e., $\xi_l = (\lambda/\pi)(E/\Delta E)$, where ΔE is the FWHM of the energy spectrum.

Phase space arguments relate the angular spread of the beam to the coherence length, but the above calculation only uses the angular size of the source and not the angular collimation of synchrotron sources.

One would expect that high collimation would be the result of increased coherence and this is indeed found to be so. A phase space description of synchrotron radiation is based on giving intensity as a function of direction and position over cross-sections of the beam. This double distribution is called the spectral brightness. Usually a cross-section of the beam intersecting a plane at a distance z is used but any surface through which the beam passes would work. For a certain class of sources there is a simple direct relation between the brightness and the cross-spectral density. Just as the time dependence of the coherence is often only a function of the time difference (stationarity) the degree of coherence is often a function of the separation of the two spatial arguments (homogeneity).

Such sources are often called Schell-model sources [19]. Furthermore, it often happens that coherence is more sharply peaked than the intensity distribution of the light. This implies the following form of the cross-spectral density:

$$W(\vec{r}_1, \vec{r}_2, \nu) = I \left(\frac{\vec{r}_1 + \vec{r}_2}{2} \right) H(\nu) \mu(\vec{r}_2 - \vec{r}_1) \quad (2.100)$$

Sources with this factored form are called quasi-homogeneous and for these sources, the brightness is related to the Fourier transform of the coherence as

$$B(\vec{r}, \hat{s}, \nu) = k^2 I(\vec{r}) H(\nu) \frac{1}{(2\pi)^2} \int \mu(\vec{u}) \exp(ik\hat{s}_\perp \cdot \vec{u}) d\vec{u} \quad (2.101)$$

Where \hat{s} is a unit vector specifying the direction and \hat{s}_\perp the part of \hat{s} in the plane upon which the brightness is defined. From this equation one can see that the information content of the cross-spectral density is as complete as the phase space description. Assuming Gaussian forms for the partial coherence a natural cross-spectral density of a synchrotron source is:

$$W(\vec{r}_1, \vec{r}_2, \nu) = \frac{I_o H(\nu)}{2\pi\sigma_h\sigma_v} \exp\left(-\left(\frac{(x_1+x_2)^2}{8\sigma_h^2} + \frac{(y_1+y_2)^2}{8\sigma_v^2}\right)\right) \exp\left(-\left(\frac{(x_2-x_1)^2}{2\rho_h^2} + \frac{(y_2-y_1)^2}{2\rho_v^2}\right)\right) \quad (2.102)$$

with coherence lengths ρ_i and source sizes σ_i . Thus, after integration

$$B(\vec{r}, \hat{s}, \nu) = \left(\frac{k}{2\pi}\right)^2 I_o H(\nu) \frac{\rho_h\rho_v}{\sigma_h\sigma_v} \exp\left(-\left(\frac{x^2}{2\sigma_h^2} + \frac{y^2}{2\sigma_v^2}\right)\right) \exp\left(-\left(\frac{(k\rho_h s_x)^2}{2} + \frac{(k\rho_v s_y)^2}{2}\right)\right) \quad (2.103)$$

$$= \frac{1}{4\pi^2} \frac{I_o H(\nu)}{\sigma_{s_h} \sigma_{s_y} \sigma_h \sigma_v} \exp\left(-\left(\frac{x^2}{2\sigma_h^2} + \frac{y^2}{2\sigma_v^2}\right)\right) \exp\left(-\left(\frac{s_x^2}{2\sigma_{s_h}} + \frac{s_y^2}{2\sigma_{s_y}}\right)\right) \quad (2.104)$$

which has the usual Gaussian form often given for synchrotron radiation. The angular spreads σ_{s_i} of the synchrotron source are seen to be related to the intrinsic coherence

lengths, ρ_i , by $\sigma_{s_i} = 1/(k\rho_i)$. Note that in the paraxial limit x and $y \ll z$ and

$$\hat{s} = (s_x, s_y, 1) = (x/z, y/z, 1).$$

The cross-spectral density at a distance z as implied above

$$\begin{aligned} W(x_1, y_1, x_2, y_2, z, \nu) = & \frac{I_o H(\nu)}{2\pi\Delta_h\Delta_v} \exp\left(-\frac{(x_1+x_2)^2}{8(\sigma_h\Delta_h)^2}\right) \exp\left(-\frac{(x_2-x_1)^2}{2(\delta_h\Delta_h)^2}\right) \exp\left(-\frac{ik(x_2^2-x_1^2)}{R_h}\right) \\ & \exp\left(-\frac{(y_1+y_2)^2}{8(\sigma_v\Delta_v)^2}\right) \exp\left(-\frac{(y_2-y_1)^2}{2(\delta_v\Delta_v)^2}\right) \exp\left(-\frac{ik(y_2^2-y_1^2)}{R_v}\right) \end{aligned} \quad (2.105)$$

where we have defined (subscript i represents either v or h):

$$r = (x_i, y_i, z_i), \quad (2.106)$$

$$\delta = \frac{2\sigma_i\rho_i}{\sqrt{(2\sigma_i)^2 + \rho_i^2}} \quad (2.107)$$

$$\Delta_i = \sqrt{1 + \left(\frac{z}{k\sigma_i\delta_i}\right)^2} \quad (2.108)$$

and

$$R_i = z \left[1 + \left(\frac{k\sigma_i\delta_i}{z}\right)^2 \right] \quad (2.109)$$

This form shows how both the beam size and the coherence lengths grow with distance from the source. The phase factors in the above form (the complex exponentials) are related to the curvature of the spherical wavefronts intersected by a plane. By inspection of these equations, it is seen that the transverse coherence lengths of the synchrotron begin at δ_i and at large distances grows linearly with distance. Typically the coherence lengths are much smaller than the source dimensions and so $\delta_i = \rho_i$. From this form for $W(x_1, y_1, x_2, y_2, z, \nu)$ we find $\Gamma(x_1, y_1, x_2, y_2, z, t_2 - t_1)$.

2.3 DYNAMIC LIGHT SCATTERING

2.3.1 The Intensity and Electric Field Autocorrelation Functions $g^{(2)}$ and $g^{(1)}$

To investigate the properties of the scattered light field from a field of identical spherical scatterers, we write the general expression for the instantaneous amplitude of the field $E(\mathbf{q}, t)$ scattered by N particles to a point in the far field

$$E(\mathbf{q}, t) = -E_o \frac{\exp[i(kR - t)]}{R} \sum_{j=1}^N b_j(\vec{q}, t) \exp[-i\vec{q} \cdot \vec{R}_j(t)] \quad (2.110)$$

Here q is the scattering vector, $b_j(q, t)$ is the time-dependent amplitude of the field scattered by particle j , and $R_j(t)$ is the position of the center of mass of particle j at time t . For identical spherical particles all $\{b_j(q, t)\}$ have the same time-independent value $b(q)$

and can therefore be taken out of the sum. Dynamic light scattering deals with normalized quantities, thus we can omit the pre-factors

$$-E_o \frac{\exp[i(kR - t)]}{R} \quad (2.111)$$

and can write

$$E(q, t) = \sum_{j=1}^N \exp[-i\vec{q} \cdot \vec{R}_j(t)] \quad (2.112)$$

Each of the phase factors $\exp[-i\vec{q} \cdot \vec{R}_j(t)]$ can be represented by unit vectors in the complex plane making an angle $\vec{q} \cdot \vec{R}_j$ with the real axis.

The average value of the scattered field is

$$\langle E(q, t) \rangle = \sum_{j=1}^N \langle \exp[-i\vec{q} \cdot \vec{R}_j(t)] \rangle = \sum_{j=1}^N [\langle \cos(\vec{q} \cdot \vec{R}_j(t)) \rangle - i \langle \sin(\vec{q} \cdot \vec{R}_j(t)) \rangle] = 0 \quad (2.113)$$

since the phase angles are uniformly distributed between 0 and 2π . The average of the scattered intensity is

$$\langle I(q, t) \rangle = \langle |E(q, t)|^2 \rangle = \sum_{j=1}^N \sum_{k=1}^N \langle \exp\{-i\vec{q} \cdot [\vec{R}_j(t) - \vec{R}_k(t)]\} \rangle \quad (2.114)$$

$$= \sum_j 1 + \sum_{j \neq k} \langle \exp[-i\vec{q} \cdot \vec{R}_j(t)] \rangle \langle \exp[i\vec{q} \cdot \vec{R}_k(t)] \rangle \quad (2.115)$$

$$= N \quad (2.116)$$

The observed time correlation function is a light intensity autocorrelation function as follows:

$$G^{(2)}(t) = \langle I(0)I(t) \rangle \quad (2.117)$$

An electric field autocorrelation function is

$$G^{(1)}(t) = \langle E^*(t)E(0) \rangle \quad (2.118)$$

where $E^*(t)$ is the complex conjugate of electric field $E(t)$. By introducing normalized autocorrelation functions of

$$g^{(1)}(t) \equiv \frac{G^{(1)}(t)}{\langle I \rangle} \quad (2.119)$$

and

$$g^{(2)}(t) \equiv \frac{G^{(2)}(t)}{\langle I \rangle^2} \quad (2.120)$$

Where we can now write the following relationship between the first order (electric field) autocorrelation function $g^{(1)}(t)$ (a Fourier transform of the spectrum)

$$g^{(1)}(t) = N^{-1} \sum_j \langle \exp\{-iq \cdot [R_j(0) - R_j(\tau)]\} \rangle \quad (2.121)$$

$$= \langle \exp\{-iq \cdot [R(0) - R(\tau)]\} \rangle \quad (2.122)$$

The last step follows from the fact that the average motions of identical particles are themselves the same.

As previously mentioned, dynamic light scattering measures directly the time correlation function of the scattered intensity

$$\langle I(q,0)I(q,\tau) \rangle = \left\langle \sum_{j=1}^N \sum_{k=1}^N \exp\{-iq \cdot [R_j(0) - R_k(0)]\} \sum_{l=1}^N \sum_{m=1}^N \exp\{-iq \cdot [R_l(0) - R_m(0)]\} \right\rangle \quad (2.123)$$

$$= \left\langle \sum_j \sum_k \sum_l \sum_m \langle \exp\{-iq \cdot [R_j(0) - R_k(0) + R_l(\tau) - R_m(\tau)]\} \rangle \right\rangle \quad (2.124)$$

this can be factored...

$$\langle I(q,0)I(q,\tau) \rangle = \sum_j 1 \sum_l 1 + \sum_j \langle \exp\{-iq \cdot [R_j(0) - R_j(\tau)]\} \rangle \sum_k \langle \exp\{iq \cdot [R_k(0) - R_k(\tau)]\} \rangle \quad (2.125)$$

$$= N^2 + N^2 \left| \langle \exp\{-iq \cdot [R(0) - R(\tau)]\} \rangle \right|^2 \quad (2.126)$$

By defining the normalized time correlation function of the scattered intensity by

$$g^{(2)}(t) \equiv \frac{G^{(2)}(t)}{\langle I \rangle^2} \quad (2.127)$$

where

$$G^{(2)}(t) = \langle I(q,0)I(q,\tau) \rangle \quad (2.128)$$

$$G^{(2)}(t) = N^2 + N^2 \left| \langle \exp\{-iq \cdot [R(0) - R(\tau)]\} \rangle \right|^2 \quad (2.129)$$

therefore

$$g^{(2)}(t) = \frac{G^{(2)}(t)}{\langle I \rangle^2} \quad (2.130)$$

$$= \frac{N^2 + N^2 \left| \langle \exp\{-iq \cdot [R(0) - R(\tau)]\} \rangle \right|^2}{N^2} \quad (2.131)$$

$$= \frac{N^2}{N^2} + \frac{N^2 \left| \langle \exp\{-iq \cdot [R(0) - R(\tau)]\} \rangle \right|^2}{N^2} \quad (2.132)$$

and the second order (intensity) autocorrelation function $g^{(2)}(t)$ can now be given by the Siegert relation:

$$g^{(2)} = 1 + A[g^{(1)}(t)]^2 \quad (2.133)$$

In an ideal apparatus, the constant A , often called the ‘speckle contrast’, determined largely by the size of the detection aperture in the experiment optics, is equal to 1, so that, in such a case, the normalized intensity autocorrelation function starts at a value of 2 at time equals zero and eventually decays to 1. This is shown as follows:

In a dynamic light scattering experiment a detector reads the intensity of light scattered from a given sample volume. The qualitative features of light scattering by ergodic and non-ergodic media can be described in simple terms. The amplitude of the scattered light field $E(q, t)$ at a time t scattered to a point in the far field associated with a scattering vector q . If it is assumed that the scattering volume contains many uncorrelated regions then $E(q, t)$, sampled over the full ensemble, is a zero-mean complex Gaussian variable. The intensity of the scattered light is

$$I(q, t) \equiv |E(q, t)|^2 \quad (2.134)$$

This intensity is considered to be an ensemble average of scattered intensities I at a given scattering vector q from sub-ensembles $\{m\}_p$. First let us assume that the medium is completely rigid so that no motion of the scatterers is possible. Then the intensity $I_p(q, t)$ of the light scattered by a particular volume V in configuration p , viewed as a function of the scattering vector q , constitutes a non-fluctuating random Gaussian speckle

pattern. If the intensity at a particular point in the pattern is constant in time (no scatterer motion) then

$$I_p(q, t) = I_p(q). \quad (2.135)$$

Then, if one were to measure by dynamic light scattering the normalized intensity correlation function, one would obtain:

$$\frac{\langle I_p(q, 0) I_p(q, t) \rangle_T}{\langle I_p(q) \rangle_T^2} = \frac{I_p^2(q)}{I_p^2(q)} = 1 \quad (2.136)$$

graphically represented in Figure 7:

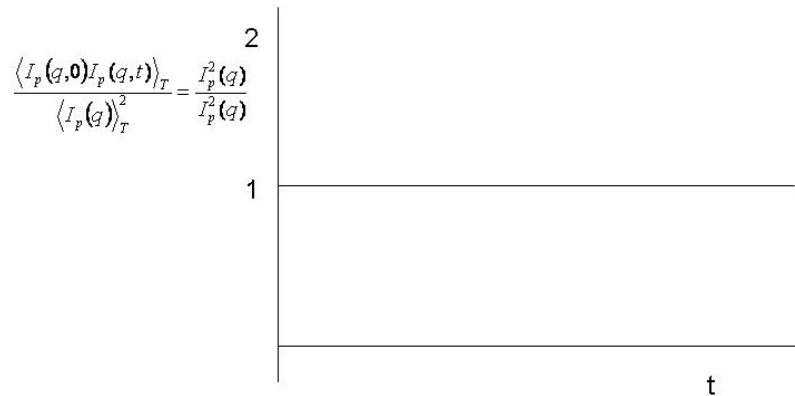


Fig. 7: The normalized time-averaged intensity correlation function for a localized sub ensemble

If the sample is moved so that a different volume is illuminated the detector will measure a different intensity $I_p(q, t)$. Clearly the normalized correlation function of this intensity will also have the value of 1. On the other hand, if one were to combine the time averaged intensities and the un-normalized ICF's, measured in series, $p=1$ to P , of differing scattering volumes, one would obtain for the normalized ensemble-averaged intensity correlation function

$$\frac{\langle\langle I_p(q,0)I_p(q,t) \rangle\rangle_T \rangle_E}{\langle\langle I_p(q) \rangle\rangle_T \rangle_E} \equiv \frac{\frac{1}{P} \sum_P I_p^2(q)}{\left[\frac{1}{P} \sum_P I_p(q) \right]^2} = \frac{\langle I^2(q) \rangle_E}{\langle I(q) \rangle_E^2} = 2 \quad (2.137)$$

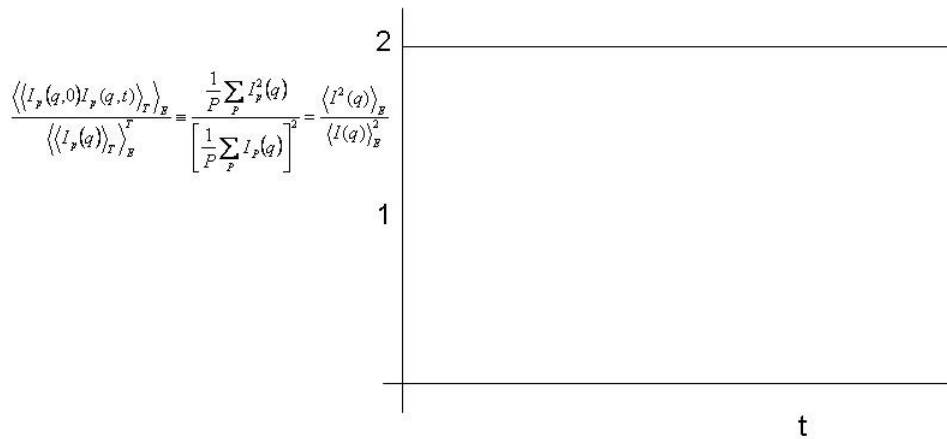


Fig.8: The normalized ensemble-averaged intensity correlation function

Now consider the case of an ergodic medium. As the scatterers move the intensity at a point in the speckle pattern will fluctuate in time. Furthermore, in time a representative fraction of all possible configurations will be sampled so therefore the speckle pattern

will undergo the full range of Gaussian fluctuations. Here, the value of 2 results from the zero-mean Gaussian statistical properties of $E(q,t)$. When the decay time $t = 0$, the normalized ICF has the Gaussian value of 2

$$\lim_{t \rightarrow 0} \frac{\langle I(q,t)I(q,0) \rangle_E}{\langle I(q) \rangle_E^2} = \frac{\langle I^2(q) \rangle_E}{\langle I(q) \rangle_E^2} = 2 \quad (2.138)$$

And as $t \rightarrow \infty$, $I(q,t)$ and $I(q,0)$ become uncorrelated such that

$$\lim_{t \rightarrow \infty} \frac{\langle I(q,t)I(q,0) \rangle_E}{\langle I(q) \rangle_E^2} = \frac{\langle I^2(q) \rangle_E}{\langle I(q) \rangle_E^2} = 1 \quad (2.139)$$

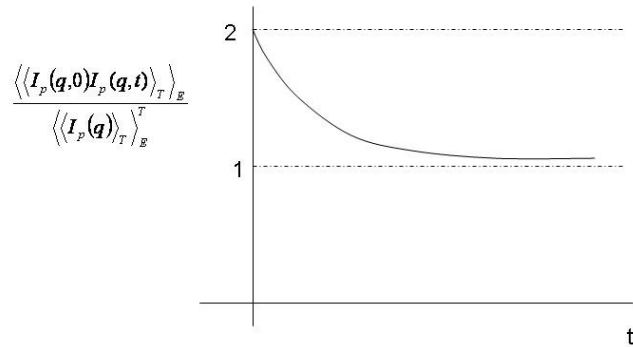


Fig.9: The ensemble averaged intensity correlation function as a function of time.

The decay of the ICF between these limits is determined by the nature of the motion of the scatterers.

Now consider the case of a non-ergodic medium where the motion is limited about a set of fixed positions. As the scatterers move, the intensity $I(q,t)$ at a point in the speckle pattern will fluctuate in time. Now the light scattered by a particular scattering volume will constitute a speckle pattern that is composed of both fluctuating and non-fluctuating components.

$$\langle I \rangle_T = \langle I_S \rangle_T + \langle I_D \rangle_T \quad (2.140)$$

Whereas $\langle I_S \rangle_T$ is related to the frozen-in static component and varies with position, $\langle I_D \rangle_T$ is related to the mobile dynamic component so that so that it is independent of the sample position. Because we are looking at the relaxation dynamics, we can model the MRE as an ergodic system concentrating on $\langle I_D \rangle_T$ and setting $\langle I_S \rangle_T = 0$. $g^{(2)}(q,t)$ is related to the normalized electric-field autocorrelation function $g_E^{(1)}(q,t)$

$$g_E^{(1)}(q,t) \equiv \frac{\langle E(q,t)E(q,0) \rangle_E}{\langle E(q) \rangle_E^2} \quad (2.141)$$

via the Siegert relation

$$g^{(2)}(q,t) = 1 + A[g_E^{(1)}(q,t)]^2 \quad (2.142)$$

A is a positive optical experimental constant less than 1 and is referred to as the speckle contrast.

By using the earlier definitions for the upper and lower limits on the intensity correlation function, we can define the data in our experiment by

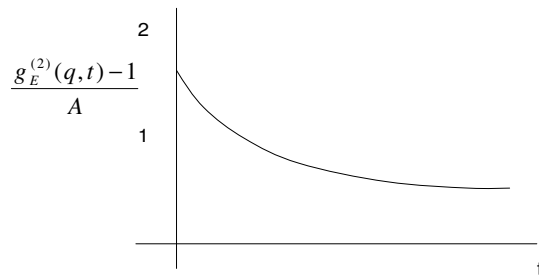


Fig.10: A representation of the electric field correlation function, $[g_E^{(1)}(t)]^2$, versus time via the Siegert relation.

$$0 \leq \left[\frac{g_E^{(2)}(q,t) - 1}{A} \right] \leq 2$$

The electric field correlation function $g^{(1)}(q,t)$ is frequently called the ‘measured intermediate scattering function’ $f^M(q,t)$ i.e.

$$f^M(q,t) \equiv g^{(1)}(q,t) \quad (2.143)$$

For identical interacting spheres $[all\{b_j(q,t)\}=b(q)]$ this becomes

$$f^M(q,t) \equiv f(q,t) \equiv \frac{F(q,t)}{S(q)} \quad (2.144)$$

where $F(q,t)$ is defined as the “dynamic structure factor” and is defined as

$$F(q,t) = N^{-1} \sum_j \sum_k \langle \exp[-iq \cdot [R_j(0) - R_k(t)]] \rangle \quad (2.145)$$

and $S(q) = F(q,0)$ is defined as the static structure factor

$$S(q) = \sum_j \sum_k \langle b_j(q) b_k^*(q) \exp[-iq \cdot [R_j(0) - R_k(0)]] \rangle \quad (2.146)$$

in the absence of interactions, the cross-terms $j \neq k$ vanish to give

$$S(q) \cong 1 \quad (2.147)$$

The expression for the dynamic structure factor

$$F(q, t) = \exp\langle -iq \bullet [R_j(0) - R_k(t)] \rangle \quad (2.148)$$

can be re-written for one dimension as

$$F(q, t) = \exp\langle -iq \bullet \Delta\vec{x}(t) \rangle \quad (2.149)$$

where $\Delta\vec{x}$ is a single Cartesian component of the particle displacement. If $\Delta\vec{x}$ is assumed to be a Gaussian random variable then dynamic light scattering gives a direct measurement of the particle mean square displacement as

$$F(q, t) = \exp(-q^2 \langle \Delta\vec{x}^2(t) \rangle) \quad (2.150)$$

and the Siegert relation is shown to decay exponentially.

The mean square displacement $\langle \Delta x^2(t) \rangle$ of the ferrous filler in the MRE under influence of an external magnetic field can be examined using the analogy of the simple physical picture of the scattering from colloidal gels. Using the fundamental relation of $q = 2\pi/L_0$ we can write the dynamic structure factor as a function of the average relative length changes

$$q^2 \langle \Delta x^2 \rangle = 4\pi^2 \left(\frac{\langle \Delta x(q, t) \rangle}{L_o} \right)^2 \quad (2.151)$$

therefore

$$f(q, t) = \exp \left(-4\pi^2 \left(\frac{\langle \Delta x(q, t) \rangle}{L_o} \right)^2 \right) \quad (2.152)$$

For monodisperse particles in a dilute solution, we may view the motion of the particles with a given relaxation coefficient (denoted by Γ) as contributing its own exponential to the first order correlation function such that

$$g^{(1)}(t) = \sum_i A_i \exp(-\Gamma_i t) \quad (2.153)$$

Where Γ_i is the reciprocal decay time and A_i is a weighting factor proportional to the fraction of the scattered intensity contributed by this subset of particles. It has been experimentally shown by several authors [29] [18] [8] that for these types of systems

$$\Gamma = Dq^2 \quad (2.154)$$

D is the diffusion coefficient of the particles and q is the magnitude of the scattering wave vector. Hansen has mathematically derived the diffusion coefficient for single particle motion using the velocity autocorrelation function. For identical scatterers

(colloids or polymers) D has been identified as a q -dependent collective diffusion coefficient which, in the limit $q \rightarrow 0$, is equal to the gradient diffusion coefficient.

2.3.2 Method of Cumulants

We have previously shown the first order time correlation function is now a sum of exponentials. The correlation function of the light scattered by this type of colloidal system lends itself to an analysis in terms of moments and cumulants. The formal correspondence between the form of the correlation function given above and the moment generating function is:

$$M(\tau, \Gamma) \equiv \langle \exp(-\Gamma t) \rangle_{av} \quad (2.155)$$

$$= |g^{(1)}(t)| \quad (2.156)$$

$\langle \exp(-\Gamma t) \rangle_{av}$ here signifies an average over Γ , weighted by the distribution function $G(\Gamma)$. The moments of the distribution are related to the derivatives of $M(t, \Gamma)$ with respect to t .

One can also define the cumulant generating function as the natural logarithm of the moment generating function

$$\ln[M(t, \Gamma)] = \ln[g^{(1)}(t)] = \sum_n \frac{K_n (-t)^n}{n!} \quad (2.157)$$

Therefore, one technique for characterizing this sum of exponentials is the method of cumulants. In the cumulants method, the logarithm of the normalized correlation function $g^{(1)}(t)$ is expanded as a power series in time

$$\ln(\sqrt{g^{(2)} - 1}) = \ln[g^{(1)}(t)] \quad (2.158)$$

$$\ln[g^{(1)}(t)] = \sum_n \frac{K_n (-t)^n}{n!} \quad (2.159)$$

In macromolecular and colloidal systems, the forces constraining the scatterers are usually weak and their motions can be described by coupled over-damped Langevin equations or the many-body diffusion, Smoluchowski, equation. Then on short-time scales, expansion of the dynamic structure factor can be written as

$$\ln(f(q, t)) \rightarrow \sum_n \frac{K_n (-t)^n}{n!} \quad (2.161)$$

Thus

$$K_1 = -\lim_{t \rightarrow 0} \frac{d}{dt} \ln \left[\frac{F(q, t)}{S(q)} \right] \quad (2.162)$$

$$= -\lim_{t \rightarrow 0} \frac{1}{S(q)} \frac{dF(q,t)}{dt} \quad (2.163)$$

and

$$K_2 = -\lim_{t \rightarrow 0} \frac{d^2}{dt^2} \ln \left[\frac{F(q,t)}{S(q)} \right] \quad (2.164)$$

$$= -\lim_{t \rightarrow 0} \left\{ \frac{1}{S(q)} \frac{d^2 F(q,t)}{dt^2} - \frac{1}{[S(q)^2]} \left[\frac{dF(q,t)}{dt} \right]^2 \right\} \quad (2.165)$$

Recalling

$$g^{(1)}(q,t) \equiv \frac{F(q,t)}{S(q)} \quad (2.166)$$

and the definition

$$F(q,t) \equiv N^{-1} \sum_i^N \sum_j^N \left\langle \exp[i\vec{q} \cdot (\vec{r}_i(t) - \vec{r}_j(t + \tau))] \right\rangle. \quad (2.167)$$

We are interested in the initial time dependence of $F(q,t)$, we differentiate with respect to the delay time τ :

$$\frac{dF}{d\tau} = -iqN^{-1} \sum_i^N \sum_j^N \left\langle V_j(t+\tau) \exp[i\vec{q} \cdot (\vec{r}_i(t) - \vec{r}_j(t+\tau))] \right\rangle \quad (2.168)$$

this is rearranged using the stationarity condition

$$\frac{dF}{dt} \equiv 0 = iqN^{-1} \sum_i^N \sum_j^N \left\langle (V_i(t) - V_j(t+\tau)) \exp[i\vec{q} \cdot (\vec{r}_i(t) - \vec{r}_j(t+\tau))] \right\rangle \quad (2.169)$$

to give,

$$K_2 = \lim_{t \rightarrow 0} \left\{ \frac{1}{S(q)} \frac{d^2 F(q,t)}{dt^2} - \frac{1}{[S(q)]^2} \left[\frac{dF(q,t)}{dt} \right]^2 \right\} \quad (2.170)$$

the identity

$$r_j(t+\tau) = r_j(t) + \int_t^{t+\tau} V_j(t') dt' \quad (2.171)$$

leads to

$$\frac{dF}{d\tau} = -iqN^{-1} \sum_i^N \sum_j^N \left\langle V_i(t) \exp[i\vec{q} \cdot (\vec{r}_i(t) - \vec{r}_j(t))] \exp\left(-iq \int_t^{t+\tau} V_j(t') dt'\right) \right\rangle \quad (2.172)$$

for delay times short enough such that

$$q \int_0^{\tau} V_j(t') dt' \ll 1, \quad (2.173)$$

we keep only the first two terms in the expansion of the last exponential, thus

$$\left. \frac{dF}{d\tau} \right|_{small\tau} = -q^2 N^{-1} \sum_i^N \sum_j^N \int_0^{\tau} dt' \langle V_i(0) V_j(t') \exp[i\vec{q} \cdot (\vec{r}_i(0) - \vec{r}_j(0))] \rangle \quad (2.174)$$

and therefore

$$\left. \frac{d^2 F}{d\tau^2} \right|_{small\tau} = -q^2 N^{-1} \sum_i^N \sum_j^N \langle V_i(0) V_j(t') \exp[i\vec{q} \cdot (\vec{r}_i(0) - \vec{r}_j(0))] \rangle \quad (2.175)$$

recalling that Δr is a Gaussian random variable.

where the time correlation function of two dynamical variables $A(t)$ and $B(t)$ is written as

$$C_{BA}(t) = \langle B(t + \Delta) A(t) \rangle \quad (2.176)$$

$C_{AA}(t)$ (corresponding to the case when $B \equiv A$) is called the autocorrelation function of the variable A [9]. The time correlation is written as an average over time:

$$\langle B(t + \Delta)A(t) \rangle = \lim_{\tau \rightarrow 0} \frac{1}{\tau} \int_0^{\tau} B(t + \Delta + t')A(t') dt' \quad (2.177)$$

The Hamiltonian is a constant of the motion and therefore $C_{AB}(t)$ is independent of the choice of time origin t ; the correlation function is said to be stationary with respect to t .

The stationary property of the time correlation function means that we can write

$$\frac{d}{dt} \langle B(t + \Delta)A(\Delta) \rangle = \langle \dot{B}(t + \Delta)A(\Delta) \rangle + \langle B(t + \Delta)\dot{A}(\Delta) \rangle \quad (2.178)$$

$$= 0$$

Thus

$$\langle \dot{B}(t + \Delta)A(\Delta) \rangle = - \langle B(t + \Delta)\dot{A}(\Delta) \rangle \quad (2.179)$$

In particular:

$$\langle \dot{A}A \rangle = 0 \quad (2.180)$$

repeated differentiation yields

$$\frac{d^2}{dt^2} \langle B(t)A \rangle = \langle \ddot{B}(t)A \rangle \quad (2.181)$$

$$= \lim_{\tau \rightarrow \infty} \frac{1}{\tau} \int_0^\tau \ddot{B}(t+t')A(t')dt' \quad (2.182)$$

$$= -\lim_{\tau \rightarrow 0} \frac{1}{\tau} \int_0^\tau \dot{B}(t+t')\dot{A}(t')dt' + \lim_{\tau \rightarrow 0} \frac{1}{\tau} [\dot{B}(t+t')A(t')]_0^\tau$$

$$= -\langle \dot{B}(t)\dot{A} \rangle \quad (2.183)$$

using these rules along with the following property of the expectation value

$$\langle aE \rangle = a \langle E \rangle \quad (2.184)$$

where a is a constant. We can begin to express the terms K_1 and K_2 as functions of the dynamic structure factor $F(q, \tau)$ as

$$K_1 = -\lim_{t \rightarrow 0} \frac{d}{dt} \ln \left[\frac{F(q, t)}{S(q)} \right] \quad (2.185)$$

$$= -\lim_{t \rightarrow 0} \frac{1}{S(q)} \frac{dF(q, t)}{dt} \quad (2.186)$$

$$= -\frac{1}{S(q)} q^2 N^{-1} \sum_i^N \sum_j^N \int_0^\tau dt' \langle V_i(0)V_j(t') \exp[i\vec{q} \cdot (\vec{r}_i(0) - \vec{r}_j(0))] \rangle \quad (2.187)$$

and

$$K_2 = -\lim_{t \rightarrow 0} \frac{d^2}{dt^2} \ln \left[\frac{F(q,t)}{S(q)} \right] \quad (2.188)$$

$$= -\lim_{t \rightarrow 0} \left\{ \frac{1}{S(q)} \frac{d^2 F(q,t)}{dt^2} - \frac{1}{[S(q)^2]} \left[\frac{dF(q,t)}{dt} \right]^2 \right\} \quad (2.189)$$

$$= - \left\{ \frac{1}{S(q)} \left(-q^2 N^{-1} \sum_i^N \sum_j^N \langle V_i(0) V_j(t) \exp[i\vec{q} \cdot (\vec{r}_i(0) - \vec{r}_j(0))] \rangle \right) \right. \\ \left. - \frac{1}{[S(q)^2]} \left[q^2 N^{-1} \sum_i^N \sum_j^N \int_0^t dt' \langle V_i(0) V_j(t') \exp[i\vec{q} \cdot (\vec{r}_i(0) - \vec{r}_j(0))] \rangle \right]^2 \right\} \quad (2.190)$$

$$\frac{d^2 F(q,t)}{dt^2} \gg \left[\frac{dF(q,t)}{dt} \right]^2 \text{ or equivalently } q^2 \gg q^4 \quad (2.191)$$

$$\cong \frac{q^2}{S(q)} N^{-1} \sum_i^N \sum_j^N \langle V_i(0) V_j(t) \rangle \exp[i\vec{q} \cdot (\vec{r}_i(0) - \vec{r}_j(0))] \quad (2.192)$$

we assume that for ballistic motion

$$\langle V_i(0)V_j(t) \rangle = \delta_{ij} \langle V_i(0)V_i(t) \rangle \quad (2.193)$$

whereupon

$$K_1 = \frac{dF(q,t)}{dt} = -\frac{1}{S(q)} q^2 N^{-1} \sum_i^N \sum_j^N \int_0^\tau dt' \langle V_i(0)V_j(t') \exp[i\vec{q} \cdot (\vec{r}_i(0) - \vec{r}_j(0))] \rangle \quad (2.194)$$

becomes

$$-\frac{1}{S(q)} q^2 N^{-1} \sum_i^N \sum_j^N \int_0^\tau dt' \delta_{ij} \langle V_i(0)V_i(t') \rangle \exp[i\vec{q} \cdot (\vec{r}_i(0) - \vec{r}_j(0))] \quad (2.195)$$

and we can approximate K_2 as

$$K_2 \cong \frac{q^2}{S(q)} N^{-1} \sum_i^N \sum_j^N \langle V_i(0)V_j(t) \rangle \exp[i\vec{q} \cdot (\vec{r}_i(0) - \vec{r}_j(0))] \quad (2.196)$$

Therefore the constants in the cumulant expansion can be written as

$$K_1 = Dq^2 \quad (2.197)$$

and

$$K_2 = v^2 q^2 \quad (2.198)$$

The internal dynamics and dynamics of colloidal gels using dynamic light scattering techniques has been studied by Hobbie and Stewart [13] amongst several others. Their approach was to use the particle tracking methods of the correlation function. They found that the correlation function decays exponentially in space and exhibits a scaling in terms of the first moment. The second moment was found to be proportional to the mean-square particle displacement.

In general, the first cumulant K_1 defines an effective diffusion coefficient governing the initial decay of $F(q, t)$ and K_2 is proportional the velocity of the scatterer as it moves in the medium [29]. K_2 can be re-written in terms of the mean square particle displacement as

$$K_2 = v^2 q^2 \quad (2.199)$$

$$K_2 = 4\pi^2 \left(\frac{1}{L_o} \frac{d\langle \Delta x(t) \rangle}{dt} \right)^2 \quad (2.200)$$

It is well known that methods of statistical mechanics are appropriate to describe the thermo-elastic material behavior of rubber-like polymers [38]. Elastomers are considered a thermodynamic “system” since they have a definable boundary. The intensive thermodynamic state of an isotropic elastic solid is determined by the stress components and the temperature. Hence, at constant mass and composition, all the dependent variables of state (the volume V , the length L , the internal energy U , the entropy S , etc.) the elastomeric properties can now be considered in terms of stress, strain, time and

temperature. Discussions of this topic define these relationships either as phenomenological or molecular. The phenomenological or mathematical basis would include the works of Mooney [25] and Rivlin [31] which subsequently produced the Mooney-Rivlin coefficients. The molecular basis, primarily using thermodynamics, originally was referred to as the statistical theory and is more commonly referred to as the Gaussian theory. Several authors have shown how network theory for a Gaussian chain can be extended through thermodynamic models to obtain a more general conceptual understanding of viscoelasticity [30][27].

2.4 MICROMECHANICAL CONSIDERATIONS

2.4.1 Elasticity of a Network

The behavior of the polymeric host material we are considering, which contains chains of molecules or fiber-like structures, follows from the understanding of the behavior of a representative fiber [24].

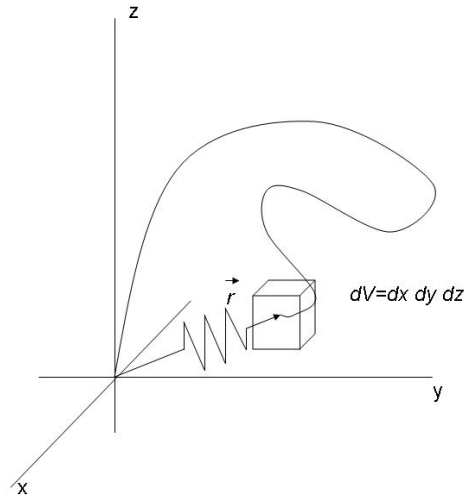


Fig.11: A representative elastic chain detached from the network

To build up the statistical theory, one derives the probability for the end-to-end distance of an average chain lying between r and $r + dr$. The quantity ρ represents the mean length of a fiber segment. The probability density based on a Gaussian distribution is given by

$$P(r) = \frac{1}{(\rho\sqrt{\pi})^3} \exp\left[-\frac{r^2}{\rho^2}\right] \quad (2.201)$$

For a detached Gaussian fiber, the mean-square end-to-end displacement averaged over time is

$$\langle r^2 \rangle_o = \frac{3}{2} \rho^2 \quad (2.202)$$

and the quantity ρ is a representative fiber length of polymer. The subscript “o” signifies that average over r^2 is taken with the chain out of the network. Since this is the length of all chains n taken with the chain out of the network-the value of $\langle r^2 \rangle_o$ averaged over all chains is $(3/2)\rho^2$. Imagine the chain now transferred back into the specimen to reform the network. Any deformation will now cause the chain to have an end-to-end length of $\langle r^2 \rangle_i$. This value of $\langle r^2 \rangle_i$ is not an intrinsic property of the molecule, but is a function of the specimen volume V . If V is changed then $\langle r^2 \rangle_i$ changes accordingly. $\langle r^2 \rangle_o$ is an intrinsic property of the macromolecule and does not depend on the volume change.

Consider a volume of initial dimensions $X_o Y_o Z_o$ to be deformed along the principal directions x, y, and z to the new dimensions X, Y, Z . Rubber is deformed at essentially no change in volume; therefore $X_o Y_o Z_o = XYZ$. The extension ratios in the three principal directions are

$$\lambda_x = \frac{X}{X_o}, \lambda_y = \frac{Y}{Y_o}, \lambda_z = \frac{Z}{Z_o} \quad (2.203)$$

From this it follows that the product of the extension ratios are a constant, i.e. constant volume:

$$\lambda_x \lambda_y \lambda_z = 1 \quad (2.204)$$

Assuming any chain in the network deforms like the bulk rubber (affine deformation), all constituent chains and subsequently all points in the polymer will be subject to the same deformation:

$$\vec{r}_i = \hat{i}x_i + \hat{j}y_i + \hat{k}z_i \quad (2.205)$$

becomes

$$\vec{r} = \hat{i}\lambda_x x_i + \hat{j}\lambda_y y_i + \hat{k}\lambda_z z_i \quad (2.206)$$

the change in the end-to-end vector produces a change in the end-to-end force from \vec{f}_i before deformation

$$\vec{f}_i = K[\hat{i}x_i + \hat{j}y_i + \hat{k}z_i], \quad (2.207)$$

to \vec{f} after deformation

$$\vec{f} = K[\hat{i}\lambda_x x_i + \hat{j}\lambda_y y_i + \hat{k}\lambda_z z_i]. \quad (2.208)$$

The stress-strain properties are calculated by equating the work done by internal forces to that done by external forces which create the deformation. Considering the work done by a uniaxial force on a representative fiber in the elastomer:

$$w_z = \int_{z_i}^{\lambda_z z_i} f_z dz \quad (2.209)$$

$$= \left(\frac{2kT}{\rho^2} \right) \int_{z_i}^{\lambda_z z_i} z dz \quad (2.210)$$

$$= \left(\frac{kT}{\rho^2} \right) [\lambda_z^2 - 1] z_i^2 \quad (2.211)$$

Now this is the work done by the force f_z of one fiber. It depends on the square of the initial value of the z component of the end-to-end vector of that fiber. The work done by the force f_z of all n fibers in the specimen is obtained by averaging over all values of z^2 :

$$\sum_1^n w_z = \sum_1^n \left(\frac{kT}{\rho^2} \right) [\lambda_z^2 - 1] z_i^2 \quad (2.212)$$

All chains have the same ρ and imposed stretch (or compression) λ_z , therefore

$$\sum_1^n w_z = \left(\frac{kT}{\rho^2} \right) [\lambda_z^2 - 1] \sum_1^n z_i^2 \quad (2.213)$$

And by definition

$$\sum_1^n z_i^2 = n \langle z^2 \rangle_i \quad (2.214)$$

where $\langle z^2 \rangle_i$ is the mean-square value of z_i in the undeformed state. The undeformed state is isotropic therefore

$$\langle z^2 \rangle_i = \langle y^2 \rangle_i = \langle x^2 \rangle_i = \frac{\langle r^2 \rangle_i}{3} \quad (2.215)$$

It therefore follows that

$$\sum_1^n w_z = \left(\frac{kT}{\rho^2} \right) [\lambda_z^2 - 1] n \frac{\langle r^2 \rangle_i}{3} \quad (2.216)$$

For a Gaussian fiber ρ^2 controls the mean-square end-to-end distance $\langle r^2 \rangle_o$ of the fiber when it is unperturbed. It therefore follows that

$$\sum_1^n w_z = \frac{nkT}{2} \frac{\langle r^2 \rangle_i}{\langle r^2 \rangle_o} [\lambda_z^2 - 1]. \quad (2.217)$$

The equations for the work done by all the f_x and f_y forces allow an identical argument, so that the total work done during the deformation is

$$W = \sum_1^n [w_x + w_y + w_z] \quad (2.218)$$

$$= \frac{NkT}{2} \frac{\langle r^2 \rangle_i}{\langle r^2 \rangle_o} [\lambda_x^2 + \lambda_y^2 + \lambda_z^2 - 3] \quad (2.219)$$

2.4.2 The Strain Tensor

When a body is deformed, the distances between points change. Let us consider two closely spaced points separated by a radius vector dx_i . The new radius vector joining the same points after deformation is defined as $dx'_i = dx_i + du_i$. The distance between the points are given by vector addition as $dl = \sqrt{(dx_1^2 + dx_2^2 + dx_3^2)}$ prior to the deformation and $dl' = \sqrt{(dx_1'^2 + dx_2'^2 + dx_3'^2)}$ after. Using the general summation rule, we can write $dl^2 = dx_i^2$, $dl'^2 = dx_i'^2 = (dx_i + du_i)^2$. Substituting $du_i = (\partial u_i / \partial x_k) dx_k$, we can write

$$dl'^2 = \left(dx_i + \frac{\partial u_i}{\partial x_k} dx_k \right)^2 \quad (2.220)$$

$$dl'^2 = dx_i^2 + 2 \frac{\partial u_i}{\partial x_k} dx_i dx_k + \left(\frac{\partial u_i}{\partial x_k} dx_k \right)^2 \quad (2.221)$$

Since the summation is taken over both suffixes i and k in the second term on the right, we can put $(\partial u_i / \partial x_k) dx_i dx_k = (\partial u_k / \partial x_i) dx_i dx_k$. In the third term, the suffixes i and l can be interchanged.

$$dl'^2 = dl^2 + 2 \frac{\partial u_i}{\partial x_k} dx_i dx_k + \frac{\partial u_i}{\partial x_k} \frac{\partial u_i}{\partial x_l} dx_k dx_l \quad (2.222)$$

$$dl'^2 = dl^2 + \left(2 \frac{\partial u_k}{\partial x_i} + \frac{\partial u_l}{\partial x_k} \frac{\partial u_l}{\partial x_i} \right) dx_k dx_i \quad (2.223)$$

$$dl'^2 = dl^2 + \left(\frac{\partial u_k}{\partial x_i} + \frac{\partial u_i}{\partial x_k} + \frac{\partial u_l}{\partial x_k} \frac{\partial u_l}{\partial x_i} \right) dx_k dx_i \quad (2.224)$$

Then dl'^2 takes the final form

$$dl'^2 = dl^2 + 2u_{ik} dx_i dx_k \quad (2.225)$$

where

$$u_{ik} \equiv \frac{1}{2} \left[\left(\frac{\partial u_i}{\partial x_k} \right) + \left(\frac{\partial u_k}{\partial x_i} \right) + \frac{\partial u_l}{\partial x_i} \frac{\partial u_l}{\partial x_k} \right] \quad (2.226)$$

and for small strains becomes

$$u_{ik} \equiv \frac{1}{2} \left[\left(\frac{\partial u_k}{\partial x_i} \right) + \left(\frac{\partial u_i}{\partial x_k} \right) \right] \quad (2.227)$$

2.4.3 Hooke's Law

Two independent scalars of the second degree can be formed from the components of the symmetrical tensor u_{ik} . They can be taken as the squared sum of the diagonal components (u_{ii}^2) and (u_{ik}^2) . Expanding the free energy F in powers of u_{ik}

$$F = F_o + \frac{1}{2} \lambda u_{ii}^2 + \mu u_{ik}^2 \quad (2.228)$$

This is the general equation for the free energy of a deformed isotropic body. The quantities λ and μ are called the Lamé coefficients. Any deformation can be represented as the sum of a pure shear and a hydrostatic compression

$$u_{ik} = \left(u_{ik} - \frac{1}{3} \delta_{ik} u_{ll} \right) + \frac{1}{3} \delta_{ik} u_{ll} \quad (2.229)$$

Where the first term on the right is pure shear and the second term is a hydrostatic compression.

As a general expression for the free energy of a deformed body, it is convenient to write

the free energy in terms of $\left(u_{ik} - \frac{1}{3} \delta_{ik} u_{ll} \right)^2$ and u_{ii}^2 as

$$F = \mu \left(u_{ik} - \frac{1}{3} \delta_{ik} u_{ll} \right)^2 + \frac{1}{2} K u_{ll}^2 \quad (2.230)$$

The quantities K and μ are called the modulus of hydrostatic compression and the modulus of rigidity. K is related to the Lamé coefficients by

$$K = \lambda + \frac{2}{3}\mu \quad (2.231)$$

Using the general thermodynamic expression

$$\sigma_{ik} = \left(\frac{\partial F}{\partial u_{ik}} \right)_T \quad (2.232)$$

to determine the stress tensor by calculating the derivatives $\partial F / \partial u_{ik}$. Writing the total differential dF (for constant temperature):

$$dF = Ku_{ll}du_{ll} + 2\mu(u_{ik} - \frac{1}{3}u_{ll}\delta_{ik})d(u_{ik} - \frac{1}{3}u_{ll}\delta_{ik}) \quad (2.233)$$

In the second term, multiplication of the first parenthesis by δ_{ik} gives zero, leaving

$$dF = Ku_{ll}du_{ll} + 2\mu(u_{ik} - \frac{1}{3}u_{ll}\delta_{ik})du_{ik} \quad (2.234)$$

or writing $du_{ll} = \delta_{ik}du_{ik}$

$$dF = \left[K u_{ii} du_{ik} + 2\mu \left(u_{ik} - \frac{1}{3} u_{ii} \delta_{ik} \right) \right] du_{ik} \quad (2.235)$$

Hence the stress tensor is related to the displacement vector u as

$$\sigma_{ik} = K \nabla \cdot u \delta_{ik} + 2\mu \left(u_{ik} - \frac{1}{3} \nabla \cdot u \delta_{ik} \right). \quad (2.236)$$

The first term shows the stress produced by a volume change and the second term is the stress caused by shear deformation. The coefficients K and μ are the bulk and shear modulus of the polymer.

2.4.4 Thermodynamics of Deformation

Let us consider the deformation of a body and suppose that the deformation is done in such a way that the displacement vector u_i changes by a small amount δu_i ; and let us determine the work done by the internal stresses in this change.

Multiplying the force $F_i = \partial \sigma_{ik} / \partial x_k$ by the displacement δu_i and integrating over the volume of the body

$$\int \delta W dV = \int \frac{\partial \sigma_{ik}}{\partial x_k} \delta u_i dV \quad (2.237)$$

where δW denotes the work done by the internal stresses per unit volume. We integrate by parts using Green's theorem, obtaining

$$\int \delta W dV = \oint \sigma_{ik} \delta u_i df_k - \int \sigma_{ik} \frac{\partial \delta u_i}{\partial x_k} dV \quad (2.238)$$

By considering the medium infinite and not deformed at infinity, we can make the surface integration in the first integral tend to infinity; then $\sigma_{ik} = 0$ on the surface, and the integral is zero. The second integral can because of symmetry of the stress tensor σ_{ik} be written as

$$\int \delta W dV = -\frac{1}{2} \int \sigma_{ik} \left(\frac{\partial \delta u_i}{\partial x_k} + \frac{\partial \delta u_k}{\partial x_i} \right) dV \quad (2.239)$$

$$\int \delta W dV = -\frac{1}{2} \int \sigma_{ik} \delta \left(\frac{\partial u_i}{\partial x_k} + \frac{\partial u_k}{\partial x_i} \right) dV \quad (2.240)$$

$$\int \delta W dV = -\frac{1}{2} \int \sigma_{ik} \delta u_{ik} dV \quad (2.241)$$

thus

$$\delta W \equiv -\sigma_{ik} \delta u_{ik} \quad (2.242)$$

Giving the work δW in terms of the change in the strain tensor assuming processes in the case of elastic deformations are occurring slowly enough that thermodynamic equilibrium is established in the body at every point. An infinitesimal change dE in the internal energy E of a unit volume of the body is equal to the difference between the heat acquired by the unit volume considered and the work dW done by the internal stresses.

Thus

$$dE = TdS - dW \quad (2.243)$$

$$dE = TdS + \sigma_{ik} du_{ik} \quad (2.244)$$

This is the thermodynamic identity for deformed bodies. In hydrostatic compression, the stress tensor is $\sigma_{ik} = -p\delta_{ik}$. Then $\sigma_{ik} du_{ik} = -p\delta_{ik} du_{ik} = -pdu_{ii}$. By considering a unit volume, the change in the displacement vector is $du_{ii} = dV$. Therefore the thermodynamic identity becomes

$$dE = TdS - pdV \quad (2.245)$$

Introducing the free energy of the body, $F = E - TS$, we find the form

$$dF = -SdT + \sigma_{ik} du_{ik} \quad (2.246)$$

for the thermodynamic identity. Finally, the components of the stress tensor can be obtained by differentiating F with respect to the components of the strain tensor for constant temperature

$$\sigma_{ik} = \left(\frac{\partial F}{\partial u_{ik}} \right)_T \quad (2.247)$$

2.4.5 Cauchy Stress

The stress-strain relationship sample volume in tension will be shown as the simplest case. For a specimen deformed along the z-axis from initial length L_o , to a final length L , by an applied force F .

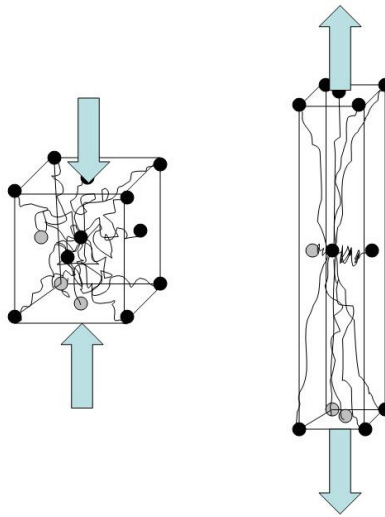


Fig.12: Deformation of an elastomer volume

The initial assumption of constant volume deformation will be made so that the volume V is

$$V = A_i L_i = AL \quad (2.248)$$

in which A_i and A are the cross-sectional areas before and after deformation. The theory is formulated simultaneously for compression, in which case the force F is negative, so $L < L_i$, and $A > A_i$ still holding the constant volume assumption.

The stress-deformation or stress-strain response of an incompressible, hyperelastic material can be written in terms of the strain energy density function, U , and the principal stretch ratios $\lambda_i, \lambda_j, \lambda_k$ and the principal values of the stress are obtained

via

$$\sigma_i = \lambda_i \frac{\partial U}{\partial \lambda_i} + p \quad (2.249)$$

where the subscripts refer to the direction of the deformation, p is a hydrostatic pressure, and σ_i is the stress in the i -direction. Again, for affine deformation $\lambda_1 \lambda_2 \lambda_3 = 1$. For the uniaxial deformations such as tension or compression, the stress-strain response can be given in terms of the principal stress difference $\sigma_1 - \sigma_2$:

$$\sigma_1 - \sigma_2 = \lambda_1 \frac{\partial U}{\partial \lambda_1} - \lambda_2 \frac{\partial U}{\partial \lambda_2} \quad (2.250)$$

It is often the case that the behavior of rubber is represented in a simple stress-deformation diagram. Early in the development of both phenomenological and molecular theories of rubber elasticity, an alternative method of looking at data arose based on the so called Mooney-Rivlin representation. This method of representation in terms of reduced stress arises when one examines the stress-strain relations that arise when the strain energy density function is assumed to have the Mooney form

Mooney-Rivlin strain energy function

$$U = C_0(\lambda_1^2 + \lambda_2^2 + \lambda_3^2 - 3) + C_1(\lambda_1^{-2} + \lambda_2^{-2} + \lambda_3^{-2}) \quad (2.251)$$

where C_0 and C_1 are material parameters (Mooney-Rivlin constants).

$$\sigma_1 - \sigma_2 = \lambda_1 \frac{\partial U}{\partial \lambda_1} - \lambda_2 \frac{\partial U}{\partial \lambda_2} \quad (2.252)$$

$$= \lambda_1 [C_0(2\lambda_1) + C_1(-2\lambda_1^{-3})] - \lambda_2 [C_0(2\lambda_2) + C_1(-2\lambda_2^{-3})] \quad (2.253)$$

For the ideal case of uniaxial tension/compression, where $\lambda_1 = \lambda$, $\lambda_2 = \lambda_3 = 1/\sqrt{\lambda}$, the first principal stress difference $\sigma_1 - \sigma_2$ for a uniaxial deformation is given by

$$\sigma_1 - \sigma_2 = \left(2C_o + \frac{2C_1}{\lambda} \right) \left(\lambda^2 - \frac{1}{\lambda} \right) \quad (2.254)$$

$$\sigma_1 - \sigma_2 = Nk\theta v_p^{\frac{1}{3}} \left(\lambda^2 - \frac{1}{\lambda} \right) \quad (2.255)$$

where $Nk\theta$ can be shown in the limit of small deformations to be the shear modulus, G , of the matrix material and v_p is the classification of swelling ($v_p = 1$ refers to the unswelled state). Therefore the change in principal stress is given by

$$\sigma_1 - \sigma_2 = G \left(\lambda^2 - \frac{1}{\lambda} \right). \quad (2.256)$$

The shear modulus G , is defined as the ratio of shear stress to engineering shear strain on the loading plane,

$$G = \frac{\sigma_{xy}}{\varepsilon_{xy} + \varepsilon_{yx}} = \frac{\sigma_{xy}}{2\varepsilon_{xy}} = \frac{\sigma_{xy}}{\gamma_{xy}} \quad (2.257)$$

$$= \frac{E}{2(1+\nu)} \quad (2.258)$$

where the engineering shear strain is

$$\gamma_{xy} = \frac{\partial v}{\partial x} + \frac{\partial u}{\partial y} \quad (2.259)$$

$$\gamma_{xy} = \epsilon_{xy} + \epsilon_{yx} = 2\epsilon_{xy} . \quad (2.260)$$

γ_{xy} is a total measure of the shear strain in the x - y plane.

2.5 THEORY OF VISCOELASTICITY-MODELS

Before attempting to devise a model to duplicate the viscoelastic behavior of an actual material, it is well to examine the response ϵ of ideal systems to a stress σ using analogical models. Ideal analogical models are assemblies of mechanical elements such as springs and dashpots with responses similar to those expected in the real material. They are used, very often, to provide a concrete illustration of the constitutive equations. The analogy stops there and never concerns itself with the physical mechanisms themselves.

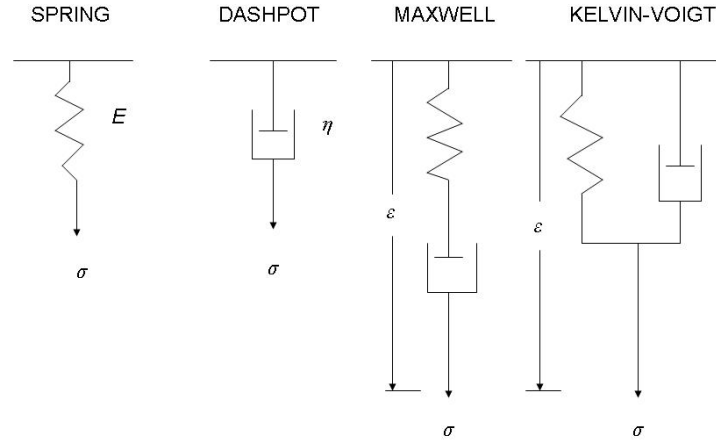


Fig.13: Symbolic representation of the analogical models of viscoelasticity

THEORY OF VISCOELASTICITY-MODELS

2.5.1 The Maxwell Model

An ideal elastic element is represented by a spring which obeys Hooke's law, with a modulus of elasticity E . This is the representation for linear elasticity where the elastic deformation is instantaneous and independent of time:

$$\sigma = E\epsilon \quad (2.261)$$

A completely viscous response is that of a Newtonian fluid. This is a material whose deformation is linear with time while the stress is applied and is completely irrecoverable.

A damper is used to represent linear or non-linear viscosity:

$$\sigma = \eta \frac{d\epsilon}{dt} = \eta \dot{\epsilon} \quad (2.262)$$

The two elements of spring and dashpot can be combined in two ways. If they are placed in series, the resulting Maxwell element exhibits flow plus elasticity on the application of stress. When the stress is applied, the spring elongates while the dashpot slowly yields. On the removal of the stress the spring recovers but the dashpot does not. Since both elements are connected in series, the total elongation is

$$\varepsilon_T = \varepsilon_S + \varepsilon_D \quad (2.263)$$

and the time rate of change in elongation is written as

$$\frac{d\varepsilon_T}{dt} = \frac{d\varepsilon_S}{dt} + \frac{d\varepsilon_D}{dt} . \quad (2.256)$$

Therefore, the strain is given by the equation

$$\frac{d\varepsilon}{dt} = \frac{\sigma}{\eta} + \frac{1}{E} \frac{d\sigma}{dt} \quad (2.257)$$

If we apply a constant stress $\sigma = \sigma_o$ to this system at $t = 0$ the solution will have the form

$$\varepsilon(t) = \frac{\sigma_o}{\eta} t + C_1 \quad t > 0 . \quad (2.258)$$

To find the constant C_1 , an initial condition is needed. The sudden application of the stress σ_o at $t = 0$ means that $\dot{\sigma}(t)$ has a singularity at this point. To deal with it, we must integrate across this point:

$$\int_{-\tau}^{+\tau} \sigma dt + p_1 [\sigma(+\tau) - \sigma(-\tau)] = q_1 [\varepsilon(+\tau) - \varepsilon(-\tau)] \quad (2.259)$$

When $\tau \rightarrow 0$, the first term goes to zero and we are left with

$$p_1 \sigma_o = q_1 \varepsilon_o \quad \text{that is} \quad \varepsilon_o = \frac{p_1 \sigma_o}{q_1} = \frac{\sigma_o}{E_o}, \quad (2.260)$$

where $\varepsilon_o = \varepsilon(0^+)$ is the value of ε immediately to the right of $t = 0$. When we now find that

$$C_1 = \varepsilon_o = p_1 \sigma_o / q_1, \quad (2.261)$$

and hence

$$\varepsilon(t) = \frac{\sigma_o}{q_1} (p_1 + t) \quad (2.262)$$

2.5.2 Fractional Models

Through combinations of springs and dashpots one arrives at standard viscoelastic models, such as the Maxwell or Kelvin-Voigt model. Usually, these models involve a fairly small number of single elements. The problem here is that the corresponding ordinary differential equations have a relatively restricted class of solutions, which is, in general, too limited to provide an adequate description for the complex systems of the type dictated by a magnetorheological elastomer.

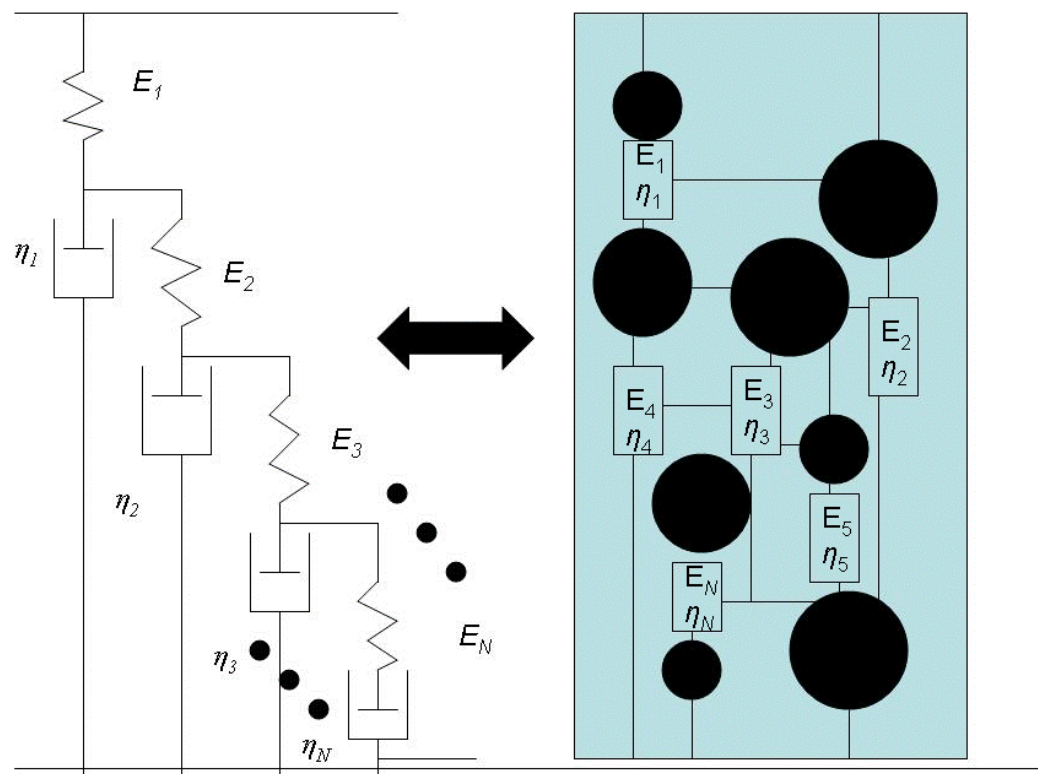


Fig.14: Sequential realization of the fractional element model and a model representation of an MRE. This helps to illustrate the motivation for the use of fractional calculus. The volumes between inclusions at different length scales can be considered to have differing dynamic viscosities and elastic moduli. This model leads to a distribution spectrum of viscoelastic relaxation times as a function of probed length scales.

To overcome this, one can relate the stress and strain through viscoelastic models based on fractional derivatives with respect to time. In general, models based on fractional derivatives need fewer input parameters and allow for the interpolation between the purely elastic behavior of the Maxwell model and the purely viscous pattern of the Kelvin-Voigt model. Studies such as the ones by Koeller[17] and [34] have written on the theory of generalized fractional viscoelastic equations and their solutions.

The study of viscoelastic behavior of a material by means of fractional calculus implies its modeling using differential equations with non-integer derivative order or transfer functions such as the quotient of polynomials in real powers of s . Modification of classical models can be obtained by relating the stress through a differential equation of order q : considering that the response functions $J(t)$ and $G(t)$ are a linear combination of those found in the previous models. $J(t)$ and $G(t)$ are the summation of vanishing exponentials with different relaxation times, linear functions and Dirac delta functions, as follows;

$$G(t) = G_e + \sum_n G_n \exp(-t / \tau_n) + G_- \delta(t) \quad (2.263)$$

with $G_- \delta(t)$ being a response in the form of a delta function.

By performing the Laplace transform on the previous models we obtain

$$sG(s) = G_e + \sum G_n - \sum \frac{G_n}{1 + s\tau_n} + G_- s. \quad (2.264)$$

$sG(s)$ can be expressed as a rational function in the complex plane with real poles and zeros:

$$\frac{1}{sG(s)} = \frac{P(s)}{Q(s)}, \text{ where } P(s) = 1 + \sum_{k=1}^p a_k s^k, \quad (2.265)$$

$$Q(s) = m + \sum_{k=1}^p b_k s^k \quad (2.266)$$

The stress-strain behavior can be modeled by the following differential equation:

$$\left(1 + \sum_{k=1}^p a_k \frac{d^k}{dt^k}\right) \sigma(t) = \left(m + \sum_{k=1}^p b_k \frac{d^k}{dt^k}\right) \varepsilon(t) \quad (2.267)$$

Formally, a fractional model extending the derivative order k in the last expression to non-integer values can be obtained. This implies the substitution of the classic models with a finite distribution of delay and relaxation times, for models that involve a continuous distribution.

2.5.3 Maxwell Fractional Model

The mechanical models in fractional calculus use a model intermediate between ideal springs and dashpots denominated the Scott-Blair model called a spring-pot, which is represented by a fractional derivative order α .

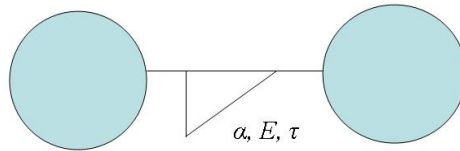


Fig.15: The Scott-Blair or fractional element in the context of our MRE model (represented in the volume between to spherical inclusions by the triangle). The fractional element is a modified combination of the traditional spring and dashpot viscoelastic models. It allows modeling of the fractional relaxation behavior of our material as interpreted by dynamic light speckle.

These elements can be built by means of structures in trees, cascades, lattices, etc., of discrete elements, springs and dashpots.

The differential fractional equation corresponding to this element is

$$\sigma(t) = E\tau^\alpha \frac{d^\alpha \varepsilon(t)}{dt^\alpha}, G(t) \approx \frac{E}{\Gamma(1-\alpha)} \left(\frac{t}{\tau}\right)^{-\alpha} \quad (2.268)$$

In Maxwell's fractional model the total strain is the sum of the partial strains in each of the Scott-Blair elements

$$\varepsilon_1(t) = E_1^{-1} \tau_1^{-\alpha} \frac{d^{-\alpha} \sigma(t)}{dt^{-\alpha}} \quad (2.269)$$

$$\varepsilon_2(t) = E_2^{-1} \tau_2^{-\alpha} \frac{d^{-\alpha} \sigma(t)}{dt^{-\alpha}} \quad (2.270)$$

for a given stress in an element. By adding both expressions and performing the α -order derivative, the fractional differential equation for Maxwell's model is obtained:

$$\sigma(t) + \tau^{\alpha-\beta} \frac{d^{\alpha-\beta} \sigma(t)}{dt^{\alpha-\beta}} = E \tau^\alpha \frac{d^\alpha \varepsilon(t)}{dt^\alpha} \quad (2.271)$$

Using the properties of the Mellin transform and the Fox integral (West, Bologna, Grigolini) [40] the time relaxation modulus is obtained as follows:

$$G(t) = E \left(\frac{t}{\tau} \right)^\beta, E_{\alpha-\beta, 1-\beta} \left[- \left(\frac{t}{\tau} \right)^{\alpha-\beta} \right] \quad (2.272)$$

where $E_{k,\mu}$ is the generalized Mittag-Leffler function defined by

$$E_{k,\mu}(x) = \sum_{n=0}^{\infty} \frac{z^n}{\Gamma(kn + \mu)}. \quad (2.273)$$

The time relaxation modulus approaches, for different ranges of time, two negative power functions of time. This fact is related to two types of relaxation processes: one for short times in which $t \ll \tau$ and the other one for long times where $t \gg \tau$:

$$t \ll \tau \rightarrow G(t) \approx \frac{E}{\Gamma(1-\beta)} \left(\frac{t}{\tau}\right)^{-\beta} \quad (2.274)$$

and

$$t \gg \tau \rightarrow G(t) \approx \frac{E}{\Gamma(1-\alpha)} \left(\frac{t}{\tau}\right)^{-\alpha} \quad (2.275)$$

Taking the Naperian logarithm of the relaxation modulus for times both much greater than and much less than the characteristic time τ :

$$t \ll \tau \rightarrow \ln G(t) = \ln \frac{E}{\Gamma(1-\beta)} - \beta \ln \left(\frac{t}{\tau}\right) \quad (2.276)$$

$$= \ln \frac{E\tau^\beta}{\Gamma(1-\beta)} - \beta \ln t \quad (2.277)$$

$$= \ln k_1 - \beta \ln t \quad (2.278)$$

and

$$t \gg \tau \rightarrow \ln G(t) = \ln \frac{E}{\Gamma(1-\alpha)} - \alpha \ln \left(\frac{t}{\tau}\right) \quad (2.279)$$

$$= \ln \frac{E\tau^\alpha}{\Gamma(1-\alpha)} - \alpha \ln t \quad (2.280)$$

$$= \ln k_2 - \alpha \ln t \quad (2.281)$$

Fitting of the plot of the natural logarithm of the true stress, found from the Mooney-Rivlin model, versus the natural logarithm of time should yield two straight lines whose slopes are in fact the orders β and α of the fractional derivatives. From the values of the two constants and the average relaxation time, τ , we can obtain the fractional elastic modulus, E , of the material from the Maxwell fractional form

$$k_1 = \frac{E}{\Gamma(1-\beta)} \tau^\beta \quad \text{and} \quad k_2 = \frac{E}{\Gamma(1-\alpha)} \tau^\alpha \quad (2.282)$$

$$E = \frac{k_1 \Gamma(1-\beta)}{\tau^\beta} \quad \text{and} \quad E = \frac{k_2 \Gamma(1-\alpha)}{\tau^\alpha} \quad (2.283)$$

Viscoelastic models based on fractional derivatives of time need fewer input parameters and avoid oscillation [3]. This model has been used to study specifically the relaxation modulus in PMMA and PTFE polymers [12].

CHAPTER 3

EXPERIMENTAL METHODS AND TECHNIQUES

3.1 Sample preparation and SEM classification

We studied the magnetostrictive properties of two types of MRE composites. The first type was an isotropic sample created at Ford Motor Company (Dearborn, MI.). This sample was one of a natural rubber (cis-polyisoprene) matrix with a magnetic dispersed phase. The dispersed filler phase was Magnox-Pulaski magnetite (Fe_3O_4) TMB-1260. This inclusion had a bulk saturation magnetization of $4.8E 5$ A/m and was present at approximately a 27% volume fraction. These materials, together with the necessary crosslinkers and processing aids, were mixed together on a conventional two-roll mill. The resulting material was thinly spread between glass slides and exposed to temperatures of order $150^\circ C$ for durations of 10 to 30 minutes.

The second type of MRE samples were created at the University of Michigan-Ann Arbor. These are samples of varying levels of anisotropy due to their cure process. The GE Silicones Red RTV 106 silicone rubber matrix was mixed with varying volume fractions of ISP Technologies Grade R-1430 carbonyl iron particles. Carbonyl Iron is known to have a bulk saturation magnetization of $1.9E6$ A/m. Immediately following mixing the combined material was placed in a rubber mold and allowed to cure in differing levels of

an applied magnetic field. The duration and magnitude of the field applied during cure dictated the level of anisotropy.

Subsequently, SEM was done on our samples to aid in the characterization of the internal structure. As can be seen, it is obvious that varying the volume fraction and the application of an external magnetic field to the MRE as the matrix cures will drastically alter the internal order.

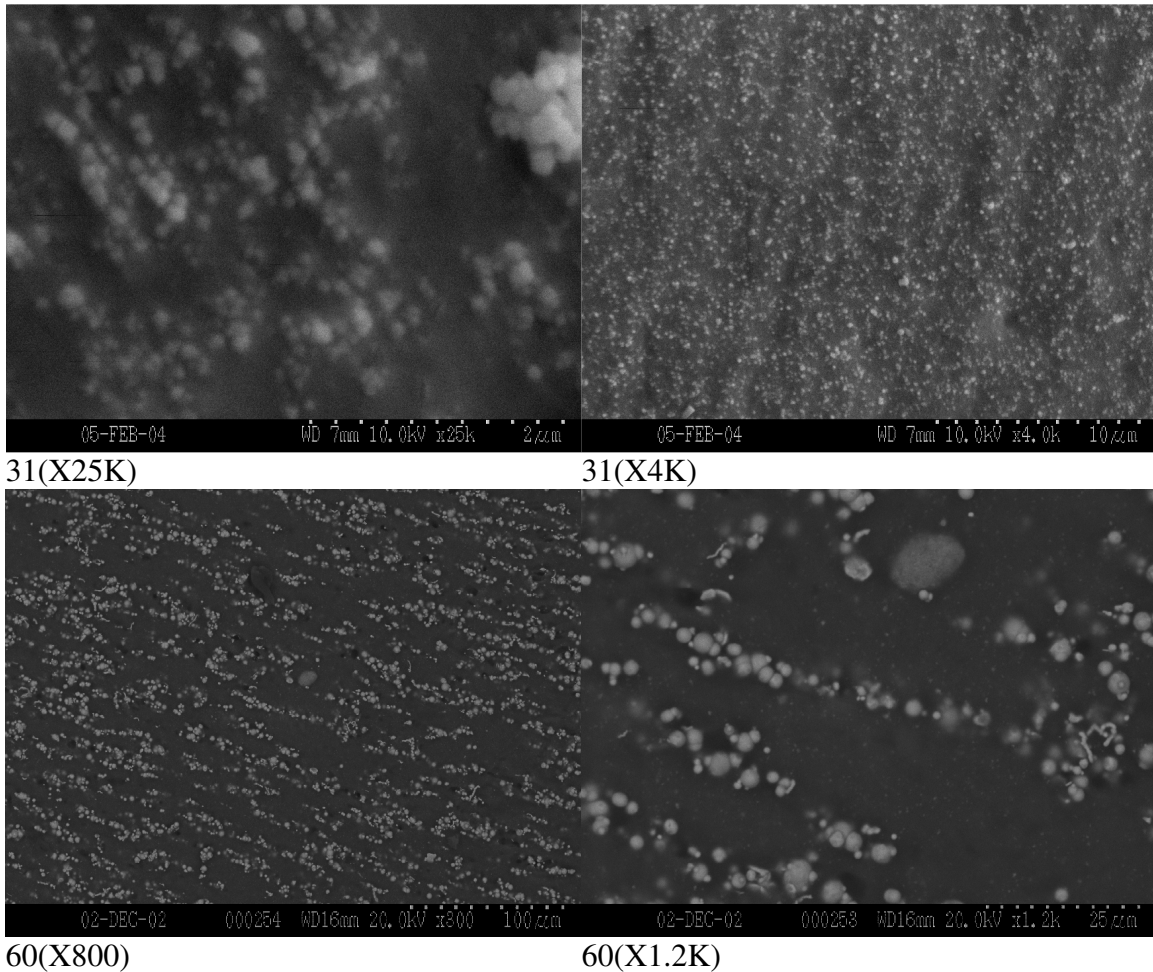


Fig. 16: Actual scanning electron microscopy images of the MRE samples used in this study

3.2 Review of the experimental set up at Argonne National Labs

The experimental approach was to apply newly developed coherent x-ray techniques to probe material dynamics and mechanical properties at relevant length scales. The interparticle dimensions that were probed were on the order of nanometers. The advantages to using x-rays in this method are the following. First, x-rays are penetrating. This allowed us to non-destructively probe our material. Secondly, the coherence lengths of our highly coherent x-rays were on the order of the interparticle separation. Most importantly x-rays are strongly scattered from heavy objects such as iron. This gave us a distinct image of the interparticle dynamics.

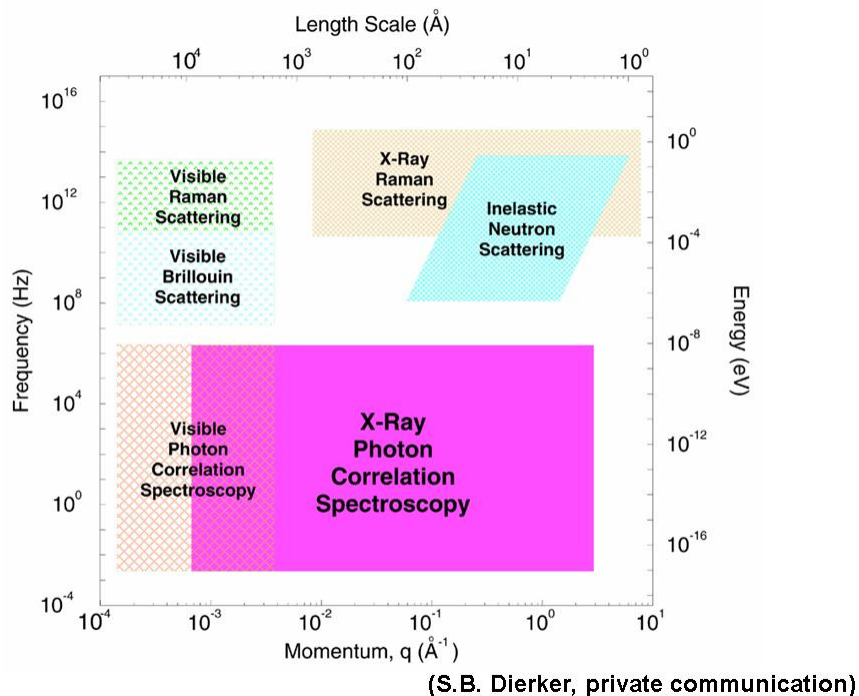


Fig.17: Application ranges for various optical probing methods.

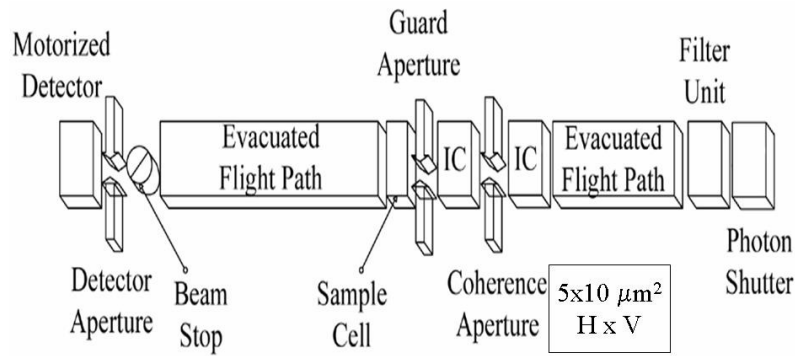
APS undulator A was the x-ray source we used for the experiments described here. For the XPCS experiments, we set the undulator fundamental at 9.0keV. The x-ray source dimensions are 350 μm in the horizontal and 50 μm in the vertical and the divergences are 25 μrad x 5 μrad . The white beam was collimated with white beam slits set to nominally 100 μm by 100 μm and placed 27m from the source. Two small Pt mirrors separated by 0.95m and set at 0.45° were used to produce a pink beam. The doubly reflected beam had a spectrum with an average energy of 7KeV, with a bandwidth of $\Delta E / E = 2.55\%$. This produced a coherent x-ray intensity as large as 3.6×10^{10} photons/s in an aperture of $(5\mu\text{m})^2$.

With these numbers, the source coherence lengths were calculated to be 1 μm x 5 μm at a wavelength of 1.62Å. At a sample distance of 55m the coherence lengths (standard deviations) were approximately 4 μm x 30 μm . Finally, although the frequency distribution of the undulator varied with position in the beam, it did not vary significantly over its coherence lengths and so an undulator is considered a monochromatic source if small sample volumes are considered.

The coherent beam characteristics used in our experiments were an x-ray energy, E of 7 keV, a wavelength, λ of 1.771Å and speckle size=24.5 μm .

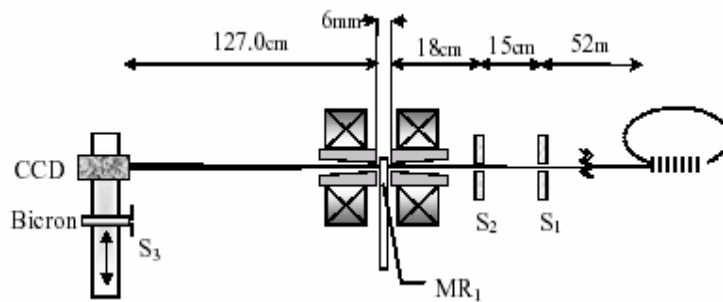
Monochromatic x-rays were used to probe the sample as shown in the configuration outlined in figures 11a), 11b) and 11c).

Small-angle XPCS Set up at 7-ID-C



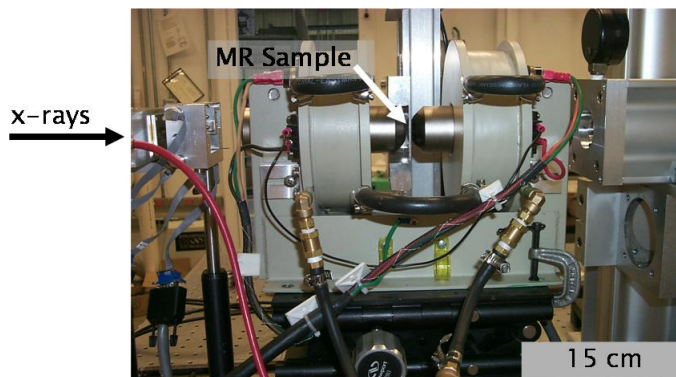
Horizontal (vertical) coherence lengths at 9 keV = 4 μm (68 μm)
37 m downstream from the undulator source.

a)



b)

Magnet and Sample



c)

Fig. 18 Schematic representation of MRE experiment performed at Argonne. Frame a) is a schematic representation illustrating the x-ray optics layout, frame b) shows the arrangement of the magnet and the detectors used to acquire the speckle data and frame c) is an actual photo of the experimental set-up.

Coherence (S_1) and guard slits (S_2) are used to select only the transversely coherent section of the beam. For this geometry and x-ray wavelength, the size of a single speckle spot was calculated to be $8\mu\text{m}$ therefore the slit openings are set to $\leq 10\mu\text{m}$. Tapered axial holes were bored in each pole piece, allowing the beam to travel parallel to the field lines in the sample. The coherent beam enters a hole in the first pole piece of the dipole electromagnet, GMW-3470, and travels 18cm to the sample (MR_1).

Time dependent speckle patterns were measured with a CCD chip positioned to capture directly the small-angle scattering. The optical components were aligned such that all the points lying on the circumference of a circle would have the same scattering vectors. The sample detector distance is chosen so that the speckle size is an appropriate match for CCD pixel resolution limited by the $7\mu\text{m}$ pixel size. A Bicron photomultiplier detector with $64\mu\text{m}$ slits (S_3) was used for calibration but the CCD was selected for data acquisition for the following attributes: efficient parallel data acquisition, the ability to access very small scattering angles (corresponding to scattering wave vectors from $0.001\text{\AA} < q < 0.01\text{\AA}$) and enhanced statistics enabled by averaging over annular regions of fixed q .

A Texas Instruments TC253 low noise, high sensitivity charge coupled device (CCD) x-ray camera specially constructed with $7.4\mu\text{m}$ pixel width in a 658×494 array was controlled by a 12-bit QMAX 650 camera. Digital images were transmitted to a microcomputer and recorded as a movie with KSA 400 image acquisition software. Using an area detector allows us to measure $I(q, t)$ for many different q vectors

simultaneously. A profile of radial intensity with respect to wave vector q was extracted from the data and fit to a Guinier curve. The temporal fluctuations in intensity were recorded for each pixel and characterized with the intensity auto-correlation function $g^{(2)}(t)$. Images of the speckle pattern were acquired into the memory of the computer with frame times varying from 50-300 ms and the correlation results for each pixel were averaged with all others at a radius q from beam axis. The time dependence of these data is a direct function of the scatter motion at a length scale in the material given by

$$L_o = 2\pi/q .$$

3.3 Experiment

In order to understand the magnetostrictive behavior we subjected the MRE composite to a time-varying magnetic field while probing the sample with x-rays. Most of the measurements were performed with a periodic (on-off) square wave variation of the applied field. The purpose of this was to measure the dynamics of the material following various magnetic field perturbation situations, including suddenly switching it on and suddenly turning it off.

The sample was rigidly constrained between kapton slides in the gap between the pole pieces in the position shown as MR₁ in figure 11. Alignment was such that the longitudinal or cure axis of the sample coincides with the x-ray beam axis. This was to ensure that the scattered x-ray wavevector had its principal component along the

magnetic axis and therefore is most sensitive in this geometry to the particle-particle interactions as illustrated in figure 12.

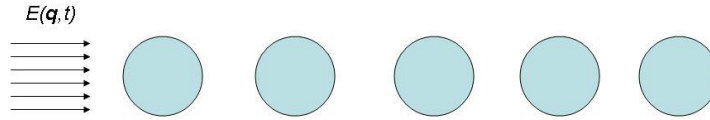


Fig.19 Optimized orientation between beam direction and inclusion chain. The incoming coherent x-rays are scattered from inclusions that have formed into highly ordered chains. The direction of the alignment (or cure axis) was dictated by the direction of the magnetic field applied during matrix cure.

The amplitude of the cyclically applied magnetic field was approximately 1.7 Tesla and was switched at 0.25Hz for samples of series 31 and 0.09Hz for samples of series 60, which were viscoelastic and required more time to relax.

The dynamic light scattering or speckle patterns created by this configuration were collected and recorded as scattering vector-dependant intensities. The data sets were recorded real time and stored as viewable AVI files. These images were then divided into rings of radius scattering vector q and autocorrelated frame-by-frame.

The data were analyzed by studying the decaying intensity autocorrelation function as a function of scattering vector.

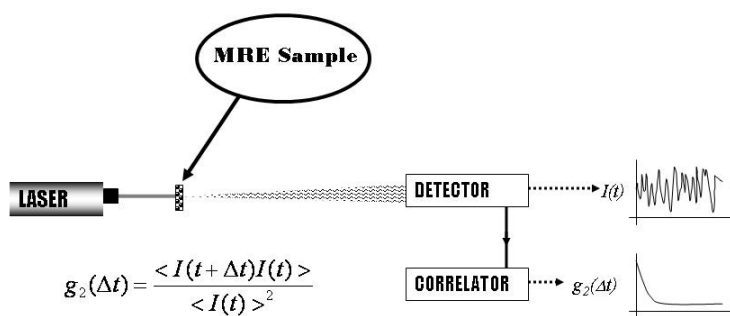


Fig. 20: Idealized experimental sequence used in the evaluation of a MRE using x-ray speckle autocorrelation.

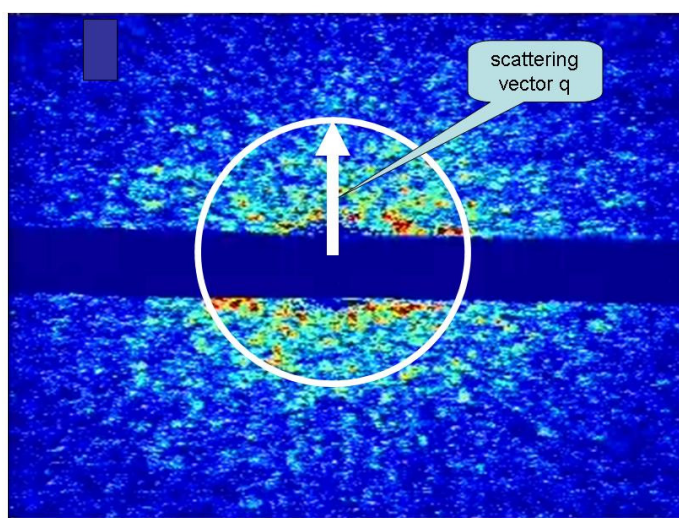


Fig. 21: Image of actual speckle as collected by a CCD camera. The white annulus superimposed on the image is a representation the area of collected data at a given radius from the beam axis. This radius is the scattering vector q .

CHAPTER 4

ANALYSIS, RESULTS AND DISCUSSION

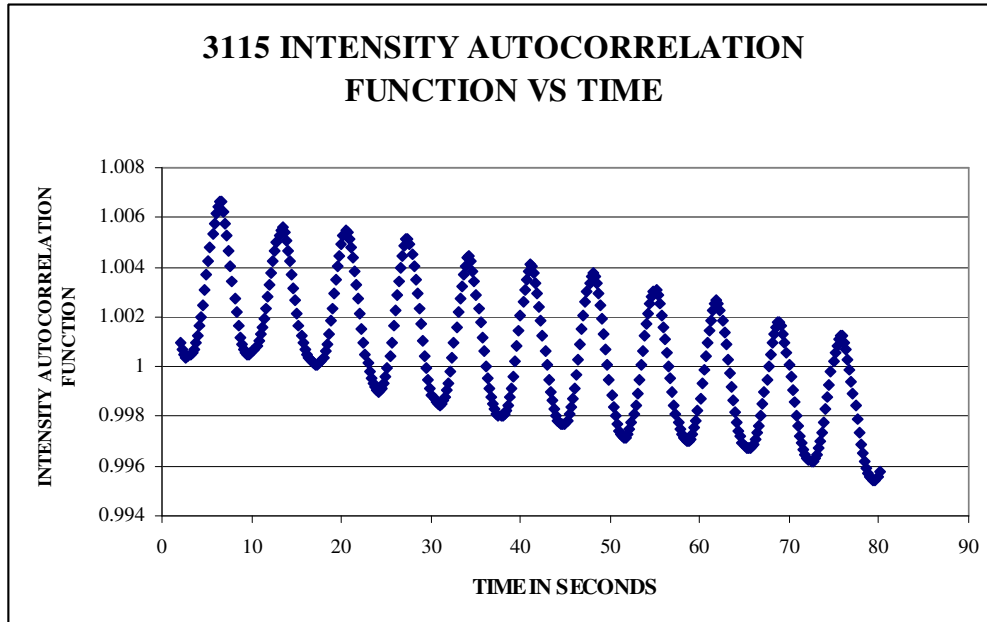
4.1 Extracting Physical Properties From Speckle Data

Several past works utilizing dynamic light scattering to explore the dynamics of non-interacting particles in colloidal gels have been recorded[29]. The interpretation of the light scattering by Brownian particles in terms of a generalized Stokes-Einstein relation has formed the basis of the interpretation of much of the experimental data[29]. In this section, we will outline, for the first time, a Stokes-Einstein type methodology to examine the dynamic behavior of magnetic solid elastomer composite. From this we will obtain the mean square displacements of the scattering sites at differing scattering vectors. This will allow us to determine different material properties and mechanical constants of the MRE.

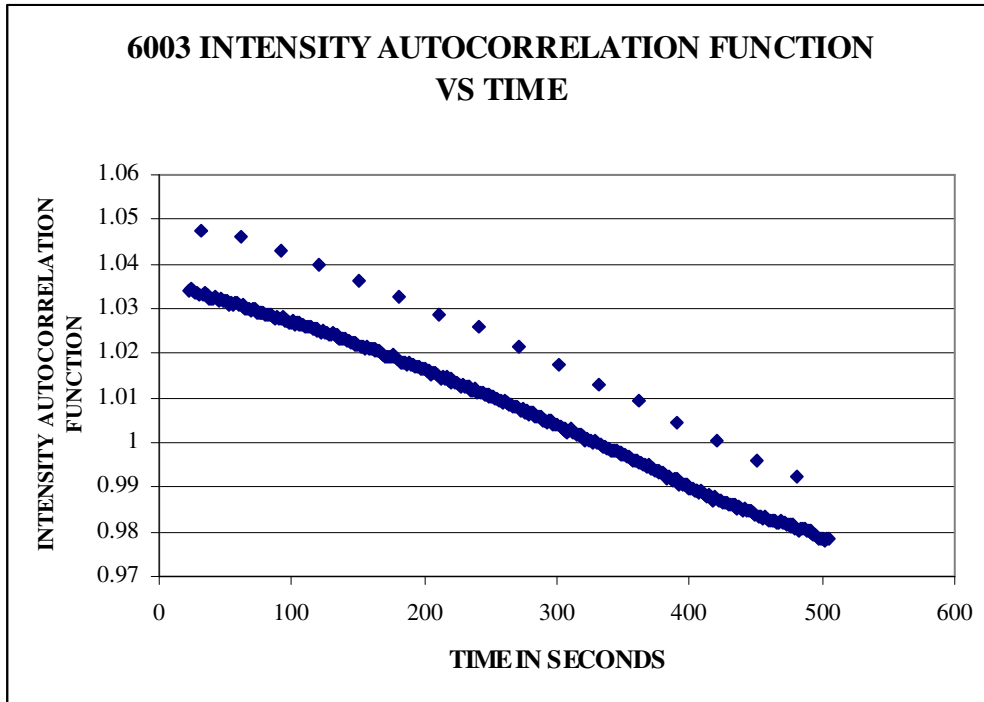
In our experiments we have excited our MR elastomer with a magnetic field and recorded the relaxation in the material via the change in the scattered light pattern. The time-dependent change in intensity of the speckle pattern is a direct function of the material relaxation. As the material relaxes the spatial arrangement of scattering sites changes. Therefore the level and time rate of change of the intensity decorrelation is proportional to the displacement and time rate of change in the particle motion. We have previously defined $g^{(2)}$ as the intensity autocorrelation function (eqn.1.1)

$$g^{(2)}(\Delta t) = \frac{\langle I(t + \Delta t)I(t) \rangle}{\langle I(t) \rangle^2}.$$

Below we have plotted the function $g^{(2)} - 1$ as a function of time for MRE samples 31 and 60. These plots represent the material behavior in response to a cyclically applied magnetic field.



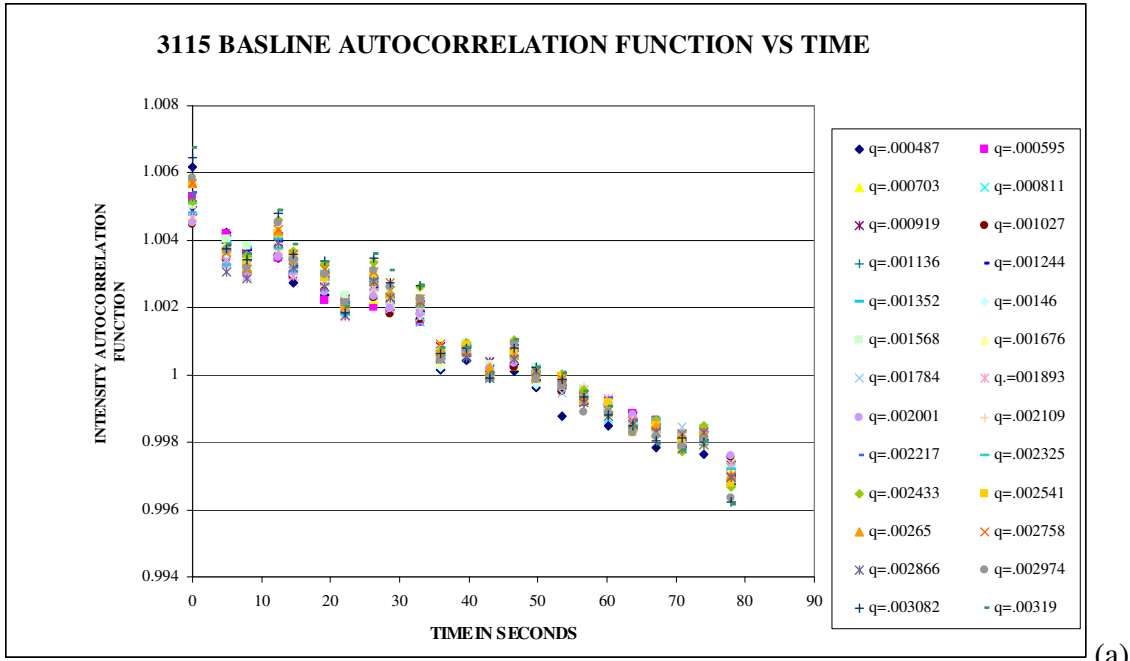
(a)



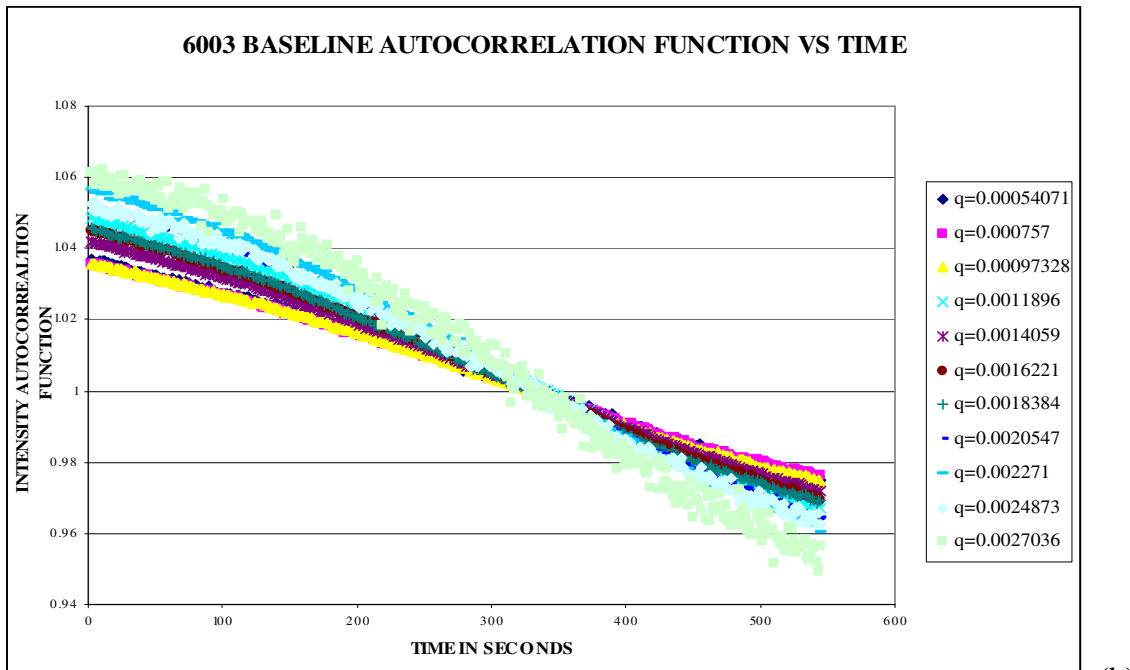
(b)

Fig .22 The autocorrelation function for MRE 31 (A) and MRE 60 (B). The behavior in each plot is composed of two portions. A creep relaxation of the bulk material (the base downward trend) with a periodic response to the actuating magnetic field superimposed. Note: the response of the system 60 was so fast following the magnetic perturbation (field on – field off) that only a single data point shows significant change in intensity. Data are recorded every 4 seconds and thus the data points during the steady state (constant field) condition appear as a continuous curve.

In each plot what is shown is the complete response to our test. This complete response is the relaxation behavior of our MRE which falls into two regimes. The first regime is one that reflects the creep relaxation at a given temperature of the composite. In the intensity plots this is shown as the overall downward trend in the correlated intensity. This room temperature relaxation will be referred to as the baseline or “slow” regime.



(a)



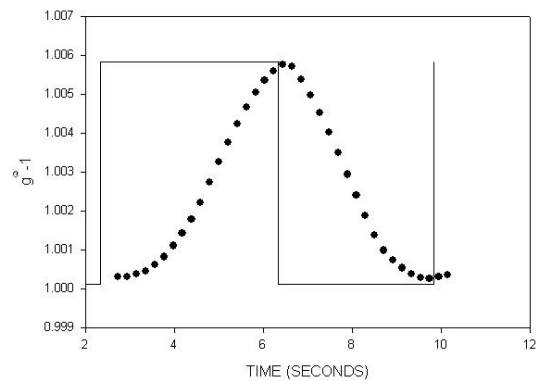
(b)

Fig .23: The autocorrelation function of the baseline relaxation for MRE 31 (a) and MRE 60 (b)

This long-time relaxation could be due to the assumption that each polymer fiber in a highly entangled system moves or “reptates” in a tube formed by other fibers.

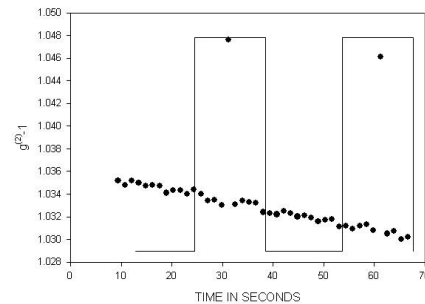
This is in contrast to the short time scale direct response to the imposed magnetic field. A state of high correlation in $g^{(2)}$ at time $t=0$, corresponds to an initial displacement of the filler by the magnetic field to an interparticle spacing approaching $2\pi/q$. When the magnetic field is removed, the material relaxes to its initial pre-field arrangement. This will be referred to as the dynamic or “fast” regime.

3115 FAST REGIME RESPONSE TO APPLIED MAGNETIC FIELD VS TIME



(a)

6003 FAST REGIME RESPONSE TO APPLIED MAGNETIC FIELD VS TIME



(b)

Fig .24: The autocorrelation function in the fast regime for MRE 30 (a) and MRE 60 (b) illustrating the response profile to the applied field.

The stimulus profile is that of a square wave, we can see from the plots of the autocorrelated intensity that the response does not have a square profile. This illustrates

that there are non-linear mechanical processes that are governing the material response behavior. Again, the total material response is a superposition of these two separate behaviors in the two time regimes.

When the field is applied there is an initial elongation of the material. After the field is turned off, the material/scattering site relaxes away from this position as a function of time given by the mean square displacement $\langle \Delta^2 L(t) \rangle$. We can consider the $t = 0$ configuration as a state of high stress, σ_1 , and a state of lower stress at a later time t , defined as σ_2 . We are concerned with the rate of relaxation that corresponds to this change in elongation and the associated change in stress.

4.2 Characteristic Relaxation Times from the Intensity Autocorrelation Function

Consider the deformation of a unit cube of viscoelastic gel with fiber network density ρ .

The displacement vector of any two points is assumed to obey the following linear equation

$$\rho \frac{\partial^2 \vec{u}}{\partial t^2} = \nabla \cdot \vec{\sigma} - f \frac{\partial \vec{u}}{\partial t} \quad (4.1)$$

This equation is a representation of Newton's second law. The term on the left represents the mass times acceleration of a unit cube of the fiber network. The terms on the right hand side represent the forces exerted on the cube. The first is the net force of the internal

stresses and is expressed as the difference of the two internal stresses on the opposing walls of the unit cube. Therefore it is given by the divergence of the stress tensor $\tilde{\sigma}$. The second term is the viscous damping force.

If this is taken to represent the volume of elastomer between two neighboring magnetic inclusions in the sample then

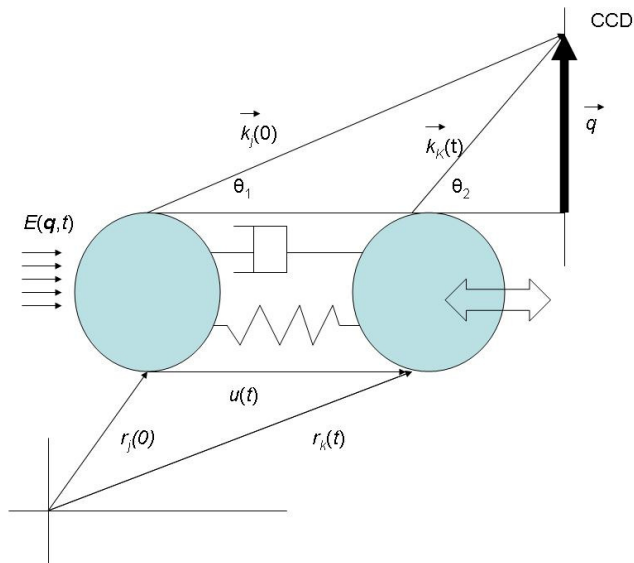


Fig .25: A simplified representation of the mechanism for relaxation in an MRE material as it relates to XPCS. The spring and dashpot are representations of the simultaneous viscous and elastic aspects of the mechanical response.

$$\rho \frac{\partial^2 u}{\partial t^2} \equiv \text{the net force on the end spheres}$$

$$\nabla \cdot \tilde{\sigma} \equiv \text{the internal stress due to loading}$$

$$f \frac{\partial u}{\partial t} \equiv \text{viscous damping}$$

$\vec{\sigma}$ is a stress tensor whose component σ_{ik} gives the force along the k axis on a unit plane perpendicular to the i axis

$$\sigma_{ik} = K \nabla \cdot u_{ik} \delta_{ik} + 2\mu \left(u_{ik} - \frac{1}{3} \nabla \cdot u \delta_{ik} \right) \quad (4.2)$$

where (eqn.2.218)

$$u_{ik} \equiv \frac{1}{2} \left[\left(\frac{\partial u_k}{\partial x_i} \right) + \left(\frac{\partial u_i}{\partial x_k} \right) \right]$$

After substitution we obtain an equation for the displacement vector u as follows,

$$\rho \frac{\partial^2 \vec{u}}{\partial t^2} = \mu \Delta u + \left(K + \frac{1}{3} \mu \right) \nabla (\nabla \cdot u) - f \left(\frac{\partial u}{\partial t} \right) \quad (4.3)$$

At this point let us introduce the Fourier transform of the displacement vector,

$$u(q, \omega) = \frac{1}{2\pi} \frac{1}{2\pi^{3/2}} \int_{-\infty}^{\infty} \int u(r, t) \exp^{-i(q \cdot r + \omega t)} dr dt \quad (4.4)$$

Restricting the motion to one dimension, we can choose the z axis in q space without loss of generality,

$$q = (0, 0, q) \quad (4.5)$$

Substituting in the transform $u(q, \omega)$ we find

$$\rho \omega^2 u_z - i f \omega u_z - \rho c_l^2 q^2 u_z = 0 \quad (4.6)$$

and

$$\rho \omega^2 u_j - i f \omega u_j - \rho c_t^2 q^2 u_j = 0 \quad (4.7)$$

for l , longitudinal modes and t transverse. Where

$$c_l = \sqrt{\left(K + \frac{4}{3}\mu\right) / \rho} \quad \text{and} \quad c_t = \sqrt{\mu / \rho} \quad (4.8)$$

Earlier works in dynamic light scattering has shown by measuring the time correlation functions of the electric field scattered from a viscoelastic gel that motions or fluctuations along the beam axis are governed by the mechanical properties of the matrix[37]

$$g^{(1)}(t) \equiv \frac{\langle E(q,t)E(q,0) \rangle}{\langle E(q) \rangle^2} = \exp \left(- \frac{\left(K + \frac{4}{3} \mu \right) q^2 t}{f} \right) \quad (4.9)$$

where

$$\left(K + \frac{4}{3} G \right) = 3G = 3C_{44} = C_{11} = E \quad (4.10)$$

and

$$\eta = \frac{f}{q^2} \quad (4.11)$$

The constant f is defined as the frictional constant of the elastomer. Therefore the displacement can be shown to be proportional to an exponential function governed by the retardation time

$$\frac{1}{\tau} = \frac{E}{\eta} \quad (4.12)$$

Where, E , and, η , are Young's modulus of elasticity and dynamic viscosity at a given length scale respectively. However, because of the Gaussian properties of the electric field, the correlation function of the intensity is given by the square of the correlation functions of the field. Thus the decay constant $\Gamma = 1/\tau$ becomes $2[E/\eta]$. The time-dependent autocorrelated speckle intensity, $g^{(2)}(t) - 1$ at a specific scattering vector is fit with

$$g^{(2)}(t) - 1 = ae^{-bt} \quad (4.13)$$

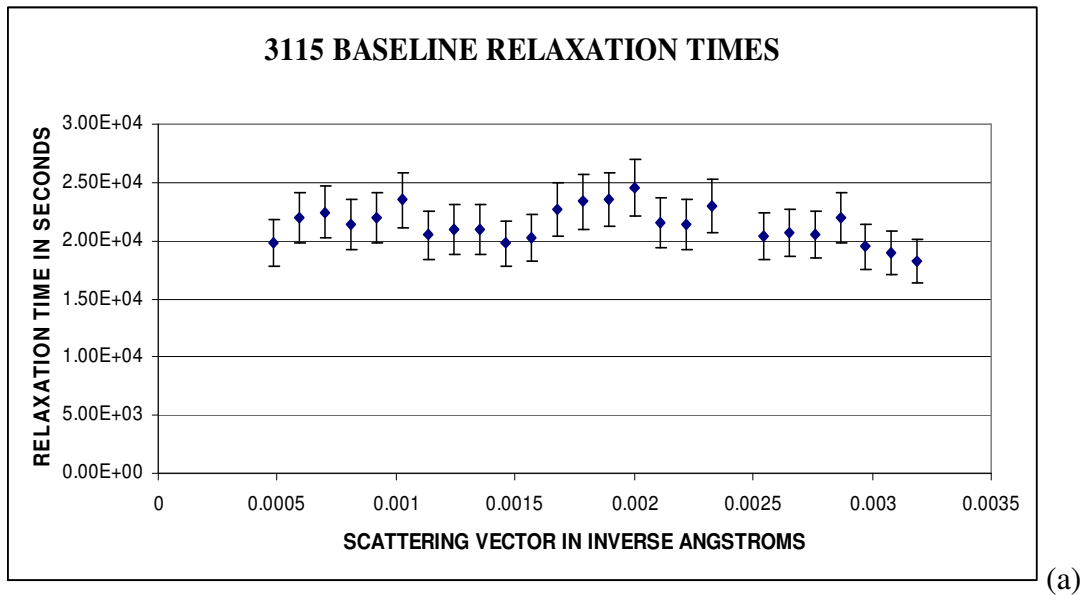
to match the form of the Siegert relation

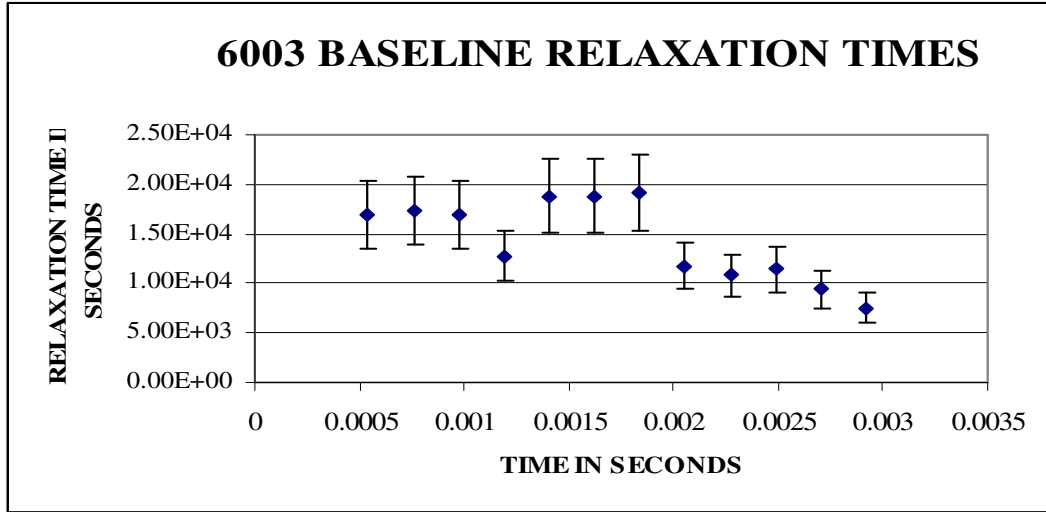
$$g^{(2)}(t) = 1 + |g^{(1)}(t)|^2 \quad (4.14)$$

Therefore, as we have shown, our characteristic times of relaxation are given by

$$b = 2\Gamma = \frac{2E}{\eta} \quad (4.15)$$

We have plotted τ as a function of scattering vector.





(b)

Fig .26: The characteristic baseline relaxation time (a) MRE 31 and (b)MRE 60

4.3 Deriving Relative Elongations From The Intensity Autocorrelation Function

The core of this unique approach is to solve for the particle displacements in this visco-elastic solid elastomer composite using only the decay in the magnitude of the intensity autocorrelation function. The decay rate of this function directly corresponds to the time scale of translation by the dispersed magnetic phase in the matrix. This can be seen to be the decay rate of the dynamic structure factor via the Siegert relation

$$g^{(2)}(t) - 1 \cong |g^{(1)}(t)|^2 \equiv \left| \frac{F(q,t)}{S(q)} \right|^2 \quad (4.16)$$

Where the ratio $F(q,t)/S(q)$ is defined as the intermediate scattering function, $F(q,t)$ the dynamic structure factor and $S(q)$ the static structure factor. Thus, we can begin to examine the relaxations through the electric field correlation function $g^{(1)}(t)$.

We will write $g^{(1)}(t)$ as an exponentially decaying function resembling a Stokes-Einstein relation

$$g^{(1)}(t) \equiv g^{(1)}|_{t=0} \exp(-q^2 \langle \Delta^2 L(t) \rangle). \quad (4.21)$$

$\langle \Delta^2 L(t) \rangle$ is the time varying mean square displacement of the scattering sites at a specific value of scattering vector q (as the scatterers move away from the configuration of high correlation).

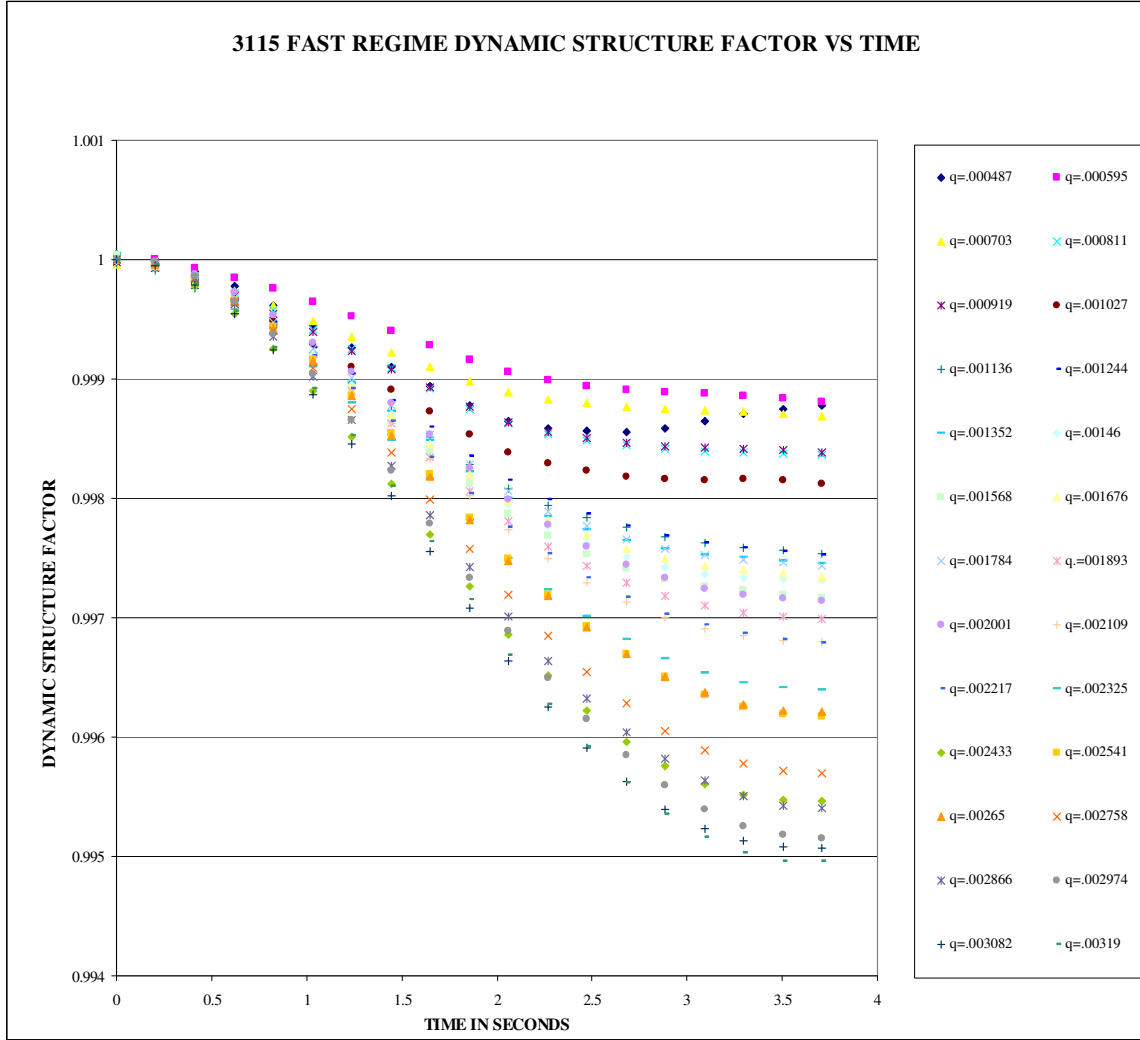


Fig.27: The dynamic structure factor MRE 30 in the fast regime. This figure demonstrates strong dependence in this regime on scattering vector.

Because we are looking at a relative change in the intensity of the speckle, $g^{(2)}(t)$ we can make the assumption that

$$|g^{(2)}(t) - 1| \cong |g^{(1)}(t)|^2 \quad (4.22)$$

$$|g^{(2)}(t) - 1| \cong g^{(1)}|_{t=0} \left| \exp(-q^2 \langle \Delta^2 L(t) \rangle) \right|^2 \quad (4.23)$$

using the definition for the scattering vector $q = 2\pi/L_o$ we can define

$$q\langle\Delta L(t)\rangle = 2\pi\frac{\langle\Delta L(t)\rangle}{L_o} \quad (4.24)$$

and rewrite the intensity autocorrelation as a function of relative elongation

$$|g^{(2)}(t) - 1| = g^{(1)}|_{t=0} \left| \exp\left(-\left(2\pi\frac{\langle\Delta L(t)\rangle}{L_o}\right)^2\right) \right|^2 \quad (4.25)$$

Taking first the square root

$$\sqrt{|g^{(2)}(t) - 1|} = \left| \sqrt{g^{(1)}|_{t=0}} \exp\left(-\left(2\pi\frac{\langle\Delta L(t)\rangle}{L_o}\right)^2\right) \right|$$

and then the natural logarithm of both sides

$$\ln\left(\sqrt{|g^{(2)}(t) - 1|}\right) = \ln\left(\sqrt{g^{(1)}|_{t=0}}\right) - \left(2\pi\frac{\langle\Delta L(t)\rangle}{L_o}\right)^2 \quad (4.26)$$

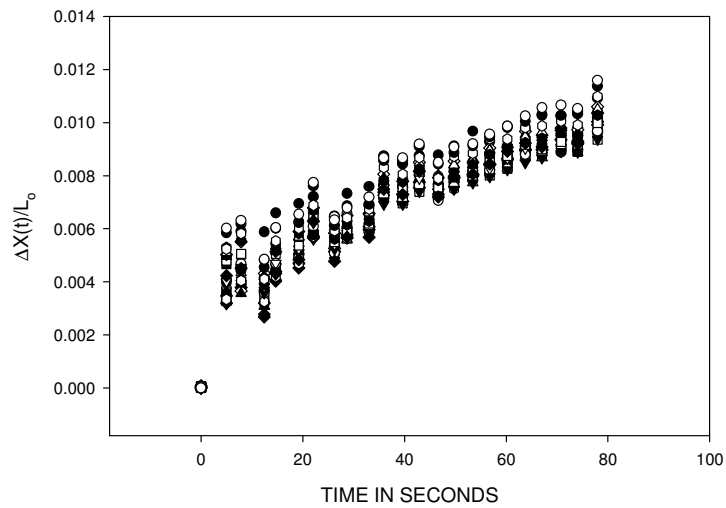
Defining

$$g^{(1)}|_{t=0} = \sqrt{g^{(2)}(0) - 1} \quad (4.27)$$

we can solve for the relative length change

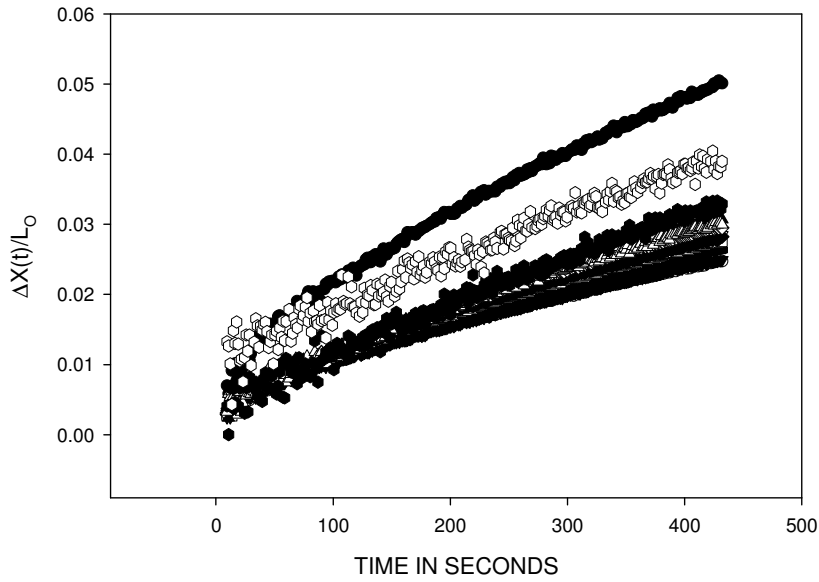
$$\frac{\langle \Delta L(t) \rangle}{L_o} = \frac{1}{2\pi} \sqrt{\ln(\sqrt{g^{(2)}(0) - 1}) - \ln(\sqrt{g^{(2)}(t) - 1})} \quad (4.28)$$

3115 BASELINE RELATIVE ELONGATION $\langle \Delta X(t) \rangle / L_o$ VS TIME

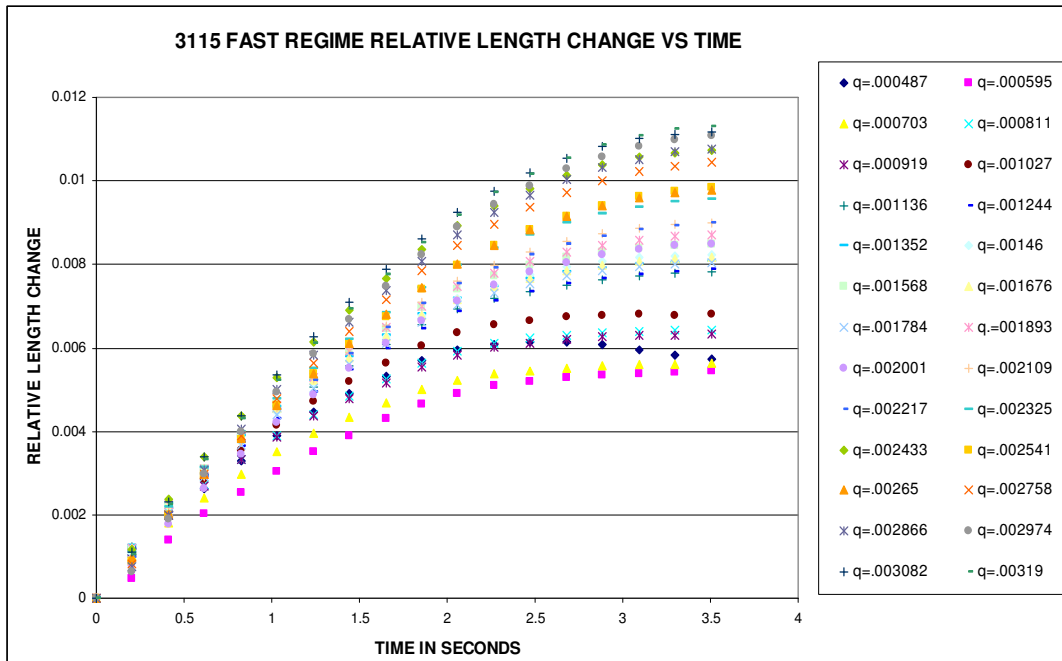


(a)

6003 BASELINE RELATIVE ELONGATION $\Delta X(t)/L_0$ VS TIME



(b)



(c)

Fig .27: The relative elongation as a function of time for (a) MRE 31, (b) MRE 60 and (c) fast regime of MRE 31

We may now easily arrive at a rate for the relative length change as

$$\frac{1}{L_o} \frac{d\langle \Delta x(t) \rangle}{dt} \quad (4.29)$$

or the slope of a plot of the relative length change as a function of time.

4.4 Calculating Elastic Modulus with Fractional Calculus

We have shown that the Cauchy stress associated with the deformation of the elastomer from the initial length L_o to a final length L , by an applied force is given by

$$\sigma_1 - \sigma_2 = G \left(\left(\frac{\langle \Delta x(t) \rangle}{L_o} \right)^2 - \frac{L_o}{\langle \Delta x(t) \rangle} \right) \quad (4.30)$$

By arriving at the principal stress difference, we can apply the technique of fractional calculus to arrive at an estimate of the relaxation modulus. We have earlier shown that the function representing the uniaxial stress can be represented in the form

$$\sigma(t) \approx \frac{E}{\Gamma(1-\alpha)} \left(\frac{t}{\tau} \right)^{-\alpha} \quad (4.31)$$

and that after algebraic manipulation

$$\ln \sigma(t) = \ln \frac{E}{\Gamma(1-\alpha)} - \alpha \ln \left(\frac{t}{\tau} \right) \quad (4.32)$$

$$= \ln \frac{E \tau^\alpha}{\Gamma(1-\alpha)} - \alpha \ln t \quad (4.34)$$

$$= \ln k - \alpha \ln t \quad (4.35)$$

So we can now plot a form of the Cauchy stress and perform a linear regression to calculate an estimate of the Young's modulus of the composite material.

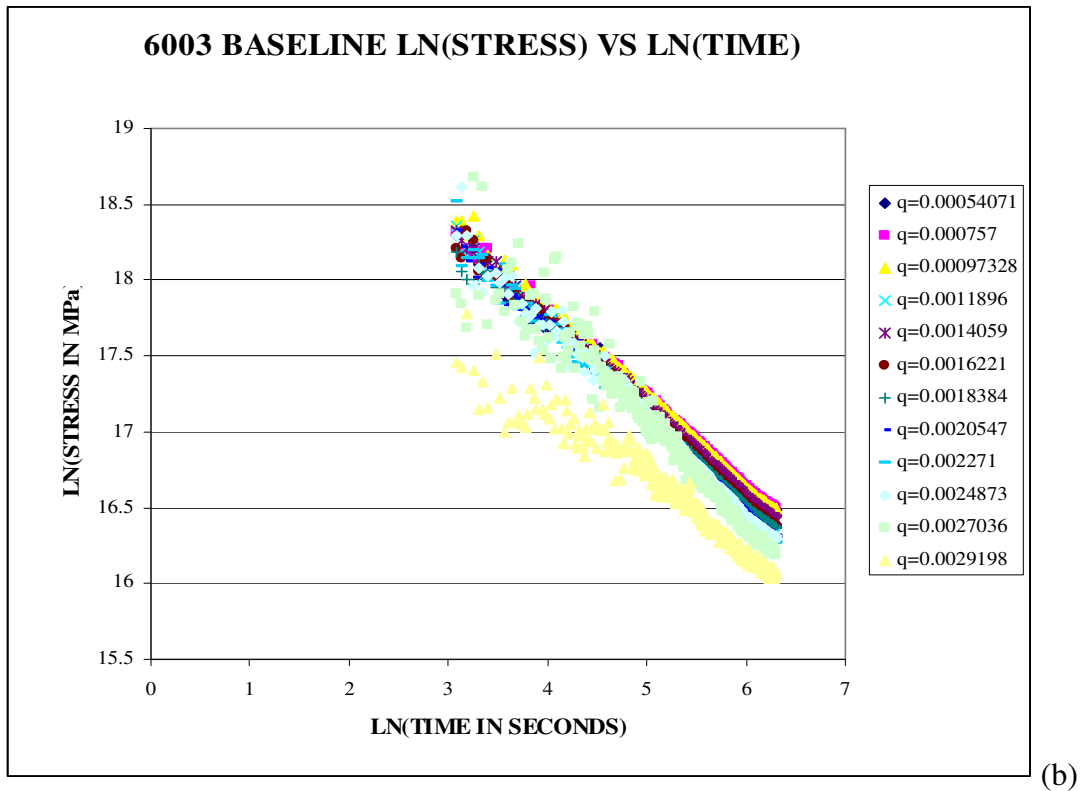
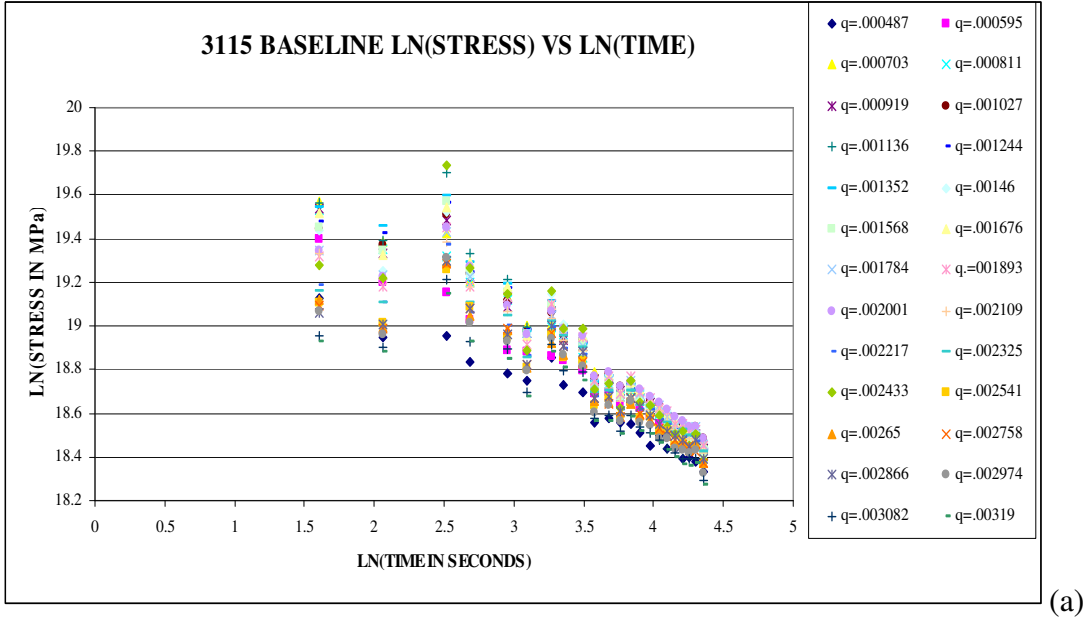
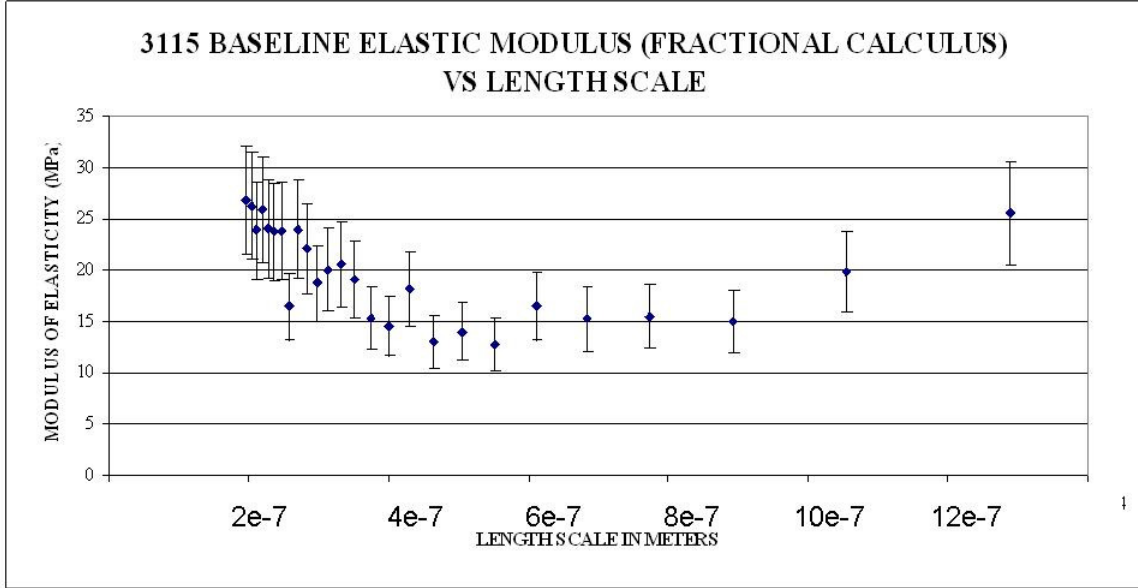
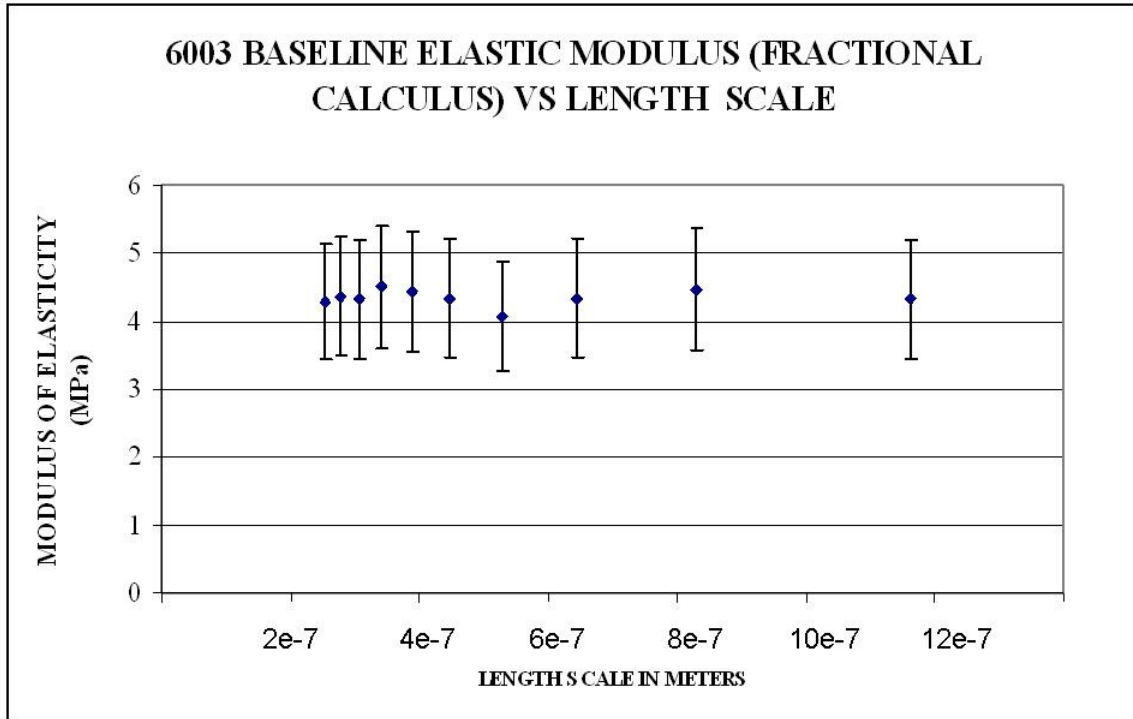


Fig .29: Ln-Ln Plots of stress relaxation data for (a) MRE 31 and (b) MRE 60

Zhou and Li [44] have used finite element analysis to calculate the zero field modulus of an MRE. Their program was based on the incursion model (rigid ferrous particles embedded orderly in a matrix) and the Ogden strain model (the model for describing the mechanical properties of rubber). This process has been reported by Davis. Using the experimental data of the extension deformation of a pure rubber MRE with a 27% volume fraction (generated by Davis), Zhou and Li generate a curve for the zero field Young's modulus versus interparticle separation. Their results are very similar in profile and magnitude as our model. Using the relative elongations found with the autocorrelation function, the Cauchy stress and techniques of fractional calculus we have found a zero-field modulus that ranges with length scale from 26MPa to 12MPa. The finite element analysis of Zhou found a length scale varying zero-field modulus that ranged from 10MPa to 2MPa. Our method has also been used to estimate the elastic modulus of MRE sample 61. This sample is similar to one tested by Bednarek [1]. Bednarek's MRE sample was one with a RTV silicone matrix and inclusions of both graphite and silicon steel particles. His tests for this material yielded a Young's modulus of 5.53MPa. The speckle relaxation tests found a length scale dependant elastic modulus ranging from 4.5MPa to 4MPa.



(a)



(b)

Fig. 30: Values of the elastic modulus for MRE 31 (a) and MRE 60 (b) samples extracted from the fractional modulus approach.

4.5 Calculating Length Scale dependant Dynamic Shear Modulus

Exploitation of the dynamic response to the cyclically applied magnetic field will now allows us to extract the scattering vector dependent dynamic shear modulus. In what we

will now refer to as our dynamic or fast regime studies of MRE response, we will use the local chain model of Jolly[15] discussed earlier.

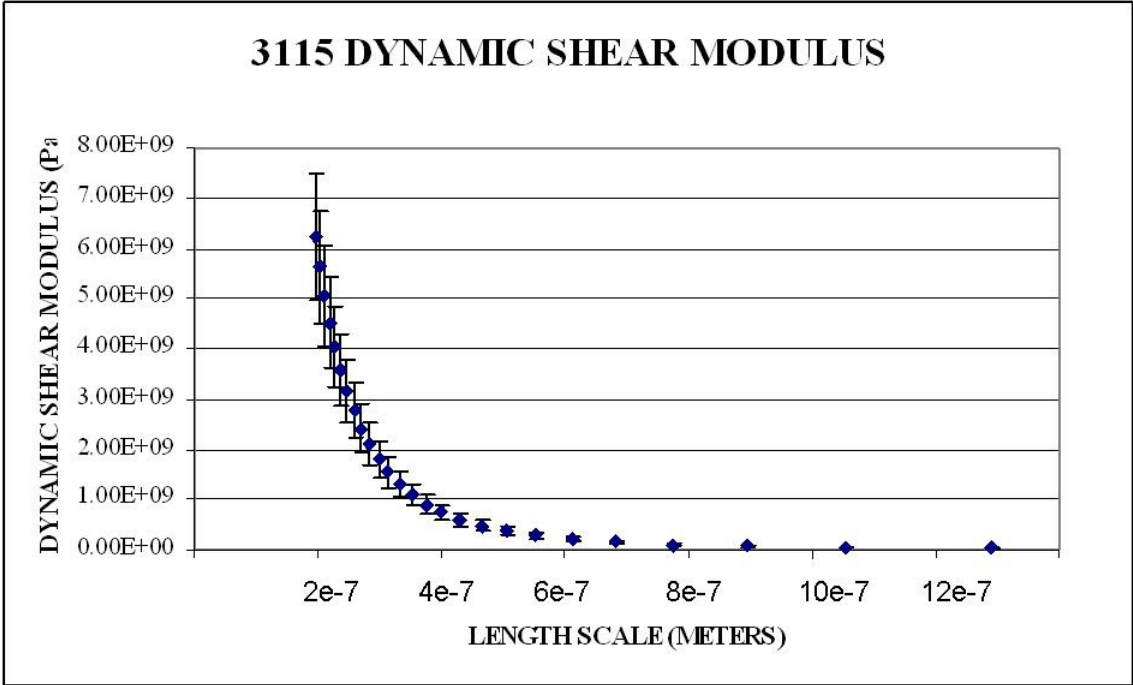
The magnetostrictive response of the MRE composite is strictly a function of the dipole-dipole interaction force between the magnetic inclusions. Jolly has put forth a simple but effective local shear model for this interaction. As shown earlier, in the small strain approximation, that (eqn.2.50)

$$\sigma(\varepsilon) \cong \left[\frac{\phi \mu_R \mu_o M^2}{2h^3} \right] \varepsilon \quad (4.35)$$

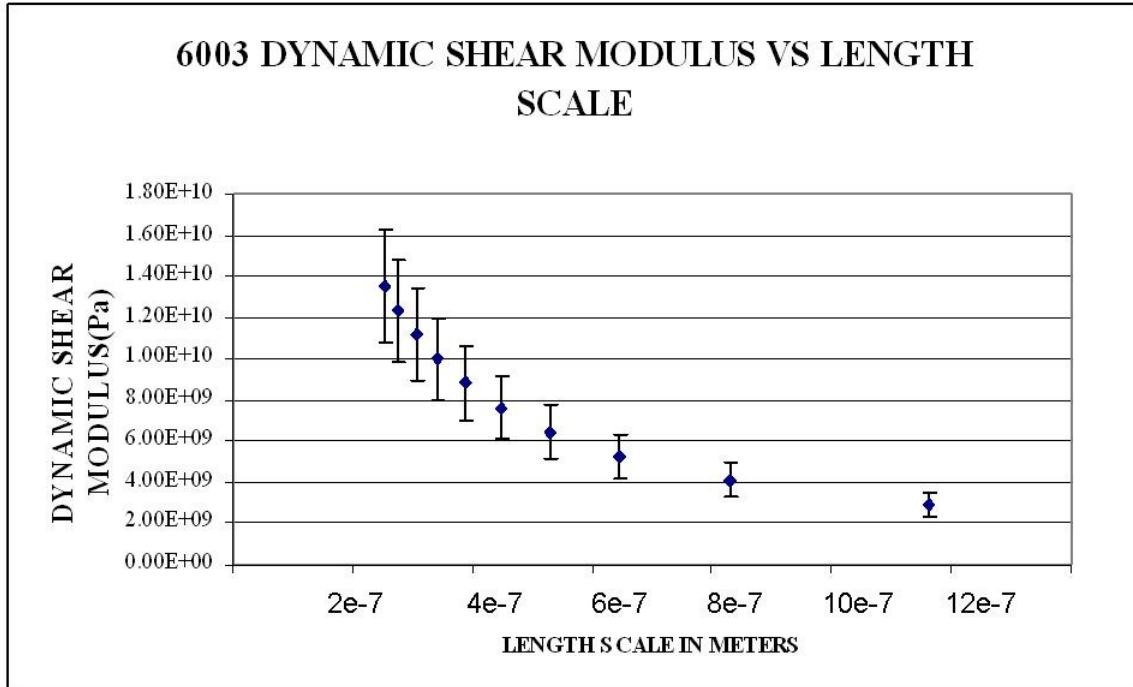
represents the local shear stress. The shear modulus G of the particle chain is (eqn.2.51)

$$G \cong \left[\frac{\phi \mu_R \mu_o M^2}{2h^3} \right] \quad (4.36)$$

where $h = L_0/d$ where d is the particle diameter and L_0 is the interparticle separation $2\pi/q$ (see fig.2).



(a)



(b)

Fig. 31: The dynamic shear modulus for MRE 31 (a) and MRE 60 (b) using the local dipole-dipole model

4.6 Using the Method of Cumulants to estimate mechanical properties

The basis of the cumulant expansion that is usually used in the analysis of dynamic light scattering lies in expanding the logarithm of $g^{(1)}$ in terms of cumulants of the distribution.

This relation follows from the fact that the n th cumulant is the coefficient of $(-t)^n/n!$ in the Taylor expansion of $K(-t, \Gamma)$ about $t=0$, as given by

$$\ln[g^{(1)}(t)] \equiv \sum_n K_n \frac{(-t)^n}{n!} = -K_1 t + \frac{K_2}{2} t^2 \quad (4.37)$$

Where we have earlier defined

$$K_1 = Dq^2 = \frac{E}{\eta} \quad (4.38)$$

and

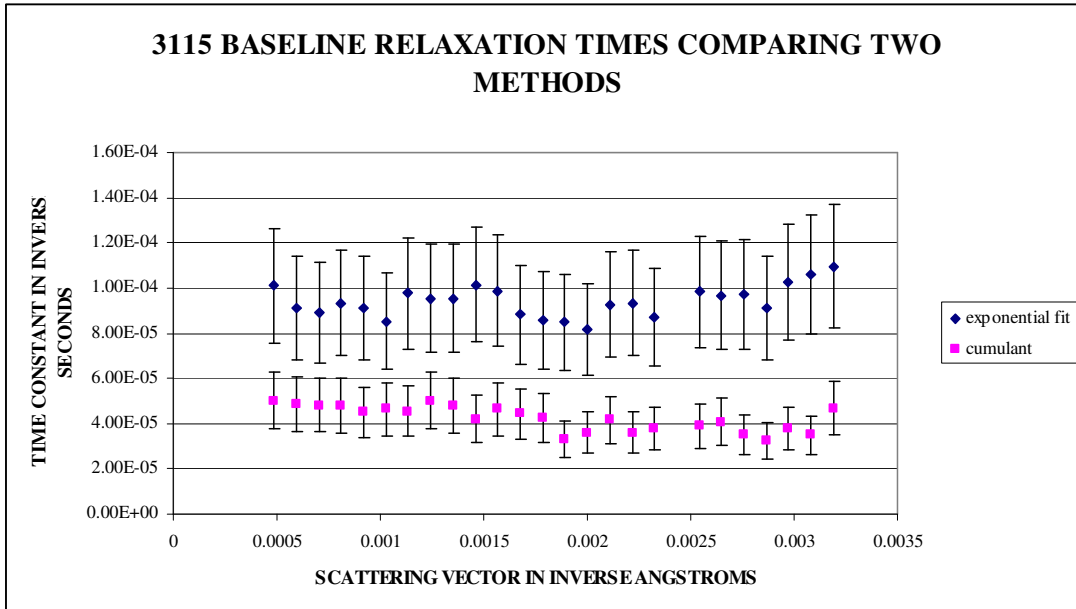
$$K_2 = 4\pi^2 \left(\frac{1}{L_o} \frac{d\langle \Delta x(t) \rangle}{dt} \right)^2 \quad (4.39)$$

We can therefore write

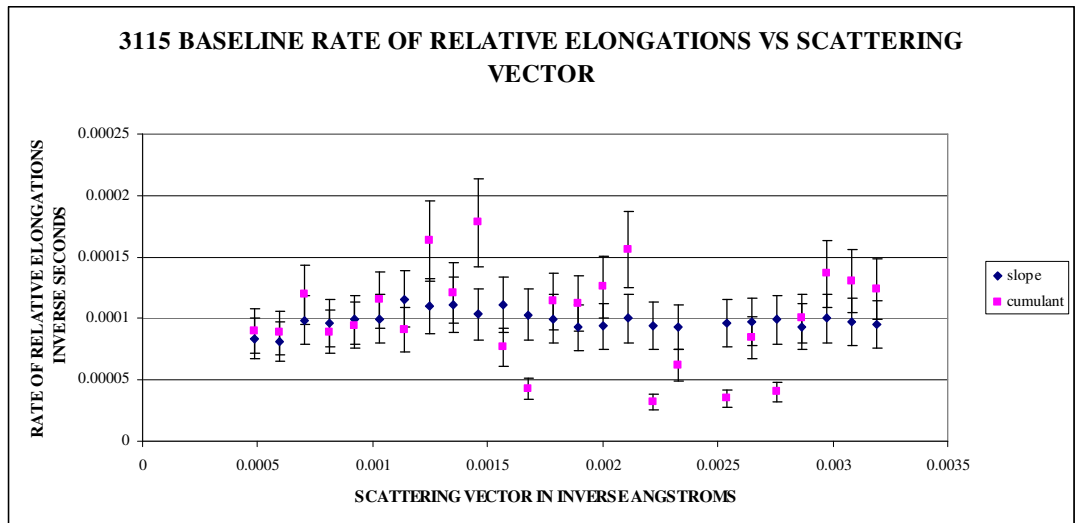
$$\ln[g^{(1)}(t)] \equiv \sum_n K_n \frac{(-t)^n}{n!} = -K_1 t + \frac{K_2}{2} t^2 = -2 \frac{E}{\eta} t + \frac{1}{2} \left(\frac{2\pi}{L_o} \frac{d\langle \Delta x(t) \rangle}{dt} \right)^2 t^2 \quad (4.40)$$

In this way we use the decaying intensity autocorrelation function to find the Young's modulus, relative elongations and dynamic viscosity of this material. We can compare the values of K_1 and K_2 found directly by a second order polynomial fit of $\ln[g^{(1)}(t)]$ to those

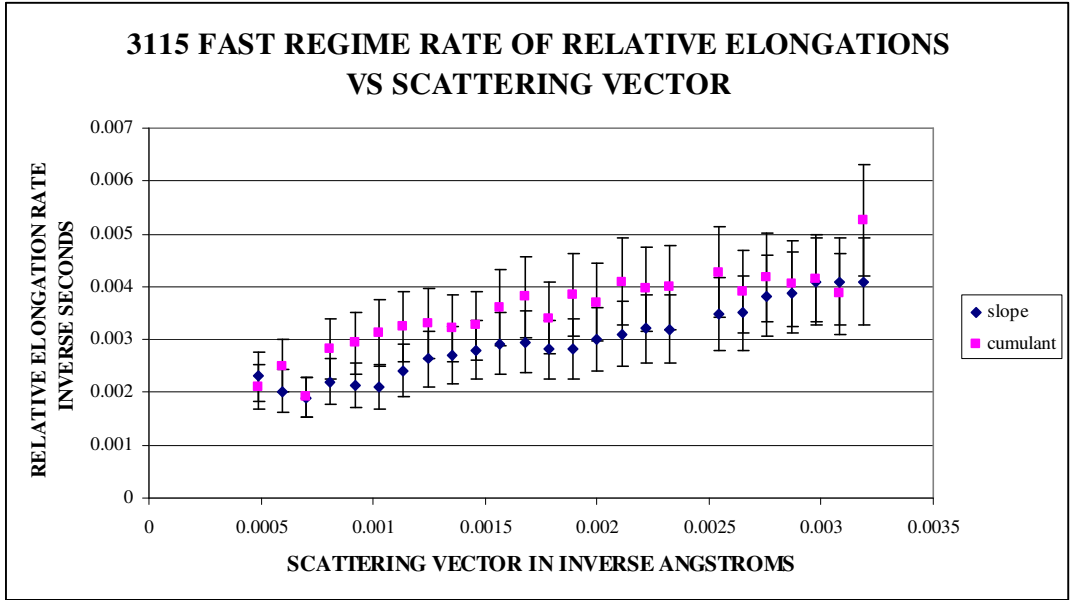
found via a mechanical evaluation of the colloidal dynamics. This allows us to physically understand the decay of the electric field autocorrelation $g^{(1)}(t)$ and thus $g^{(2)}(t)$.



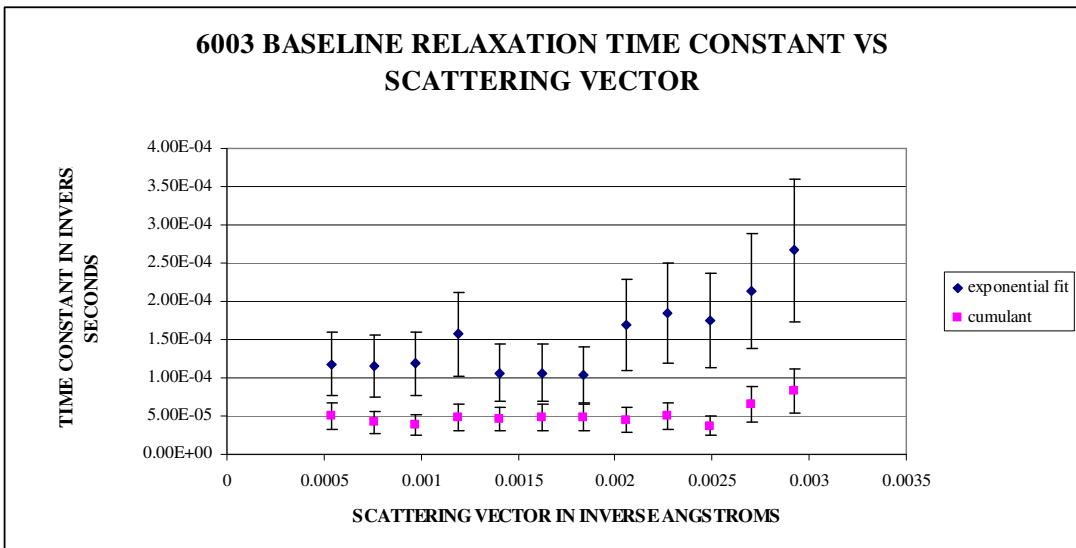
(a)



(b)



(c)



(d)

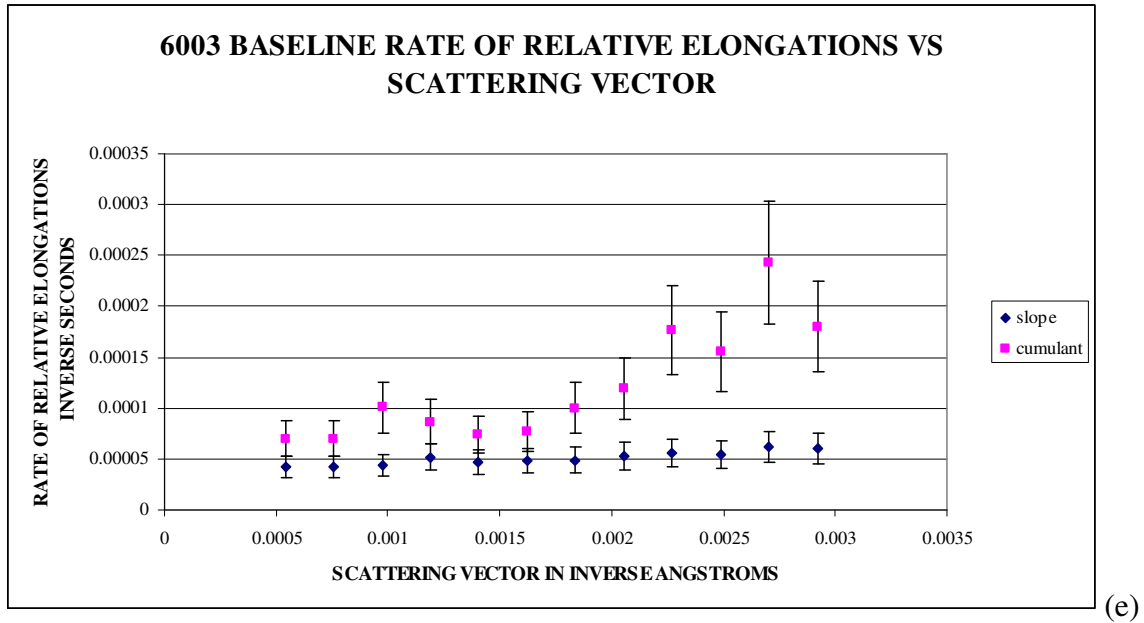


Fig. 32: A comparison of the method of cumulant fit to parameters found using other methods in the “slow” and “fast” regimes for (a-c) MRE 31 and (d and e) MRE 60

It has been emphasized by Pusey and Tough [29] that the accuracy of the cumulant method is higher for short time motions. This can be seen in the comparison in the fit of K_2 for the long term or baseline rate versus that of the direct or magnetically driven short time response of MRE sample 31. The statistical fitting accuracy associated with the method of cumulants in photon correlation spectroscopy has been evaluated by other authors [35].

4.7 Calculation of the length scale dependant magnetic interaction force

MRE response to an external magnetic field manifests itself in a contraction of the material. As we have stated, this ability to do work is accomplished due to the interaction forces and is the driving motivation for the study and production of such materials.

Therefore, of ultimate importance in the study of MRE composites is the ability to quantitatively characterize the dipole-dipole interaction forces.

As the dispersed magnetic phase responds to the applied field the spherical inclusions are displaced in the elastomer matrix. We use the model of Hertz's spherical indenter shown earlier (eqn.2.78) to find the interaction force for this displacement

$$P = \frac{8G\sqrt{R}}{3(1-\nu)} \delta^{3/2} \quad , \quad (4.41)$$

where P is the force required to displace the spherical inclusion a distance δ . The displacement δ is equal to the mean displacement $\langle \Delta x \rangle$. Therefore the force can now be written as

$$P = \frac{8G\sqrt{R}}{3(1-\nu)} (\Delta x)^{3/2} \quad (4.42)$$

This model yields a $1/r^N$ dependence law for the magnetic dipole-dipole interaction force. Considering the magnetic interaction energy

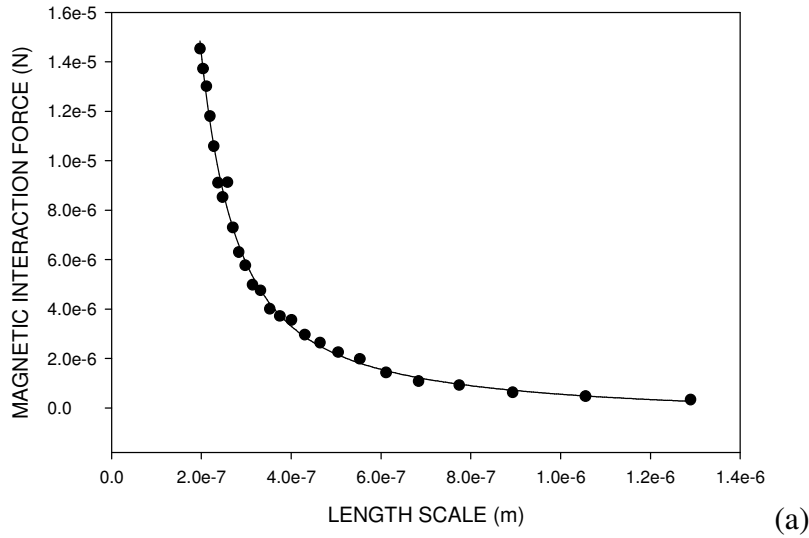
$$E_{12} = \frac{\mu_R \mu_o (MV)^2}{4\pi|r|^3} [(1 - 3\cos^2 \theta)] \quad (4.43)$$

And then the first derivative with respect to the interparticle separation r

$$F_{12} \propto -\frac{dE_{12}}{dr} \quad (4.44)$$

Furst and Gast [5] have used dual-trap optical tweezing to study the micromechanical properties of dipolar chains in MR suspensions. Using this method they were able to observe the field dependence of chain rupture. Their study was of a magnetic chain of $0.85 \mu\text{m}$ diameter polystyrene (PS) microspheres embedded with monodomain (11nm) iron oxide particles that caused the beads to exhibit a paramagnetic response. Using this method, they found tensile forces required to break the representative chain on the order of 5 to 25 pN. The force-displacement method used here allows us to make measurements in a regime where the forces are much larger than in a liquid environment where the optical trapping measurements were performed. Our samples have ferromagnetic rather than paramagnetic interactions between particles; the interactions are much stronger. For MRE sample 31, we have found forces ranging from $1.4\text{E-}5\text{N}$ to $1.0\text{E-}5\text{N}$ and $3.5\text{E-}4\text{N}$ to $5.0\text{E-}5\text{N}$ for MRE sample 60. Both samples are shown to follow a $1/r^N$ length scale dependence.

3115 MAGNETIC INTERACTION FORCE VS LENGTH SCALE



6003 MAGNETIC INTERACTION FORCE VS LENGTH SCALE

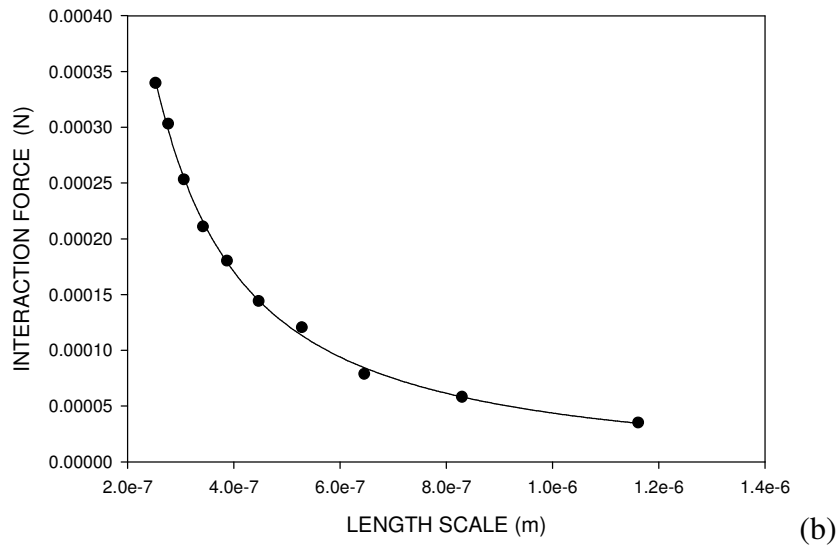


Fig. 33: The length scale dependent magnetic interaction force for (a) MRE 31 and (b) MRE 60

The parameter N classically is found to be 4 from the dipole-dipole model. Careful examination of the results of the method here allow a real examination of the magnetostrictive forces found in a MRE material under realistic conditions. Comparisons of figures 24 a) and b) show that for the highly anisotropic MRE 60 that the r dependence

goes as $N = 1.5$ and for the isotropic MRE 31 the separation interaction is best approximated with $N = 2$. The ability to examine these interparticle forces in this manner is a trait unique to this method.

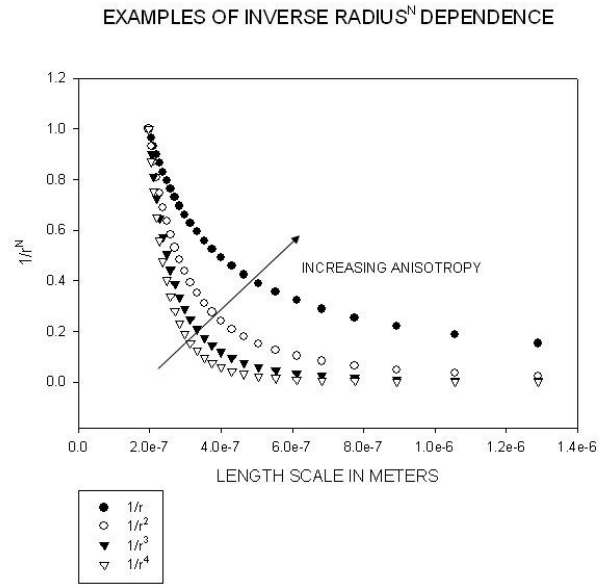


Fig. 34: A set of curves based on the length scale of the argument above to help visualize the interaction force length scale dependence.

CHAPTER 5

CONCLUSIONS AND SUGGESTIONS FOR FUTURE STUDIES

Active composite materials have several promising applications from automotive and industrial engineering to medical applications. As with any application, system optimization is of utmost importance, but this is only done by completely understanding each component. In the case of MRE materials, it is crucial to have detailed knowledge of the *microscopic* behavior which, as we have shown, is only accessible by certain specialized techniques such as XPCS.

By combining XPCS and fundamental mechanics of materials we can look at the in-situ response of a MRE and begin to truly understand how to optimize this up and coming class of materials. We have shown that the speckle patterns that arise when these disordered materials are illuminated by coherent x-rays are true representations of their structure and dynamics. The magnitude of the intensity autocorrelation function is shown to be a direct function of the time-dependent particle mean square displacement. It was also shown that by utilizing the Siegert relation, and the method of cumulants and methods of fractional calculus, that material properties and internal dynamics can be directly extracted from the relaxation curve. This is the first such study to make this connection, demonstrating that mechanical properties can be measured from x-ray speckle data.

Our study also emphasized the finding that the expansion of the electric field autocorrelation function $g^1(t)$, extracted from the coherent x-ray scattering holds important physical information on the relaxation dynamics. It was found that the second order polynomial fit of $\ln[g^1(t)]$ can give a direct first approximation of the material elastic modulus, viscosity and the short-time velocity of the particles. This has significant value to materials research. Real time knowledge of the mechanical properties of a material during use is crucial to mastering and optimizing design.

Our study has verified in a new regime of study that the following MRE parameters are important: particle size, particle ordering and the MRE matrix material. Particle size and distribution are key factors in the magnetostriction mechanism. Further studies would include using these techniques on magnetic particulate composites with differing levels of anisotropy, particle size and magnetization to compare this to the ability of the material to perform. For MRE composites this would be a study of how the internal chain structure affects the length scale dependent interaction forces.

Our results for the natural rubber MRE have found a zero-field modulus that ranges with length scale from 12 MPa at 120nm to 26 MPa at 20nm. Finite element models for a very similar material yielded a zero-field modulus that ranged from 2 MPa to 10 MPa. The RTV based sample was in good agreement with a similar material that was tensile tested. The results for the tensile tested sample yielded a Young's modulus of 5.53 MPa while speckle relaxation tests found a length scale dependant zero-field elastic modulus ranging from 4 MPa to 4.5 MPa. Subsequently, we have used continuum mechanics to study the

length scale varying magnetostrictive force. We have found forces ranging from $1.0\text{E-}5\text{ N}$ to $1.4\text{ E-}5\text{N}$ and $3.5\text{ E-}4\text{N}$ to $5.0\text{ E-}5\text{N}$ depending on the sample. The interaction force is shown to follow a $1/r^N$ length scale dependence where N is a function of the level of internal anisotropy and ranges from $1.5 \leq N \leq 2$.

Future work in magnetorheological elastomers would include, but is not limited to, MRE complex mechanical measurements and MRE transport measurements. These techniques can also be used to probe fluid based rheological systems: both electrorheological materials and ferrofluidics.

In the future, the techniques used here can be applied to a far wider class of materials than these polymeric based composites. The dynamics of any system with a high level of order on the scale of the x-ray wavelength is now accessible. These systems could include magnetic nanostructures (alternating layers of magnetic and non-magnetic materials) probing for magnetostrictive effects, domain structures and switching dynamics-fast measurements of speckle using picosecond x-ray sources (both laser based and accelerator based), stress effects in semiconductors (semiconductor superlattices, GaAs/AlAs for example) relaxation after heating or applied stress, the study of shape memory alloys and the mechanics of interfaces.

REFERENCES

- [1]Bednarek, S., Materials Science and Engineering B **55**, 201-209, 1998
- [2]Boissis G., Bellan C., International Journal of Modern Physics B **16**: 2447-2453, 2000
- [3]Bossemeyer H.G., Mechanics of Time-Dependent Materials **5**, 273-291, 2001.
- [4]Davis L.C., Journal of Applied Physics **85**, 3348-3351, 1999
- [5]Furst, E.M. and Gast, A.P., Physical Review E **61** (6), 6732-6739, 2000.
- [6]Fishbane, P.M., Gasiorowicz S., Thornton S., Physics for Scientist and Engineers, Printice-Hall, Inc., New Jersey, 1996
- [7]Ginder J.M., Proceedings of the SPIE- The International Society for Optical Engineering **3985**,418-25, 2000
- [8]Häußler W., Wilk A., Gapinski J., Patkowski A., Journal of Chemical Physics **117**, 413-426, 2002
- [9]Hansen J.P., McDonald I.R., Theory of Simple Liquids, Academic Press, New York, London, and San Francisco, 1976
- [10]Halliday D., Resnick R., Physics, Wiley, New Your, 1986
- [11]Harpavat, G., IEEE Transactions on Magnetics vMAG-10 **3**, 919-922, 1974
- [12]Hernandez-Jimenez A., Hernandez-Santiago J., Macias-Garcia A., Sanchez-Gonzalez J., Polymer Testing **21** 325-331 (2002)
- [13]Hobbie E.K., Stewart A.D., Physical Review E **61**, 5540-5544, 2000
- [14]Ivanov A.O., Kuznetsova O.B., Journal of Magnetism and Magnetic Materials **252**, 135-137, 2002
- [14]Jackson J.D., Classical Electrodynamics, Wiley, New York, 1962
- [15]Jolly, M.R., Carlson, J.D., and Munoz, B.C., Smart Materials and Structures **5**, 607-614, 1996
- [16]Kim H., Ruhm A., Lurio L.B., Basu J.K., Lai J., Mochrie S.G.J., Sinha S.K., Journal of Physics-Condensed Matter **16**, S3491-S3497, 2004

- [17]Koeller R.C., Journal of Applied Mechanics. **51**, 299-307,1984
- [18]Koppel D.E., Journal of Chemical Physics **57**, 4814-4820, 1972
- [19]Korotkova O., Salem M., Wolf E., Optics Letters **29**, 1173-1175, 2004
- [20]Kristof T., Szalai I., Physical Review E **68**, 41109-1-8, 2003
- [21]Landau L.D., Lifshitz E.M., Theory of Elasticity, Pergamon Press,Oxford-New York 1986
- [22]Lumma D., Lurio L.B., Borthwick M.A., Falus P., Mochrie S.G.J., Physical Review E **62**, 8258-8269, 2000
- [23]Mase G.E., Mase G.T., Continuum Mechanics for Engineers, CRC Press, 1992
- [24]McCrum N.G., Buckley C.P., Bucknall C.B., Principles of Polymer Engineering, Oxford University Press, Oxford and New York, 1997
- [25]Mooney M., Journal of Applied Physics **11**, 582-592, 1940
- [26]Pecora R., Journal of Nanaoparticle Reasearch **2**: 123-131, 2000
- [27]Pellicer J., Manzanares J.A., Zuniga J., Utrillas P., Fernandez J., Journal of Chemical Education **78**, 263-267, 2001
- [28]Poddar P., Wilson J.L., Srikanth H., Yoo J.H., Wereley N.M., Kotha S., Bargohouty L., Radhakrishnan R., Journal of Nanoscience and Nanotechnology **4**, 192-196, 2004
- [29]Pusey P.N., Tough, R.J.A., Dynamic Light Scattering: Applications of Photon Correlation Spectroscopy, ed. Pecora, R., 85-179, Plenum Press, New York and London, 1985
- [30]Reese S., Wriggers P., Constitutive Models for Rubber, 13-21, 1999
- [31]Rivlin R.S., Royal Society of London-Philosophical Transactions Series A **241**, 379-397, 1948
- [32]Rosensweig, R.E., Ferrohydrodynamics, Cambridge University Press, Cambridge, 1985.
- [33]Rudnitsky V.A., Djakovich V.V., Materials Science Forum **v210-213**, 391-396, 1996
- [34]Schiessel H., Metzler R., Blumen A., Nonnenmacher T.F., Journal of Physics A: (Mathematical and General) **28** 6567-6584 (1995).

- [35]Shaumeyer, J.N., Briggs, M., Gammon, R., Applied Optics **32**, 3871-3879,1993
- [36]Stadler L.M., Sepiol B., Kantelhardt J.W., Zizak I., Grubel G., Vogl G., Physical Review B **69**, Art.No.224301, 2004
- [37]Tanaka T, Hocker L.O., Benedek G.B., Journal of Chemical Physics **59**, 5151-5159, 1973
- [38]Treloar L.R.G. Transactions of the Faraday Society **39**, 241-246, 1943
- [39]Weitz D.A., Krall, A.H., Physical Review Letters **80**, 778-781, 1998
- [40]West B., Bologna M., Grigolini P., Physics of Fractal Operators, Springer-New York, 2003
- [41]Wiedmann A., Kammel M., Hoell A., Journal of Magnetism and Magnetic Materials **272**, 1487-1489, 2004
- [42]Yamazaki H., Ishikawa T., Journal of Applied Crystallograpy **37**, 48-51, 2004
- [43]Yang F., Journal of Physics D **36**, 2417-2420, 2003
- [44]Zhou, G.Y., Li, J.R., Smart Materials and Structures **12** 859-872, 2003